

**ON CONCATENATED SINGLE PARITY  
CHECK CODES AND BIT INTERLEAVED  
CODED MODULATION**

---

A thesis submitted in fulfilment  
of the requirements for the Degree of

Doctor of Philosophy

in Electrical and Electronic Engineering  
from the University of Canterbury,  
Christchurch, New Zealand

**JAMES TEE SENG KHIEN**

B. E. (Hons)

8<sup>th</sup> January 2001

000000

TK  
5102.96  
.T258  
2001

To my beloved parents, and my late grandfather



## ABSTRACT

---

In recent years, the invention of Turbo codes has spurred much interest in the coding community. Turbo codes are capable of approaching channel capacity closely at a decoding complexity much lower than previously thought possible. Although decoding complexity is relatively low, Turbo codes are still too complex to implement for many practical systems.

This work is focused on low complexity channel coding schemes with Turbo-like performance. The issue of complexity is tackled by using single parity check (SPC) codes, arguably the simplest codes known. The SPC codes are used as component codes in multiple parallel and multiple serial concatenated structures to achieve high performance. An elegant technique for improving error performance by increasing the dimensionality of the code without changing the block length and code rate is presented. For high bandwidth efficiency applications, concatenated SPC codes are combined with 16-QAM Bit Interleaved Coded Modulation (BICM) to achieve excellent performance. Analytical and simulation results show that concatenated SPC codes are capable of achieving Turbo-like performances at a complexity which is approximately 10 times less than that of a 16-state Turbo code. A simple yet accurate generalised bounding method is derived for BICM systems employing large signal constellations. This bound works well over a wide range of SNRs for common signal constellations in the independent Rayleigh fading channel. Moreover, the bounding method is independent of the type and code rate of channel coding scheme.

In addition to the primary aim of the research, an improved decoder structure for serially concatenated codes has been designed, and a sub-optimal, soft-in-soft-out iterative technique for decoding systematic binary algebraic block codes has been developed.

... ..  
... ..  
... ..

## ACKNOWLEDGMENTS

---

I am deeply indebted to Professor Des Taylor for his invaluable guidance and support over the past 3 years. He has set very high standards, and I must admit that meeting these requirements was not an easy task. I attribute the quality and success of this PhD research to his excellent supervision and constructive suggestions.

I would like to express my gratitude to all my undergraduate educators, particularly Aaron Gulliver for introducing me to coding theory. The strong dedication of Bill Kennedy in undergraduate teaching is unmatched. I would like to take this opportunity to wish him a “Happy Retirement”. I would not have gotten this far without strong support in the early years.

My thanks to all members of the communications group for their support. Also, I would like to thank the computing staff (Pieter, Florin, Mike, Dave) for their helpful technical support over the years. Last but not least, I thank my buddies – Dez, Mien, Rob, Hua and Meng – for all the foosball nights at Rockpool and suppers at Cats Pyjamas.

1. The first part of the book is devoted to a general introduction to the theory of the firm. This includes a discussion of the basic concepts of production, cost, and profit, and a review of the classical and neoclassical theories of the firm.

2. The second part of the book is devoted to a detailed analysis of the theory of the firm. This includes a discussion of the theory of the firm in a dynamic context, and a review of the modern theories of the firm.

3. The third part of the book is devoted to a discussion of the empirical evidence on the theory of the firm. This includes a review of the empirical literature on the theory of the firm, and a discussion of the implications of the empirical evidence for the theory of the firm.

## TABLE OF CONTENTS

---

<b>CHAPTER 1 : CONCATENATED CODING STRUCTURES.....</b>	<b>1</b>
1.1 INTRODUCTION .....	1
1.1.1 <i>The Pioneering Work</i> .....	2
1.1.2 <i>The Revolutionary Invention</i> .....	2
1.2 TURBO CODES .....	3
1.2.1 <i>Encoder Structure</i> .....	3
1.2.2 <i>Decoder Structure and Decoding Algorithm</i> .....	4
1.2.3 <i>Capacity Approaching Performance</i> .....	5
1.2.4 <i>Code Block Length</i> .....	6
1.2.5 <i>Higher Code Rates via Puncturing</i> .....	6
1.3 VARIANTS OF CONCATENATED CODING STRUCTURES.....	7
1.3.1 <i>Multiple Turbo Codes</i> .....	7
1.3.2 <i>Serially Concatenated Convolutional Codes (SCCC)</i> .....	7
1.3.3 <i>Product Coding Structure</i> .....	9
1.3.4 <i>Hybrid Concatenated Structures</i> .....	10
1.4 CONCATENATED BLOCK CODES .....	10
1.4.1 <i>Parallel Concatenated Block Codes (PCBC)</i> .....	11
1.4.2 <i>Serially Concatenated Block Codes (SCBC)</i> .....	11
1.4.3 <i>Product Block Codes</i> .....	12
1.5 CONCATENATED SPC CODES.....	13
1.5.1 <i>Product SPC Codes</i> .....	14
1.5.2 <i>Parallel Concatenated SPC Codes</i> .....	15
1.6 SUMMARY .....	16
<b>CHAPTER 2 : SUBOPTIMAL SISO DECODING OF SYSTEMATIC BINARY ALGEBRAIC BLOCK CODES.....</b>	<b>17</b>
2.1 INTRODUCTION .....	17
2.2 MODELLING SYSTEMATIC ALGEBRAIC BLOCK CODES .....	18
2.3 SYSTEM MODEL .....	20
2.4 DECODER STRUCTURE AND DECODING ALGORITHM.....	21

2.5	SIMULATION RESULTS .....	21
2.6	DECODING COMPLEXITY .....	31
2.7	CONVERGENCE OF THE DECODING ALGORITHM .....	32
2.8	SUMMARY .....	33

## **CHAPTER 3 : DESIGN, ANALYSIS AND PERFORMANCE OF CONCATENATED SINGLE PARITY CHECK (SPC) CODES ..... 35**

3.1	INTRODUCTION .....	35
3.2	MULTIPLE PARALLEL CONCATENATED SPC CODES .....	36
3.2.1	<i>Encoder Structure</i> .....	36
3.2.2	<i>Decoder Structure and Decoding Algorithm</i> .....	37
3.2.3	<i>Analytical Bounds</i> .....	38
3.2.3.1	The Union Bound .....	39
3.2.3.2	Pairwise Error Event Probability .....	40
3.2.3.3	The $D_h$ Term.....	40
3.2.4	<i>Bounds Compared to Simulations Results</i> .....	40
3.3	MULTIPLE SERIALY CONCATENATED SPC CODES .....	42
3.3.1	<i>Encoder Structure</i> .....	42
3.3.2	<i>Decoder Structure and Decoding Algorithm</i> .....	43
3.3.2.1	The Suboptimum Decoder Structure.....	44
3.3.2.2	An Improved Decoder Structure .....	45
3.3.2.3	Comparing the Suboptimum and Improved Decoder Structure.....	46
3.3.2.4	Generalisations of the Improved Decoder Structure .....	47
3.4.3	<i>Analytical Bounds</i> .....	48
3.4.3.1	The Union Bound .....	48
3.4.3.2	Bit Error Multiplicity .....	50
3.4.4	<i>Bounds Compared to Simulations Results</i> .....	50
3.5	SUMMARY .....	54

## **CHAPTER 4 : CODED MODULATION ..... 57**

4.1	INTRODUCTION .....	57
4.2	CODING AND MODULATION COMBINED .....	58
4.2.1	<i>Trellis Coded Modulation and Ungerboeck's Codes</i> .....	58
4.2.2	<i>Trellis Coded Modulation for the Rayleigh/Rician Fading Channels</i> .....	59

4.2.3	<i>Multilevel Codes with Multistage Decoding (MLC/MSD)</i> .....	60
4.2.3.1	Based on Euclidean Distance .....	60
4.2.3.2	Based on Equivalent Channel Capacities.....	62
4.3	CODING AND MODULATION SEPARATED .....	62
4.3.1	<i>I-Q Trellis Coded Modulation</i> .....	62
4.3.2	<i>Zehavi's Bit Interleaving Coded Modulation (Multiple Interleavers)</i> ....	63
4.3.3	<i>Channel Symbol Expansion Diversity (CSED)</i> .....	64
4.3.4	<i>Multilevel Codes with Independent Decoding on Levels (MLC/IDL)</i> ....	65
4.3.5	<i>Caire's Bit Interleaved Coded Modulation (Single Interleaver)</i> .....	66
4.4	CODED MODULATION EMPLOYING TURBO CODES .....	67
4.5	SUMMARY .....	68
<b>CHAPTER 5 : PERFORMANCE OF CONCATENATED SINGLE PARITY</b>		
<b>CHECK CODES WITH BIT INTERLEAVED CODED MODULATION ..... 69</b>		
5.1	INTRODUCTION .....	69
5.2	SYSTEM MODEL .....	69
5.3	BICM VERSUS SICM .....	71
5.3.1	<i>Equivalent Parallel Channel Model</i> .....	71
5.3.2	<i>Performance Comparison</i> .....	72
5.4	PERFORMANCE OF MULTIPLE PARALLEL CONCATENATED SPC CODES ..	75
5.5	PERFORMANCE OF MULTIPLE SERIALY CONCATENATED SPC CODES ...	77
5.6	PERFORMANCE COMPARISON AND BENCHMARK .....	79
5.7	DECODING COMPLEXITY .....	81
5.8	CONVERGENCE OF THE DECODING ALGORITHM.....	83
5.9	SUMMARY .....	85
<b>CHAPTER 6 : A GENERALISED PERFORMANCE BOUNDING</b>		
<b>TECHNIQUE FOR BICM SYSTEMS IN THE RICIAN FADING CHANNEL 87</b>		
6.1	INTRODUCTION .....	87
6.2	BICM EXPURGATED BOUND.....	88
6.3	ASYMPTOTIC APPROXIMATION BY CAIRE ET. AL.....	90
6.4	ADDING A TWIST TO THE BICM EXPURGATED BOUND.....	92
6.5	VERIFICATIONS VIA SIMULATIONS.....	96
6.6	EXTENSION TO THE RICIAN FADING CHANNEL .....	99

6.7	SUMMARY .....	104
<b>CHAPTER 7 : CONCLUSIONS AND FUTURE WORK.....</b>		<b>107</b>
7.1	ACCOMPLISHMENTS .....	107
7.2	PRACTICAL APPLICATIONS .....	108
7.3	FUTURE WORK .....	109
<b>APPENDIX I : THE MAP ALGORITHM FOR SPC CODES.....</b>		<b>113</b>
<b>APPENDIX II : EXAMPLE OF IRWEF COMPUTATION.....</b>		<b>119</b>
<b>APPENDIX III : EXAMPLE OF IOWEF COMPUTATION .....</b>		<b>123</b>
<b>REFERENCES .....</b>		<b>129</b>

## LIST OF FIGURES

---

Figure 1 : Encoder structure of a standard rate 1/3 Turbo code. ....	3
Figure 2 : Decoder structure of a Turbo code.....	4
Figure 3 : Performance of the rate 1/2 Turbo code in [6].....	5
Figure 4 : Structure of a punctured rate 1/2 Turbo code. ....	6
Figure 5 : A 3 dimensional parallel concatenated convolutional code (multiple Turbo codes).....	7
Figure 6 : Forney's serially concatenated coding structure. ....	8
Figure 7 : General encoder structure for serially concatenated codes.....	8
Figure 8 : The bit error rate curves show the error floor effect in PCCC [26]. For SCCC, the error floor effect is not present. ....	8
Figure 9 : General encoder structure for double serially concatenated codes. ....	9
Figure 10 : The 2 dimensional product coding structure.....	9
Figure 11 : The encoder structure of the hybrid concatenated code in [28].....	10
Figure 12 : Concatenated codes with tree structures. ....	10
Figure 13 : Data and parity bits of a 2 dimensional product code.....	13
Figure 14 : The (7, 4, 3) Hamming code modelled as a form of parallel concatenated SPC code.....	20
Figure 15 : The decoder structure for the (7, 4, 3) Hamming code using MAP-SPC decoders. ....	22
Figure 16 : Performance comparison of the (7, 4, 3) Hamming code in the AWGN (left curves) and fading (right curves) channels. ....	24
Figure 17 : Performance comparison of the (15, 11, 3) Hamming code in the AWGN (left curves) and fading (right curves) channels. ....	25
Figure 18 : Performance comparison of the (31, 26, 3) Hamming code in the AWGN (left curves) and fading (right curves) channels. ....	26
Figure 19 : Performance of the (63, 57, 3) Hamming code in the AWGN (left curves) and fading (right curves) channels.....	27
Figure 20 : Performance of the (127, 120, 3) Hamming code in the AWGN (left curves) and fading (right curves) channels. ....	28

Figure 21 : Performance of the (255, 247, 3) Hamming code in the AWGN (left curves) and fading (right curves) channels. ....	29
Figure 22 : Comparing the performance of the dual code technique [30] and the MAP-SPC technique. The code used is the parallel concatenated (7, 4, 3) Hamming code. ....	30
Figure 23 : Convergence behaviour of MAP-SPC decoding of the (255, 247, 3) Hamming code in the Rayleigh fading channel. ....	33
Figure 24 : General encoder structure for Multiple Parallel Concatenated Single Parity Check Codes (M-PC-SPC). ....	36
Figure 25 : Decoder structure for the 3-PC-SPC code. ....	37
Figure 26 : SISO component MAP unit for each decoder. ....	38
Figure 27 : Bounds for 2, 3, 4, 5 and 6-PC-SPC codes with the simulation results in the AWGN channel. Solid lines indicate simulation results whereas bounds are denoted by dashed lines. ....	41
Figure 28 : Bounds for 2, 3, 4, 5 and 6-PC-SPC codes with the simulation results in the fading channel. Solid lines indicate simulation results whereas bounds are denoted by dashed lines. ....	42
Figure 29 : General encoder structure for Multiple Serially Concatenated Single Parity Check Codes (M-SC-SPC). ....	43
Figure 30 : Suboptimum iterative decoder structure for the 4 dimensional serially concatenated code extended from the work of [27]. ....	45
Figure 31 : SISO component MAP unit for the inner decoder. ....	45
Figure 32 : The proposed iterative decoder structure for the 4 dimensional serially concatenated code. ....	46
Figure 33 : SISO component MAP unit for the inner decoder. ....	46
Figure 34 : Comparison of the suboptimum and improved decoders for the 4 dimensional serially concatenated single parity check (4-SC-SPC) code in the AWGN (curves on the left) and fading (curves on the right) channels. ....	47
Figure 35 : Bounds for 2, 3 and 4-SC-SPC codes with the simulation results in the AWGN channel. ....	51
Figure 36 : Bounds for 2, 3 and 4-SC-SPC codes with the simulation results in the fading channel. ....	52
Figure 37 : Bounds (dashed lines) for 5 and 6-SC-SPC codes with the simulation results (solid lines) in the AWGN channel. ....	53

Figure 38 : Bounds (dashed lines) for 5 and 6-SC-SPC codes with the simulation results (solid lines) in the fading channel. ....	54
Figure 39 : Set partitioning for a 16-QAM signal constellation.....	59
Figure 40 : The structure of a 16-QAM Ungerboeck code with a bandwidth efficiency of 3 bits/s/Hz. ....	59
Figure 41 : Multilevel code with set partitioning (multilevel partition code). ....	61
Figure 42 : Multistage decoder (MSD) for a multilevel partition code.....	61
Figure 43 : Multilevel concatenated partition code. ....	61
Figure 44 : Multilevel codes designed with equivalent channel capacities.....	62
Figure 45 : Structure of an I-Q TCM scheme.....	63
Figure 46 : Conventional coded modulation with symbol interleaving. ....	64
Figure 47 : Zehavi's coded modulation design using 3 bit interleavers. ....	64
Figure 48 : Kofman's extension of Zehavi's work to multilevel codes.....	64
Figure 49 : The decoder structure for multilevel codes with independent decoding on levels (MLC/IDL). ....	65
Figure 50 : Caire's single interleaver bit interleaving scheme, generalised from Zehavi's multiple interleaver scheme.....	66
Figure 51 : Equivalent parallel channel model for a 16-QAM BICM scheme.....	67
Figure 52 : System model .....	70
Figure 53 : Gray mapped 16-QAM signal constellation. ....	71
Figure 54 : Splitting the gray mapped 16-QAM constellation into 2 independent gray mapped 4-ASK constellations. ....	71
Figure 55 : The equivalent parallel channel model for a Gray mapped 16-QAM signal constellation. ....	72
Figure 56 : Encoder structure 3-PC-SPC.....	73
Figure 57 : Encoder structure for 4-PC-SPC.....	73
Figure 58 : Comparing SICM with BICM in the fading channel using 3-PC-SPC.....	74
Figure 59 : Comparing SICM and BICM in the fading channel using 3-PC-SPC with “better” random interleaver. ....	75
Figure 60 : Performance of 2, 3, 4, 5 and 6-PC-SPC using 16QAM in the AWGN channel. Based on [63], the channel capacity and cutoff rate for 3 bits/sec/Hz using 16-QAM BICM over the AWGN channel is about 4.5 dB and 6.7 dB respectively. ....	76

Figure 61 : Performance of 2, 3, 4, 5 and 6-PC-SPC using 16-QAM in the independent fading channel. Based on [63], the channel capacity and cutoff rate for 3 bits/sec/Hz using 16-QAM BICM over the Rayleigh fading channel is about 7.7 dB and 10.7 dB respectively.....	77
Figure 62 : 2, 3, 4, 5 and 6-SC-SPC codes using 16-QAM in the AWGN channel....	78
Figure 63 : 2, 3, 4, 5 and 6-SC SPC codes using 16-QAM in the independent fading channel.....	79
Figure 64 : Comparison of 3-SC, 4-SC, 3-PC and 4-PC in the Rayleigh fading channel.....	81
Figure 65 : Convergence characteristics of the decoding algorithm of 4-PC in the fading channel.....	83
Figure 66 : Convergence of the 4-SC-SPC code in the fading channel using the improved decoder structure. ....	84
Figure 67 : The performance of BPSK, 16-QAM and 64-QAM in the Rayleigh fading channel using the 4-PC-SPC code. ....	97
Figure 68 : Using the translated BPSK to bound the performance of 16-QAM and 64-QAM in the Rayleigh fading channel.....	98
Figure 69 : The performance of BPSK, 16-QAM and 64-QAM with 4-PC-SPC in the Rician fading channel ( $K = 5$ dB).....	100
Figure 70 : Using the translated BPSK to bound the performance of 16-QAM and 64-QAM in the Rician fading channel ( $K = 5$ dB).....	101
Figure 71 : Using the translated BPSK to bound the performance of 16-QAM and 64-QAM in the Rician fading channel ( $K = 10$ dB).....	102
Figure 72 : Using the translated BPSK to bound the performance of 16-QAM and 64-QAM in the Rician fading channel ( $K = 15$ dB).....	103
Figure 73 : Using the translated BPSK to bound the performance of 16-QAM and 64-QAM in the AWGN channel ( $K = \text{infinity}$ ).....	104
Figure 74 : 2 dimensional parallel concatenated SPC code.....	116
Figure 75 : Encoder structure for the 2 dimensional parallel concatenated Hamming code.....	119
Figure 76 : Serially Concatenated Block Code using the (4, 3, 2) SPC code and (7, 4, 3) Hamming code.....	123
Figure 77 : Encoder structure for a 3 dimensional serially concatenated block code, also known as a double serially concatenated block code [27]. ....	126

## LIST OF TABLES

---

Table 1 : Code rate and input data block lengths of product SPC codes depicted. ....	15
Table 2 : The component SPC codes used in the construction and decoding of Hamming codes. ....	22
Table 3 : Comparison of the number of codeword searches required per iteration for the MAP-SPC and dual code techniques. ....	31
Table 4 : M-PC-SPC schemes being investigated. ....	76
Table 5 : M-SC-SPC schemes considered. ....	78
Table 6 : Performance comparison of the best schemes in literature at BER = $10^{-4}$ ...	80
Table 7 : Values for $d_h^2$ and the gap in $E_b/N_0$ , reproduced from [63]. ....	95



## PREFACE

---

In recent years, the wireless communications industry has experienced a phenomenal growth rate. Many multinational wireless service providers are now betting heavily on 3<sup>rd</sup> generation cellular systems such as IMT-2000 [1][2]. Throughout the world, billions of dollars have been invested to secure the spectrum allocated for these systems. For example, the recent UK spectrum auction was worth almost US\$34 billion, whereas the German auction attracted about US\$46 billion. Clearly, what was once a small industry is now a big business in the global economy.

The industry is very upbeat about the future of wireless systems. Advanced wireless infrastructures are expected to offer data capabilities much faster than what we have today. Around the world, current GSM (Global System Mobile) systems are expected to evolve towards EDGE (Enhanced Data Rate for GSM Evolution) systems [3]. To accommodate the 384 kbps data rate, the GMSK modulation in GSM will be replaced by the larger offset-8-PSK modulation in EDGE. With all these services pushing for higher data rates, there is a need for spectrally efficient modulation schemes due to limited spectrum.

There is also the issue of power efficiency. To meet low power emission requirements (co-channel interference, EM emissions, etc), modern systems employ sophisticated digital baseband signal processing techniques. Because the signal processing techniques are very computationally intensive, powerful chips and digital signal processors are required. These hardware consume sizeable chunks of the battery's capacity. The comparatively lagging development of battery technologies amplifies the need for low complexity wireless systems.

This thesis is aimed at addressing part the problems and requirements for future wireless systems. Specifically, efforts are focused on the design of low complexity channel coding techniques with good error performance. These techniques are then applied to large signal constellations to counter the problems of power and spectral efficiency.

The first chapter provides an introduction to concatenated coding structures. Key developments in concatenated codes since the invention of Turbo codes are presented. Chapter 2 describes a novel technique for suboptimal soft-in-soft-out (SISO) decoding of systematic binary algebraic block codes. Simulations using Hamming codes compare the performance of this decoding strategy to those of soft decision brute force and hard algebraic/syndrome decoding. Chapter 3 presents the analysis and performance of concatenated single parity check (SPC) codes. Multiple SPC codes are applied in both parallel and serial concatenated structures to achieve excellent error performances. An improved decoder structure for serially concatenated codes is also presented. Chapter 4 touches on recent developments in coded modulation techniques. Chapter 5 combines the channel coding techniques developed in Chapter 3 with bit interleaved coded modulation (BICM). Simulation results compare the various schemes in Chapter 3. Also, the error performance is benchmarked against the best schemes in literature under identical channel conditions and code parameters. A decoding complexity estimate is provided. The convergence of the decoding algorithm is also discussed briefly. In Chapter 6, a generalised performance bounding method for BICM systems in the Rician fading channel is derived. Using this simple method, we show that it is possible to accurately estimate the bit error performance of large signal constellation BICM systems using the bit error performance of BPSK systems employing the same channel coding scheme. Simulation results are presented to verify this bounding technique. Conclusions and suggestions for future work are discussed in Chapter 7.

The contributions considered original for this PhD research are Chapters 2, 3, 5 and 6. The work reported in this thesis was performed during the period of March 1998 to December 2000. As a result of this research, the following papers have been published, submitted or are in preparation.

J. S. K. Tee & D. P. Taylor, "Multiple Serially Concatenated Single Parity Check Codes", proceedings of IEEE International Communications Conference (ICC), June 2000, New Orleans, USA, paper number MNC5\_5.

J. S. K. Tee & D. P. Taylor, "Iterative Decoding of Systematic Binary Algebraic Block Codes", proceedings of IEEE GlobeCom Conference, November 2000, San Francisco, USA, paper number CT4-7.

J. S. K. Tee & D. P. Taylor, "Multiple Parallel Concatenated Single Parity Check Codes", accepted for the IEEE International Communications Conference (ICC), June 2001, Helsinki, Finland.

J. S. K. Tee & D. P. Taylor, "Suboptimal SISO Decoding of Systematic Binary Algebraic Block Codes", submitted in September 2000 to IEEE International Symposium on Information Theory (ISIT), June 2001, Washington, USA.

J. S. K. Tee & D. P. Taylor, "An Improved Iterative Decoder Structure for Multiple Serially Concatenated Codes", submitted in October 2000 to IEEE Communications Letters.

J. S. K. Tee & D. P. Taylor, "Multiple Parallel Concatenated Single Parity Check Codes", submitted in December 2000 to IEEE Transactions on Communications.

J. S. K. Tee & D. P. Taylor, "Multiple Serially Concatenated Single Parity Check Codes", submitted in December 2000 to IEEE Transactions on Communications.

J. S. K. Tee & D. P. Taylor, "Suboptimal SISO Decoding of Systematic Binary Algebraic Block Codes", submitted in December 2000 to IEEE Transactions on Communications.

J. S. K. Tee & D. P. Taylor, "A Generalised Performance Bounding Technique for Bit Interleaved Coded Modulation Systems in the Rician Fading Channel", submitted in January 2001 to IEEE Transactions on Communications.

J. S. K. Tee & D. P. Taylor, "A Generalised Performance Bounding Technique for Bit Interleaved Coded Modulation Systems in the Rayleigh Fading Channel", submitted in January 2001 to IEEE GlobeCom 2001, San Antonio, USA.



# CHAPTER 1 : CONCATENATED CODING STRUCTURES

## 1.1 Introduction

Over the past 50 years, there has been much development in the field of coding theory. Looking back today, it is tempting to summarize the developments in this comparatively young field as a “Tale of 2 Papers”; one by Shannon [4], the other by Berrou et. al [5]. These 2 revolutionary papers stand out in the 20<sup>th</sup> century as the classic works; the former started a field from nothing, the latter contributed towards major advancements to the field of error coding.

Over the past 7 years, there has been a tremendous explosion of works on Turbo codes. This chapter presents an overview of concatenated coding structures. Because the scope of turbo codes is too wide, only works relevant to this thesis are included. In particular, concatenated coding structures are emphasised, instead of the exact details of the error correction codes and their related decoding algorithms. The interested reader can pursue further details in the listed references. As the chapter progresses, the emphasis is gradually narrowed down to concatenated block codes, and finally, to concatenated single parity check (SPC) codes.

### 1.1.1 The Pioneering Work

The first paper, written by Claude E. Shannon in 1948, is entitled “A Mathematical Theory of Communications” [4]. It is this paper that started the field of Information Theory and Error Correction Coding. In this seminal paper, Shannon defined the concept of channel capacity. Using this concept, he proved that, as long as the rate at which information is transmitted is less than the channel capacity, there exist error correction codes that can achieve an arbitrarily low probability of error. This proof is known as the Channel Coding Theorem. Although the theorem asserts the existence of these codes, it does not provide any clue as to how such codes can be constructed. Based on this remarkable theorem, researchers started the crusade to find ways to construct this capacity achieving code.

### 1.1.2 The Revolutionary Invention

Many decades went by, and despite extreme efforts, no one has succeeded in getting anywhere close to the capacity. Just as researchers around the world were about to lose hope and label coding theory as a dead field, a few French researchers surprised the world. In 1993, Berrou, Glavieux and Thitimajshima presented a revolutionary paper entitled “Near Shannon Limit Error Correcting Coding and Decoding : Turbo Codes” [5]. Forty-five years after Shannon’s work, they came up with an iterative decoding scheme combined with an interleaver separated by multiple encoders that approached channel capacity closer than ever before. Suddenly, there is working proof that Shannon’s theorem is not “mission impossible”.

During Turbo code’s debut in ICC’ 1993, the results were greeted with very much doubts and skepticisms. It was only when researchers have successfully reproduced the capacity approaching results that others started to embrace this brilliant idea. Due to the explosion of interests in Turbo codes in the past 7 years, the reference list is very long, and here, I will not attempt to list all of them, but only refer to the key development papers and those that are related to my work.

## 1.2 Turbo Codes

Traditionally, the design of error correction codes was tackled by constructing codes with significant algebraic structures. The problem with this traditional method is that the code length must be increased significantly in order to approach channel capacity. Because the maximum likelihood decoding complexity increases exponentially with code length, a point is reached where the complexity of the decoder is so high that implementation becomes impossible. Turbo code design is based on a random coding approach [7]. It employs a soft-in-soft-out decoding algorithm.

### 1.2.1 Encoder Structure

Figure 1 shows the encoder structure of a standard rate  $1/3$  Turbo code. The input data block is first encoded by a recursive systematic convolutional (RSC) rate  $1/2$  encoder. This generates a set of parity bits. Next, the data block is interleaved and then fed to another rate  $1/2$  RSC encoder to generate a second set of parity bits. The function of the interleaver is to scramble the data block to produce a different sequence of the original data block without changing the weight of the data block. Because both parity sets are generated using the same data block, the data block needs only be transmitted once, thereby significantly reducing the loss of code rate. The interleaver can be of any type. In [5], a random interleaver was used. A wide range of interleavers have since been proposed [8].

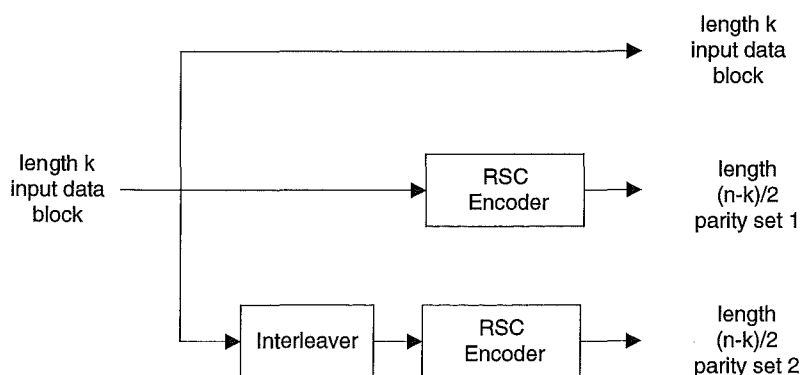


Figure 1 : Encoder structure of a standard rate  $1/3$  Turbo code.

## 1.2.2 Decoder Structure and Decoding Algorithm

The operations of a Turbo decoder are similar to the feedback configuration of a Turbo charged engine, hence, the name Turbo. Figure 2 shows the decoder structure of a Turbo code. The log-likelihood ratio<sup>1</sup> (LLR) is computed for all received bits as

$$LLR = \frac{1}{2\sigma^2} [(r - ax_0)^2 - (r - ax_1)^2]$$

where  $r$  is the received sample,  $x_1$  is the hypothesis that the transmitted data is binary 1,  $x_0$  is the hypothesis that the transmitted data is binary 0 and  $a$  represents the fade envelope.

The data LLRs are fed to both MAP decoders, whereas only the appropriate parity LLRs are fed to the constituent decoders. Decoding is performed iteratively by exchanging soft information between constituent MAP (maximum a posteriori probability) decoders. All soft informations are properly interleaved and deinterleaved before being used. In [5], the MAP decoder was implemented using the modified BCJR algorithm<sup>2</sup> [9], named after the contributors – Bahl, Cocke, Jelinek and Raviv. A variety of Turbo decoding strategies are outlined in [10], [11], [12], [13], [14].

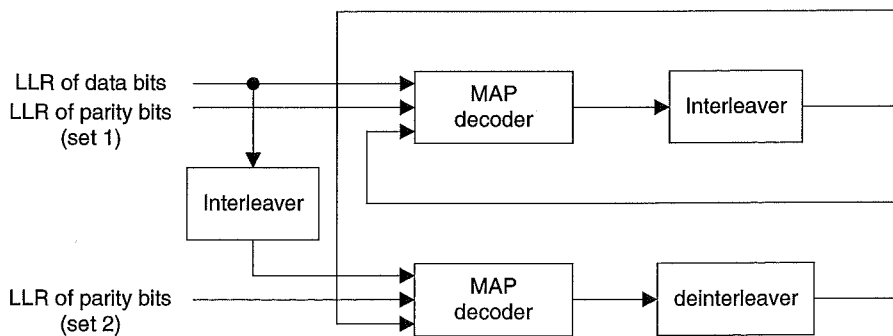


Figure 2 : Decoder structure of a Turbo code.

<sup>1</sup> Computation of the LLR is shown in Appendix I.

<sup>2</sup> The work on this thesis is focused on the decoder structure rather than the decoding algorithm. Therefore, the details will be spared here. The interested reader is directed to [9] for details.

### 1.2.3 Capacity Approaching Performance

As mentioned previously, Turbo codes are capable of approaching very closely to channel capacity. In [6], using a rate  $\frac{1}{2}$  Turbo code<sup>3</sup> with a 65,536 bit long interleaver, a bit error rate of  $10^{-5}$  is achieved at an  $E_b/N_o$  of 0.7 dB after 18 iterations of decoding. This performance is shown in Figure 3. It is very close to the theoretical limit predicted by Shannon.

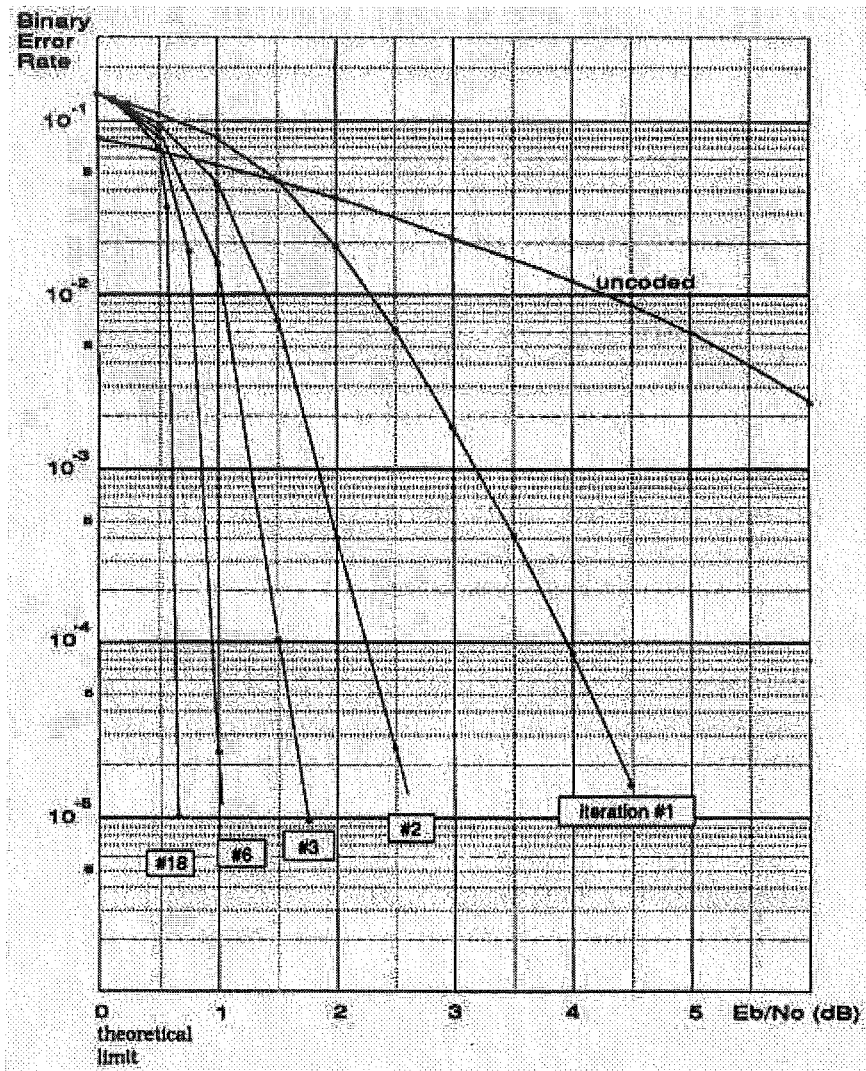


Figure 3 : Performance of the rate 1/2 Turbo code in [6].

<sup>3</sup> The rate  $\frac{1}{2}$  Turbo code was designed using two 16-state rate  $\frac{2}{3}$  RSC encoders.

### 1.2.4 Code Block Length

The performance of a Turbo coding scheme is a function of the input data block length. As the block length is decreased, the performance degrades. The performance of Turbo Codes with short frame sizes were presented in [15], [16]. In [15], it was shown that convolutional codes have better performance than 16-state Turbo codes with similar decoding complexity when the block size is under 192 bits. The performance was compared at approximately  $10^{-3}$ , which is the typical error rate required for voice communications. In [16], structured interleavers were combined with multilevel codes to improve performance for short block lengths. A comprehensive investigation of the theoretical limits of code performance as a function of block size is found in [17]. It was shown in [17] that Turbo codes can approach almost uniformly within 0.7 dB of the theoretical performance limit over a wide range of code rates and block sizes.

### 1.2.5 Higher Code Rates via Puncturing

To achieve higher code rates without significantly increasing the decoding complexity, puncturing is applied to the standard rate 1/3 turbo code. This is shown in Figure 4. In [18], spectrally efficient punctured schemes for rate 2/3 and 3/4 was proposed. In [19], puncturing designs are presented for rates  $k/(k+1)$  where  $2 \leq k \leq 16$ .

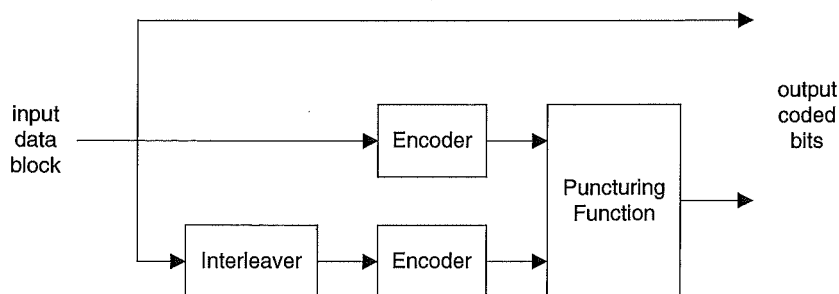


Figure 4 : Structure of a punctured rate 1/2 Turbo code.

### 1.3 Variants of Concatenated Coding Structures

Since the birth of Turbo codes, various concatenated coding structures have been introduced. They all have a Turbo-like encoder structure. This section provides an overview of common structures.

#### 1.3.1 Multiple Turbo Codes

The original Turbo code is classified as a 2 dimensional parallel concatenated convolutional code (PCCC). In [20], [21], [22] and [23], multiple Turbo codes were proposed. These codes can be modelled as 3 dimensional parallel concatenated convolutional codes, as shown in Figure 5. Multiple Turbo codes offer very good performances.

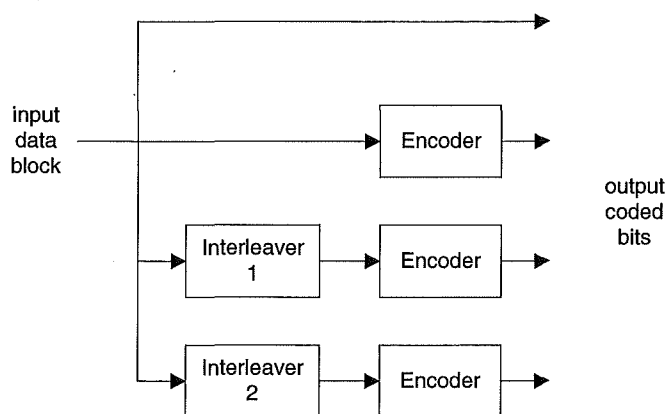


Figure 5 : A 3 dimensional parallel concatenated convolutional code (multiple Turbo codes).

#### 1.3.2 Serially Concatenated Convolutional Codes (SCCC)

The serially concatenated coding structure was originally proposed by Forney [24]. His design consists of a non-binary outer code and a binary inner code as shown in Figure 6. Usually, a Reed-Solomon code was chosen as the outer code and a binary convolutional code is used as the inner code. In [25], an interleaver is inserted between the inner and outer encoders. The resultant serially concatenated code structure is shown in Figure 7. Binary convolutional codes are used in both the inner and outer encoders to form Serially Concatenated Convolutional Codes (SCCC).

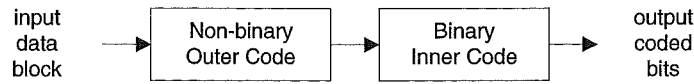


Figure 6 : Forney's serially concatenated coding structure.



Figure 7 : General encoder structure for serially concatenated codes.

One disadvantage of the original Turbo codes is the error floor problem. At low to medium SNR, the bit error rate curve falls steeply, resulting in a waterfall shaped curve. However, at high SNR, the bit error rate does not decrease as rapidly with increasing SNR and the curve flattens (hitting an error floor). Figure 8 shows the performance of a rate 1/3 PCCC using 4 state RSC encoders in the AWGN channel [26]. The input block length is 16,384 bits. The bit error rates after 6 and 9 decoding iterations are shown.

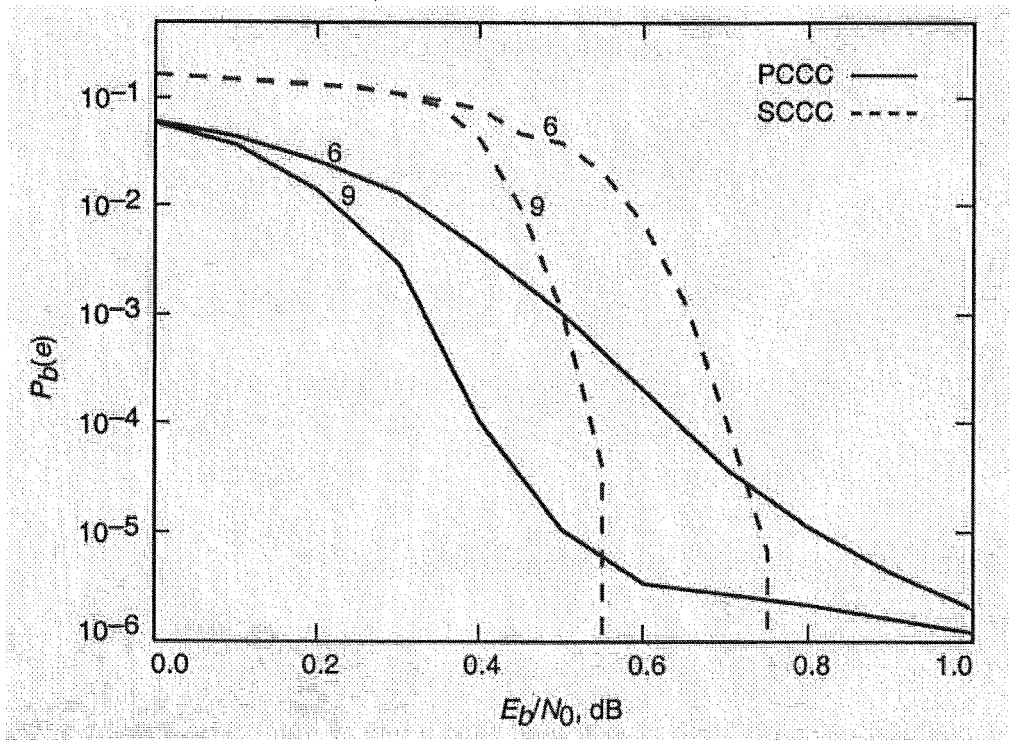


Figure 8 : The bit error rate curves show the error floor effect in PCCC [26]. For SCCC, the error floor effect is not present.

From the curves, it is observed that after 9 iterations, an error floor starts to occur at around  $10^{-5}$ . At that point, the slope of the bit error rate curve starts to flatten out,

leading to an error floor effect. Due to the error floor, the SNR must be increased significantly if very low error rates are required. The error floor is associated with the minimum distance of the code, and it has been shown that, in general, SCCC has a larger minimum distance compared to PCCC.

In Figure 8, the performance of the SCCC with the same block length is compared to that of the PCCC. To result in a rate  $1/3$  code, a rate  $1/2$  outer encoder is combined with a rate  $2/3$  inner encoder. The curves show that the SCCC does not suffer from an error floor problem in the range of bit error rates simulated. PCCC is superior at bit error rates above  $10^{-5}$  whereas SCCC is the better scheme below  $10^{-5}$ . In [27], serially concatenated codes were extended to double serially concatenated codes, shown in Figure 9.

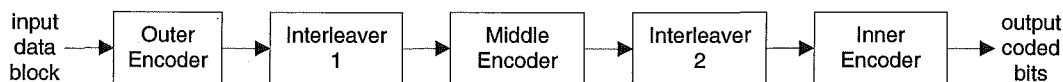


Figure 9 : General encoder structure for double serially concatenated codes.

### 1.3.3 Product Coding Structure

Another commonly used structure is the product coding structure [34]. The 2 dimensional product code is shown in Figure 10. This structure is almost exclusively used in conjunction with block codes. The unique feature of this structure lies in the fact that, in addition to the interleaved data bits, the second encoder operates on the parity bits generated by encoder 1. This results in the so-called parity on parity bits. The most widely used interleaver in product codes is the rectangular block interleaver. More will be detailed in section 1.4.3.

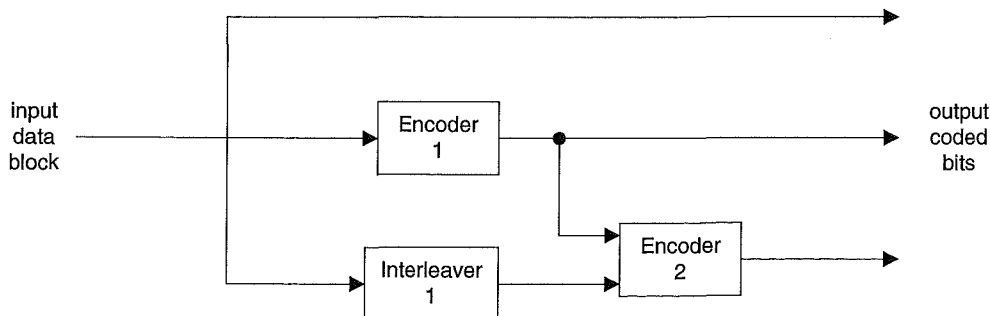


Figure 10 : The 2 dimensional product coding structure.

### 1.3.4 Hybrid Concatenated Structures

Apart from the parallel, serial and product coding structures, various hybrid structures were proposed. In [28], a hybrid concatenated code was constructed as in Figure 11. This structure consists of a combination of parallel and serial concatenations. Compared to parallel concatenated convolutional codes and serially concatenated convolutional codes, the hybrid schemes offer better performance at very low bit error rates when low complexity codes are used. In [29], a tree structure, shown in Figure 12, is proposed.

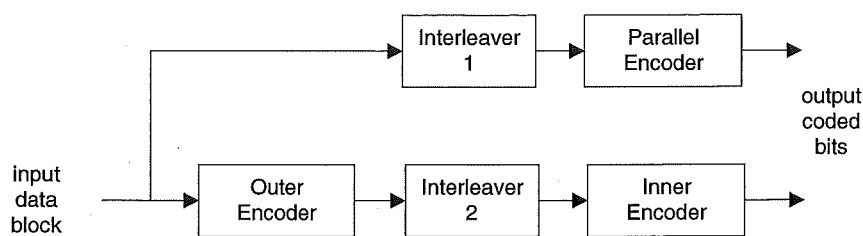


Figure 11 : The encoder structure of the hybrid concatenated code in [28].

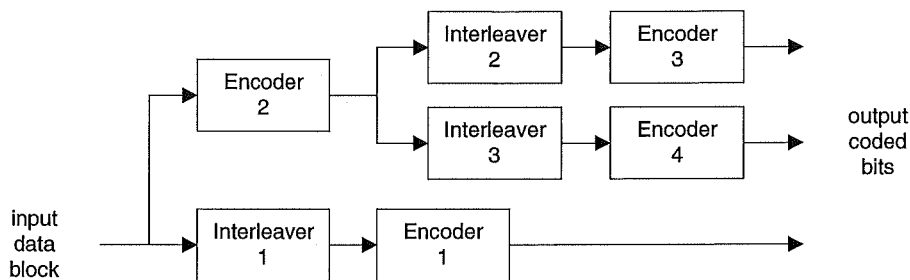


Figure 12 : Concatenated codes with tree structures.

## 1.4 Concatenated Block Codes

Since the discovery of turbo codes, there has been very much interest in concatenated convolutional codes, resulting in many publications. Comparatively, there is only a limited amount of effort focused on iteratively decoded concatenated block codes. One of the most comprehensive studies on iterative decoding of block codes in the literature is the work of [30]. In [30], the iterative decoding algorithm is generalised to

block codes using trellises of the original code and its dual code. This provided a basis for extensions to other linear block codes used in concatenated fashion. Related works on BCH, Reed-Muller, Quadratic Residue, Difference-Set Cyclic, Double Circulant and Euclidean Geometry codes are found in [31]

In this section, the 3 basic and most commonly used concatenated coding structures for block codes are briefly described. Main works in literature are cited. Work on SPC codes are emphasised in Section 1.5.

#### **1.4.1 Parallel Concatenated Block Codes (PCBC)**

Parallel Concatenated Block Codes (PCBC) have the same encoder structure as Turbo codes. The only difference is that the constituent encoders are made up of block codes instead of convolutional codes. Significant efforts on PCBC were primarily contributed by [32]. The authors presented analytical bounds for parallel concatenated linear block codes. Examples for the (7, 4, 3) Hamming code were presented. Some work based on the (63, 57, 3) and (63, 51, 5) BCH codes was also performed. In [33], 2 dimensional (1023, 1013) Hamming codes were shown to approach as close as 0.27 dB of AWGN channel capacity. The block length is in the range of 1 million bits and the decoder was implemented using a fast neurocomputer.

#### **1.4.2 Serially Concatenated Block Codes (SCBC)**

The work of [25] provides analytical performance bounds for serially concatenated block codes. The paper also provided some asymptotic design rules for SCBC. Examples using the (4, 3) single parity check (SPC) code, the (7, 4) Hamming code, the (15, 5) and the (15, 7) BCH codes were given. The interleaver gain effect was also demonstrated. Bounds for double serially concatenated block codes were presented in [27]. An example using the (3, 2) SPC, (4, 3) SPC and (7, 4) Hamming code was given.

### 1.4.3 Product Block Codes

Compared to the 2 structures previously mentioned, product block codes have attracted considerably more research interests. Elias first described product codes in 1954 [34]. By the early 1980s, at least one paper [35] and textbook [36] had described the advantages of the iterative decoding of product codes. In the same conference as the unveiling of the Turbo codes, Lodge et. al. presented a decoding technique for product and concatenated codes based on separable MAP filters [37]. Results presented for a 3 dimensional product code constructed using the (16, 11, 4) extended Hamming codes show promising potential. In [38], this work was shown to be related to cross entropy minimisation techniques.

Very soon after the introduction of Turbo codes, Pyndiah started to work on product block codes [39]. The data and parity bits of a 2 dimensional product code using a rectangular block interleaver are shown in Figure 13. Note that if the parity on parity bit is omitted, the resultant code is similar to a parallel concatenated code employing a rectangular block interleaver. In [39], product codes were constructed using 2 BCH codes and a rectangular block interleaver. Results were presented for a range of BCH codes. This technique is of significant interests because the minimum Hamming distance of the product code is equal to the product of the minimum Hamming distances of the component codes. Using component codes of minimum Hamming distance 4 and 6, product codes of minimum distance 16 and 36 are constructed respectively. The codes produce excellent performance over QPSK and 64-QAM in the AWGN and Rayleigh fading channel. An iterative decoder was implemented using a modified Chase algorithm with fixed scaling factors to decode the component codes. A version of the decoding algorithm with adaptive scaling factors was presented in [40].

Product codes were also investigated in [31]. 2 and 3 dimensional product codes based on extended Hamming codes and rectangular block interleavers have been successfully commercialised [41].

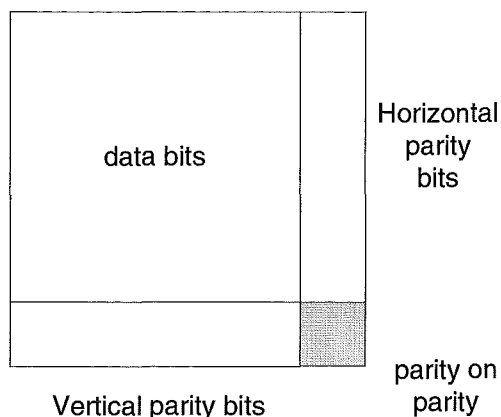


Figure 13 : Data and parity bits of a 2 dimensional product code.

### 1.5 Concatenated SPC codes

Turbo codes provide the means to get very good bit error performance. The decoding complexity is low compared to that previously predicted. However, it is still relatively complex for practical implementation. In order to design high performance codes with low decoding complexity, many conventional efforts are initiated using a high performance code. Usually, a high performance coding scheme is selected, and efforts are focused on lowering its decoding complexity to a practical level at the cost of losing some performance. The work in this thesis tackles this problem from the opposite end, starting from a low complexity code. A low complexity coding technique is chosen, and efforts are focused on improving the performance of the scheme. From the practical implementation perspective, this is a logical approach.

In the efforts to find low complexity yet high performance codes, the following question were asked : “What is the simplest possible channel coding scheme that can be iteratively decoded ?” and “How badly does it perform ?”. The answers are found in Single Parity Check (SPC) codes. This code was originally used for error detection, but has been cleverly adapted for error correction purposes using concatenated coding structures. The simplicity of this code is its deceiving feature. Concatenated SPC codes have surprisingly good error performance. In this section, published works on

concatenated SPC codes are reviewed. Various practical application problems are also outlined

### 1.5.1 Product SPC Codes

The original work on iterative decoding of product SPC codes was performed by Lodge et. al. In [42], a 4 dimensional product code using (10, 9, 2) SPC codes as component codes was designed. The asymptotic gain, defined as the relative energy efficiency of a coding and uncoded technique at low error probability (dependent on the minimum distance of the code), was estimated to be 10.2 dB. The resultant code rate is  $(0.9)^4 = 0.6561$ , which is approximately  $2/3$ . The performance of this code is superior to that of a rate  $2/3$  256 state convolutional code at error rates below  $10^{-3}$ . In [37], the potential application to a 4 dimensional product code using (25, 24, 2) component SPC codes was suggested, though no simulation results were presented. At a code rate of about 0.85, this code promises an asymptotic coding gain of 11.3 dB.

In [122], the weight spectrum for iterated product SPC codes was examined. It was shown that the weight of the code converges to the binomial distribution associated with good random codes. The work of Battail provided a significant conceptual, theoretical and analytical perspective on random-like codes [123]. In [43], product SPC codes of higher dimensions were investigated. 2, 3, 4 and 5 dimensional product SPC codes were constructed using the (8, 7, 2) SPC code. These codes were shown to offer very good performances in the AWGN channel. In [44], it was shown that, in the AWGN channel, randomly interleaved product SPC perform better than the traditional product codes employing rectangular block interleavers.

All these works on product SPC codes offer very promising performance at low complexities. Due to the small minimum Hamming distance, SPC codes are very weak. As a result, good performance is only achieved at 3 dimensions and beyond. This poses 2 practical problems. Firstly, there is the issue of code rate. As the number of dimensions is increased, the code rate falls quickly. The rates for the codes mentioned above is shown in Table 1. Secondly, block length becomes a big practical issue. As the number of dimensions is increased, the input block length increases exponentially. The input data block length of the codes are shown in Table 1.

### 1.5.2 Parallel Concatenated SPC Codes

Recognizing the problem of increasing block length, Li Ping et. al.[45] proposed multi-dimensional parallel concatenated SPC codes. In [45], simulation results for 4 and 5 dimensional parallel concatenated SPC codes using (21, 20, 2) SPC codes were presented. The resultant codes have rates of 5/6 and 4/5 respectively. The input data block length of 10, 000 bits was used. The setback in these codes is the presence of error floors. In both the 4 and 5 dimensional codes, error floors start to show up around  $10^{-5}$ .

	code rate	input data block size
4-D product (10, 9, 2) SPC code [42]	$\left(\frac{9}{10}\right)^4 = 0.656$	$9^4 = 6,561$
4-D product (25, 24, 2) SPC code [37]	$\left(\frac{24}{25}\right)^4 = 0.849$	$24^4 = 331,776$
2-D product (8, 7, 2) SPC code [43]	$\left(\frac{7}{8}\right)^2 = 0.766$	$7^2 = 49$
3-D product (8, 7, 2) SPC code [43]	$\left(\frac{7}{8}\right)^3 = 0.670$	$7^3 = 343$
4-D product (8, 7, 2) SPC code [43]	$\left(\frac{7}{8}\right)^4 = 0.586$	$7^4 = 2,401$
5-D product (8, 7, 2) SPC code [43]	$\left(\frac{7}{8}\right)^5 = 0.513$	$7^6 = 16,807$

Table 1 : Code rate and input data block lengths of product SPC codes depicted.

## 1.6 Summary

An overview of concatenated codes has been provided in this chapter. Key features of Turbo codes were discussed. Developments in concatenated block codes are outlined. The search for low complexity coding schemes ends at concatenated SPC codes. The block length and code rate problems for product SPC codes were identified. These were overcome by multi-dimensional parallel concatenated SPC codes. However, error floors are present. The work in subsequent chapters is aimed at tackling the 4 main issues identified here – low decoding complexity, error floor, code rate and input data block length.

# CHAPTER 2 : SUBOPTIMAL SISO DECODING OF SYSTEMATIC BINARY ALGEBRAIC BLOCK CODES

## 2.1 Introduction

The problem of soft decision decoding of binary block codes has been around for decades. It is well known that although maximum likelihood performance can be derived from soft decision brute force decoding (ML exhaustive search over codewords), this strategy becomes a computationally impossible task as the code length increases. In [46], Wolf proposed a maximum likelihood trellis-based technique for soft decision decoding of block codes. Even though trellis-based soft decision techniques are less complex than brute force decoding, the decoding complexity increases exponentially as the block length increases. In [30], dual code soft-in-soft-out (SISO) techniques were proposed for binary block codes. This technique is also faced with the problem of computational complexity. Moreover, due to time varying trellises in both [46] and [30], implementation of the decoders can be a tricky task. Extensive work on trellis-based algorithms for linear block codes is found in [47].

With long block lengths, practical solutions for soft decision decoding mean resorting to suboptimal approaches. In [48], Chase proposed 3 suboptimal soft decoding

algorithms for block codes. One of these techniques – Chase algorithm 2 – has recently received renewed interest due to its use in several iterative soft-decision decoding algorithms for binary linear block codes [49]. Extensive analysis of Generalised Minimum Distance (GMD) and Chase decoding algorithms are presented in [50]. Much tighter bounds on these algorithms are shown in [127]. In [51], a computationally efficient technique based on ordered statistics was proposed. The performance of this technique is proportional to the number of test patterns, which in turn, is reflected in the decoding complexity.

In chapter 1, we noted works in the literature that have successfully applied the maximum a posteriori probability single parity check (MAP-SPC) decoders to the decoding of long interleaved block codes. In this chapter, the MAP-SPC decoding technique is applied to SISO decoding of systematic binary algebraic block codes. Although suboptimal, this decoding technique performs well in the AWGN and fading channels compared to ML soft decision brute force decoding. Results for a range of Hamming codes are presented. Due to the iterative nature of this decoding technique, it allows for a flexible decoding complexity versus performance trade-off. Because of the SISO property, the MAP-SPC technique is applicable to the soft iterative decoding of concatenated block codes. Applying it to the parallel concatenated (7, 4, 3) Hamming code, the bit error performance is comparable to that of the dual code SISO method proposed in [30]. The complexity advantage of the MAP-SPC technique is outlined through a decoding complexity comparison. Its convergence behaviour is also presented.

## 2.2 Modelling Systematic Algebraic Block Codes

In order to decode systematic binary block codes using MAP-SPC decoders, we show that all systematic binary block codes can be constructed using SPC codes. This is best illustrated by a simple example. The (7, 4, 3) Hamming code is chosen for this example. The generator matrix,  $G$ , of a systematic (7, 4, 3) Hamming code is given by

$$G = \begin{bmatrix} 1 & 1 & 0 & 1 & 0 & 0 & 0 \\ 0 & 1 & 1 & 0 & 1 & 0 & 0 \\ 1 & 1 & 1 & 0 & 0 & 1 & 0 \\ 1 & 0 & 1 & 0 & 0 & 0 & 1 \end{bmatrix}$$

Applying basic algebraic coding theory, a codeword,  $c$ , is formed by performing a matrix multiplication between the message vector,  $m$ , and the generator matrix,  $G$ . The resultant codeword consists of 2 parts – 4 systematic data bits ( $d_1$ ,  $d_2$ ,  $d_3$ , and  $d_4$ ) and 3 parity bits ( $p_1$ ,  $p_2$  and  $p_3$ ) in the form

$$\begin{aligned} c &= mG \\ &= [d_1 \ d_2 \ d_3 \ d_4] \begin{bmatrix} 1 & 1 & 0 & 1 & 0 & 0 & 0 \\ 0 & 1 & 1 & 0 & 1 & 0 & 0 \\ 1 & 1 & 1 & 0 & 0 & 1 & 0 \\ 1 & 0 & 1 & 0 & 0 & 0 & 1 \end{bmatrix} \\ &= [p_1 \ p_2 \ p_3 \ d_1 \ d_2 \ d_3 \ d_4] \end{aligned}$$

The 3 parity bits are obtained as

$$p_1 = (d_1 + d_3 + d_4) \bmod 2$$

$$p_2 = (d_1 + d_2 + d_3) \bmod 2$$

$$p_3 = (d_2 + d_3 + d_4) \bmod 2$$

These parity bits are actually generated by (4,3,2) single parity check (SPC) encoders. The parity bit  $p_1$  is the SPC generated by  $d_1$ ,  $d_3$  and  $d_4$ .  $p_2$  and  $p_3$  are generated in the same way. The only difference is the data bits used in the SPC encoding process. Using SPC codes as component encoders, the (7, 4, 3) Hamming code can be modelled as a form of parallel concatenated SPC code as shown in Figure 14. Because this model is similar to that of parallel concatenated SPC codes, it can be decoded in the same iterative fashion.

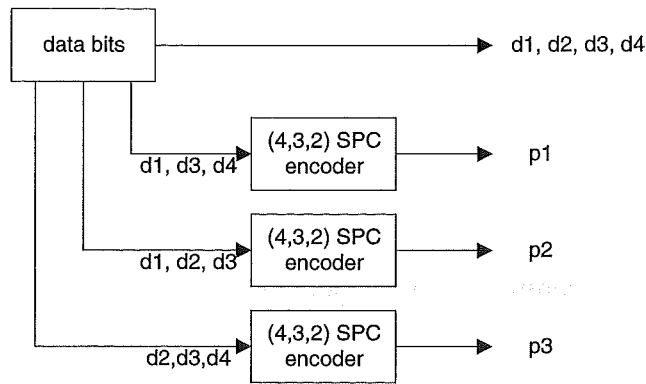


Figure 14 : The (7, 4, 3) Hamming code modelled as a form of parallel concatenated SPC code.

### 2.3 System Model

Two channels are investigated in this work – BPSK modulation over the AWGN and the independent Rayleigh fading channels. For the fading channel, interleaving is assumed to be ideal (infinite interleaving). Perfect channel state information (CSI) is assumed to be available at the receiver. Fading is slow such that perfect coherent detection is achieved. Because phase information is assumed to be recovered perfectly at the receiver, the fade samples can equivalently be represented only by their Rayleigh distributed envelope. The fade envelopes are normalised to unit average energy. Signal-to-noise ratio (SNR) is varied by scaling the complex Gaussian noise. The received baud rate complex baseband samples are represented by

$$r_i = a_i x_i + n_i$$

where  $a_i$  is the fade envelope,  $x_i$  is the transmitted (complex) symbol,  $r_i$  is the received sample (complex),  $n_i$  represents the complex Gaussian noise and  $i$  is the integer time index corresponding to  $t = iT$ , where  $T$  is the symbol duration. The maximum likelihood demodulation criteria is applied by minimizing the metric

$$metric = |r_i - a_i \hat{x}_i|^2$$

where  $\hat{x}_i$  is the hypothesised transmitted symbol. For the AWGN channel, the fade envelope is set equal to unity.

## 2.4 Decoder Structure and Decoding Algorithm

In this work, the MAP decoder for SPC codes is implemented using the repetition code method<sup>4</sup> as described in [30]. Details of this algorithm are provided in Appendix I. The decoder structure for the (7, 4, 3) Hamming code is shown in Figure 15. During each iteration, the MAP decoders only exchange extrinsic information pertaining to bits common to each decoder (not explicitly shown in Figure 15). For example, extrinsic information on d3 generated by decoder D1 is shared with decoder D2 and decoder D3. However, extrinsic information on d4 generated by decoder D1 is only shared with decoder D3 because decoder D2 does not include d4 in its SPC code. At the end of the iterative decoding process, the extrinsic informations are combined (added) appropriately to produce hard decisions.

## 2.5 Simulation Results

Simulation results for  $(2^M - 1, 2^M - 1 - M, 3)$  Hamming codes with  $M = 3, 4, 5, 6, 7, 8$  are presented in this section. The component SPC codes used in the construction and therefore, decoding, of the Hamming codes are shown in Table 2.

---

<sup>4</sup> The MAP-SPC technique uses its dual code for MAP decoding. The dual code for a  $(N, N-1, 2)$  SPC code is a  $(N, 1, N)$  repetition code. This is the simplest way to perform MAP decoding for SPC codes [30].

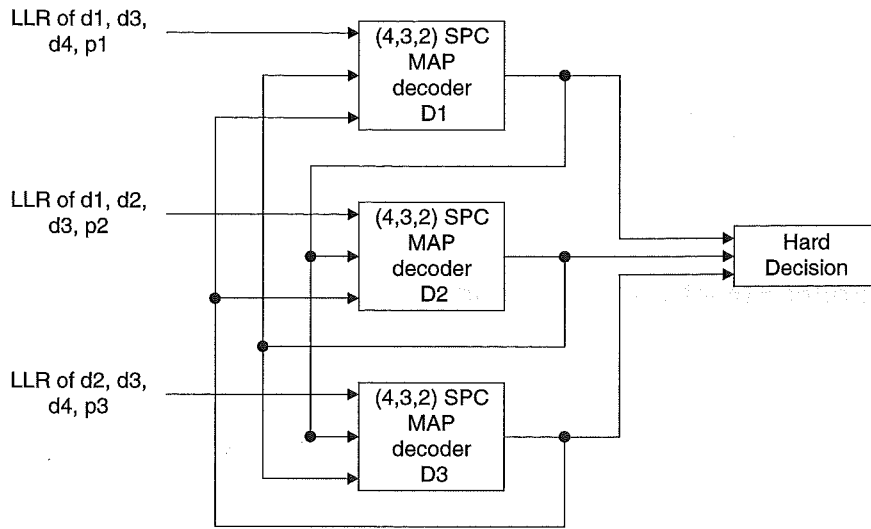


Figure 15 : The decoder structure for the  $(7, 4, 3)$  Hamming code using MAP-SPC decoders.

Hamming Codes	Component SPC codes
$(7, 4, 3)$	$(4, 3, 2)$
$(15, 11, 3)$	$(8, 7, 2)$
$(31, 26, 3)$	$(16, 15, 2)$
$(63, 57, 3)$	$(32, 31, 2)$
$(127, 120, 3)$	$(64, 63, 2)$
$(255, 247, 3)$	$(128, 127, 2)$

Table 2 : The component SPC codes used in the construction and decoding of Hamming codes.

Figure 16 shows the performance comparison of the  $(7, 4, 3)$  Hamming code in the AWGN and fading channels. Comparing the performance at  $10^{-4}$ , the MAP-SPC is about 0.3 dB worse than soft decision brute force decoding in the AWGN channel. It is about 1 dB better than hard decision decoding, represented by the hard algebraic bound [52]. In the fading channel, the suboptimality is about 0.6 dB, whereas the gain over hard decoding is about 5 dB.

Figure 17 shows the performance of the  $(15, 11, 3)$  Hamming code under the same channel conditions. Due to suboptimality, about 0.3 dB and 1.2 dB are lost in the

AWGN and fading channels respectively. Gains of about 1.0 dB and 5 dB are achieved over hard decoding.

Figure 18 compares the performance of (31, 26, 3) Hamming codes and uncoded BPSK. As in previous cases, the MAP-SPC decoding gains about 0.8 dB and 5 dB over the hard decoding in the AWGN and fading channels respectively. At  $10^{-4}$ , the MAP-SPC decoded Hamming code gains about 2 dB and 17 dB over the uncoded BPSK scheme in the respective channels.

The performance of the (63, 57, 3), (127, 120, 3) and (255, 247, 3) Hamming codes are shown in Figure 19, Figure 20 and Figure 21 respectively. In the AWGN channel, there is a slight reduction in the gain over hard decoding from 0.7 dB to 0.6 dB to 0.5 dB, as the code length increases. However, in the fading channel, the gain stays rather consistently at about 5 dB.

Figure 22 compares the performance of MAP-SPC with the dual code technique in [30] using a parallel concatenated (7, 4, 3) Hamming code in the AWGN channel. In [30], this code was decoded using the dual code of the (7, 4, 3) Hamming code, which is the (7, 3, 4) maximum length code. After 6 iterations, the MAP-SPC technique is about 0.25 inferior to the dual code technique. The advantage of the MAP-SPC technique is the lower decoding complexity, which is detailed next.

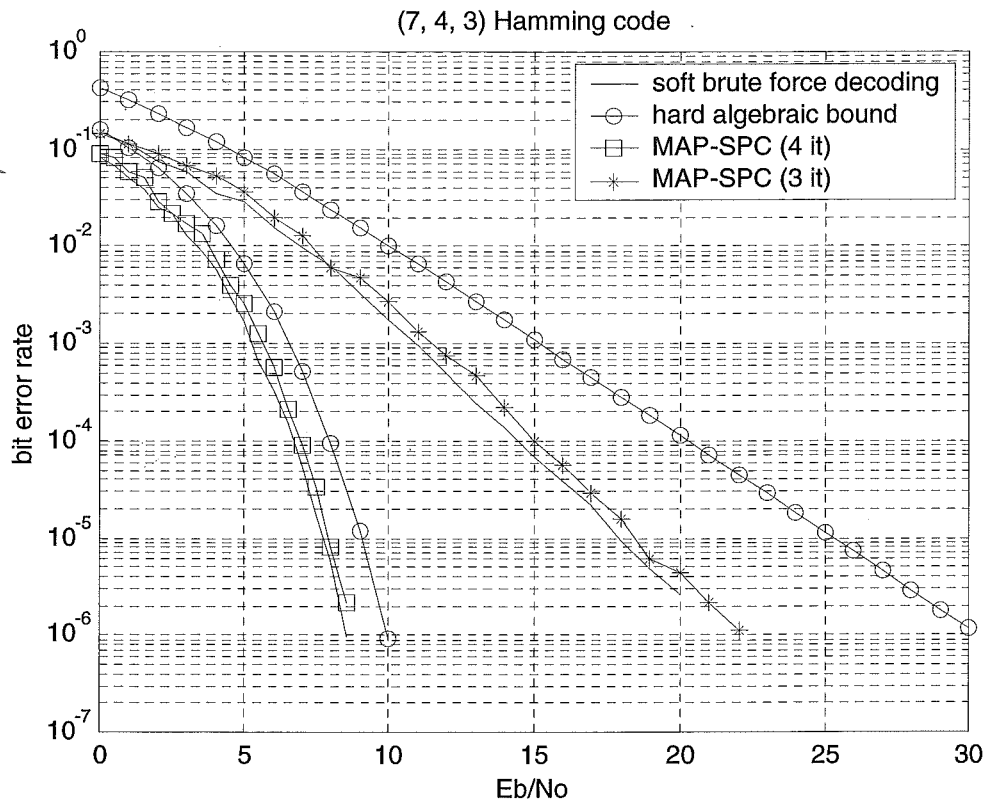


Figure 16 : Performance comparison of the (7, 4, 3) Hamming code in the AWGN (left curves) and fading (right curves) channels.

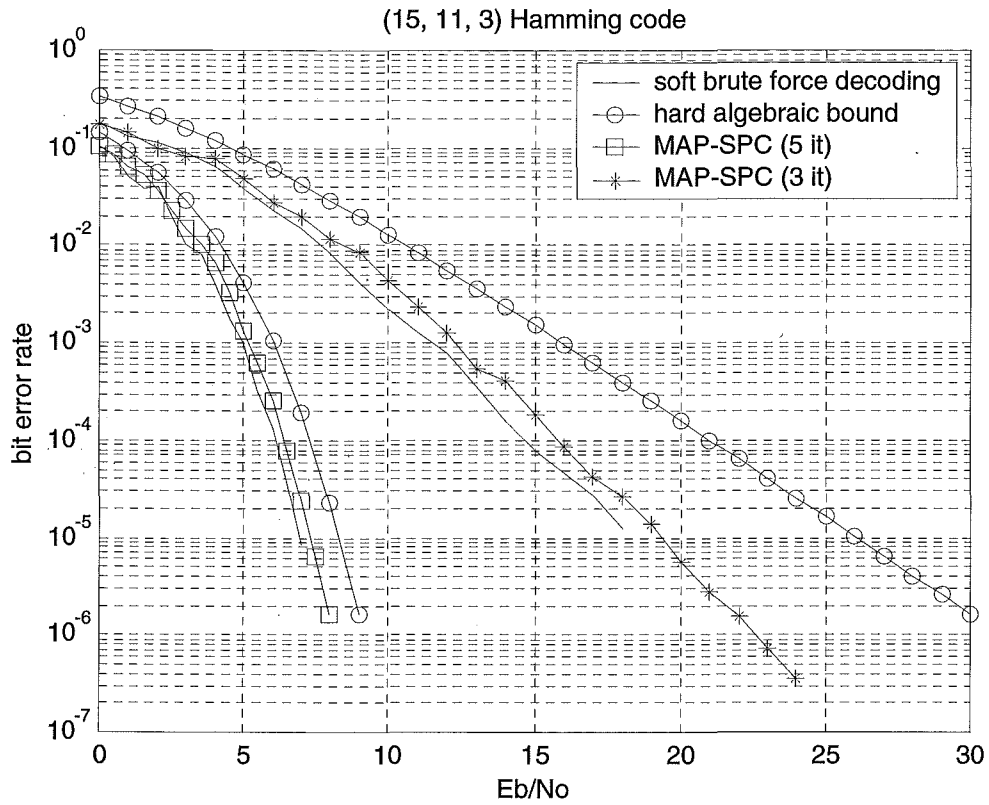


Figure 17 : Performance comparison of the (15, 11, 3) Hamming code in the AWGN (left curves) and fading (right curves) channels.

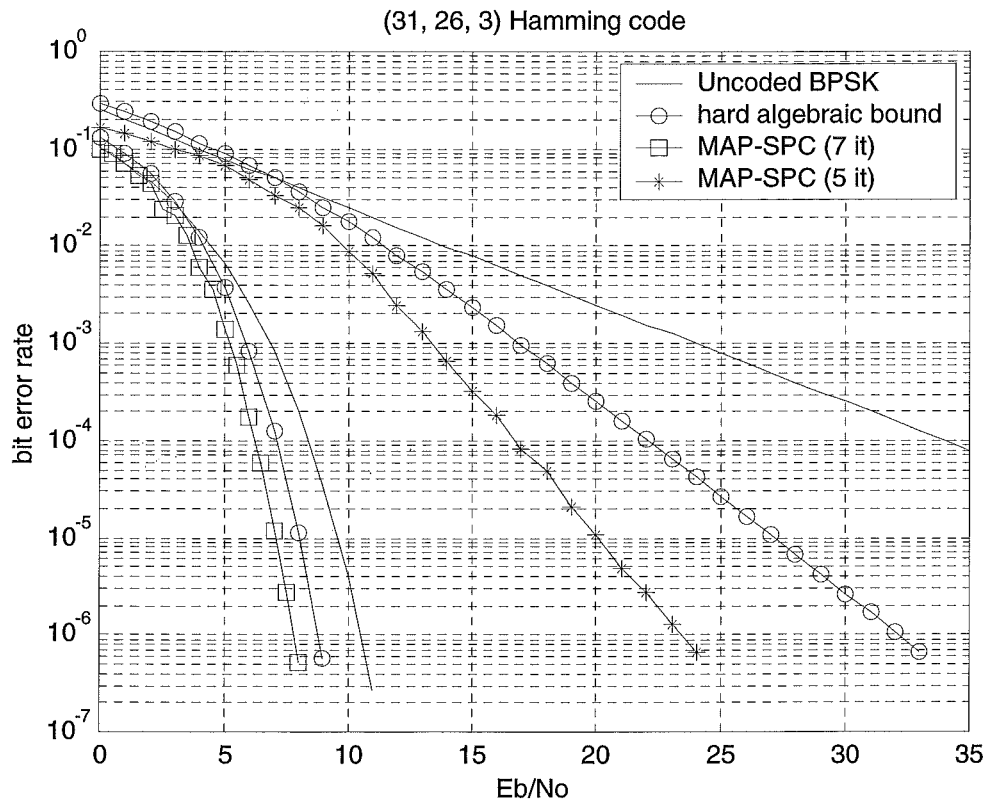


Figure 18 : Performance comparison of the (31, 26, 3) Hamming code in the AWGN (left curves) and fading (right curves) channels.

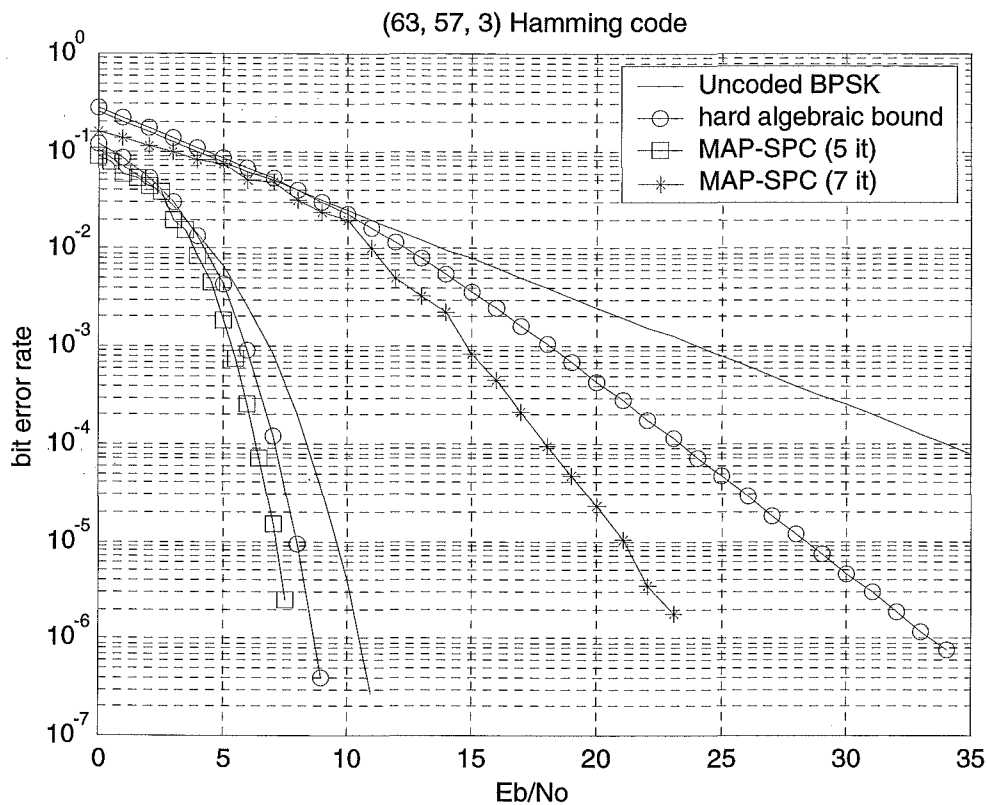


Figure 19 : Performance of the (63, 57, 3) Hamming code in the AWGN (left curves) and fading (right curves) channels.

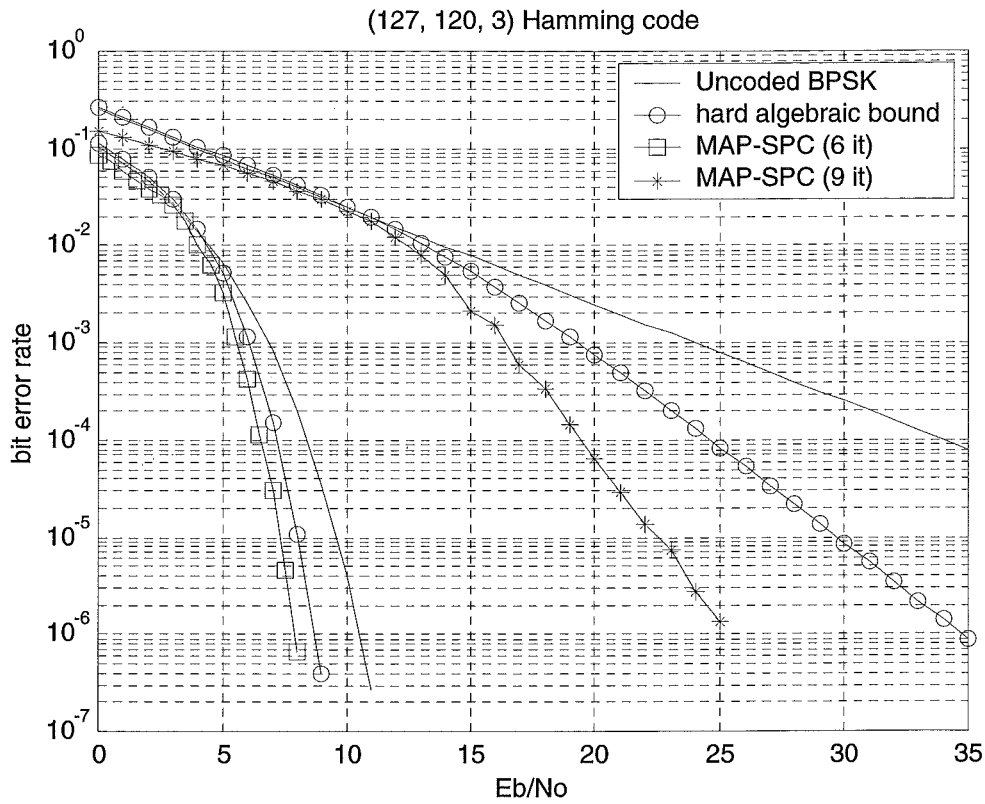


Figure 20 : Performance of the (127, 120, 3) Hamming code in the AWGN (left curves) and fading (right curves) channels.

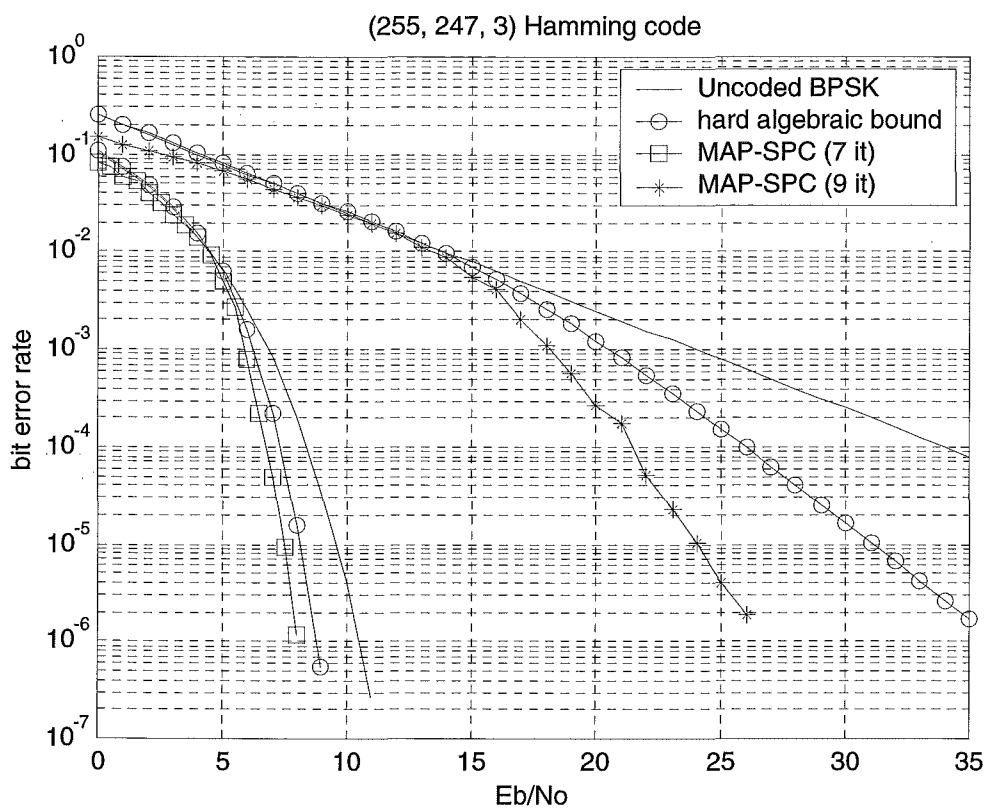


Figure 21 : Performance of the (255, 247, 3) Hamming code in the AWGN (left curves) and fading (right curves) channels.

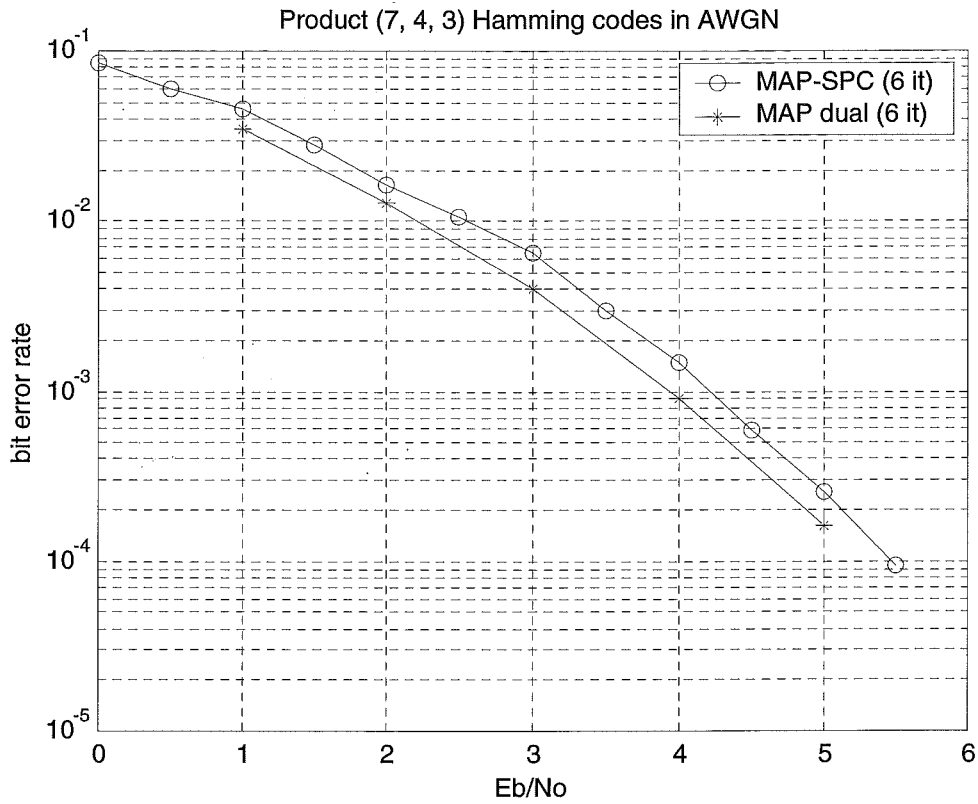


Figure 22 : Comparing the performance of the dual code technique [30] and the MAP-SPC technique. The code used is the parallel concatenated (7, 4, 3) Hamming code.

## 2.6 Decoding Complexity

The exact decoding complexity will depend on the actual implementation. However, the number of codewords that has to be searched provides a raw complexity estimate [30]. A  $(n, n-1, 2)$  MAP-SPC decoder implemented using its dual code –  $(n, 1, n)$  repetition code – requires only 2 codeword searches per iteration. Using this as a complexity measure, the complexity of the MAP-SPC scheme applied to a  $(N, K)$  systematic block code is equal to  $2*(N-K)*I$  codeword searches, where  $I$  is the number of iterations,  $K$  is the data length and  $N$  is the code length.

One of the most efficient MAP decoding techniques in the literature is the dual code technique as described in [30]. Here, the complexity of the dual code technique is compared to the MAP-SPC. For a  $(N, K)$  code, the number of codeword searches required by the dual code method of [30] is equal to  $2^{(N-K)} * I$ . Table 3 provides a comparison of the number of codeword searches required per iteration for both techniques. (Note that the dual SISO method is expected to produce better bit error rate performance compared to the MAP-SPC method. Here, both schemes are compared without taking into account the bit error rate performance.)

	MAP-SPC	Dual code
$(7, 4, 3)$ Hamming code	6	8
$(15, 11, 3)$ Hamming code	8	16
$(31, 26, 3)$ Hamming code	10	32
$(63, 57, 3)$ Hamming code	12	64
$(127, 120, 3)$ Hamming code	14	128
$(255, 247, 3)$ Hamming code	16	256

Table 3 : Comparison of the number of codeword searches required per iteration for the MAP-SPC and dual code techniques.

From Table 3, it is observed that the complexity of the dual code technique increases exponentially as the code length increases. On the other hand, the complexity of the MAP-SPC technique only increases linearly with increasing block length. Also, each

codeword search for the MAP-SPC method is conducted over repetition codes. For example, the MAP-SPC codeword search for the (63, 57, 3) Hamming code is conducted over the (32, 1, 32) repetition code. For the dual SISO technique, the codeword search is conducted over a much more complex codeword. For example, the dual SISO codeword search for the (63, 57, 3) Hamming code is conducted over the (63, 6) block code. Therefore, in effect, the complexity advantage of the MAP-SPC technique is much greater than the estimated figures.

In general, hard decision syndrome decoding is less complex than the MAP-SPC scheme. For short code lengths, the complexity of soft decision brute force decoding is lower than the MAP-SPC technique. For example, brute force decoding of the (7, 4, 3) Hamming code requires a search over  $2^4 = 16$  codewords. The MAP-SPC scheme requires a search over 6 codewords per iteration. Iterated 4 times, this translates to a total of 24 codeword searches. Nevertheless, similar to the dual code comparisons, both searches are conducted over different types of codewords. Also, the complexity of brute force decoding increases exponentially with block length at a significantly faster rate than the dual code technique.

## 2.7 Convergence of the Decoding Algorithm

Figure 23 shows the convergence behaviour of the MAP-SPC decoding algorithm for the (255, 247, 3) Hamming code in the fading channel. The convergence is stable. It is observed that as the SNR increases, more iterations are required to produce the best performance. At 20.0 dB, there is negligible gain after 6 iterations. However, at 26.0 dB, there is only negligible gains after 9 iterations. Nevertheless, the gain after 5 iterations at all SNR shown is small, perhaps too small to be worth its computation in a practical system. In general, the MAP-SPC decoding algorithm is found to converge quickly in both AWGN and fading channels. This fast convergence is a desirable feature as it results in lower overall decoding complexity and decoding delay.

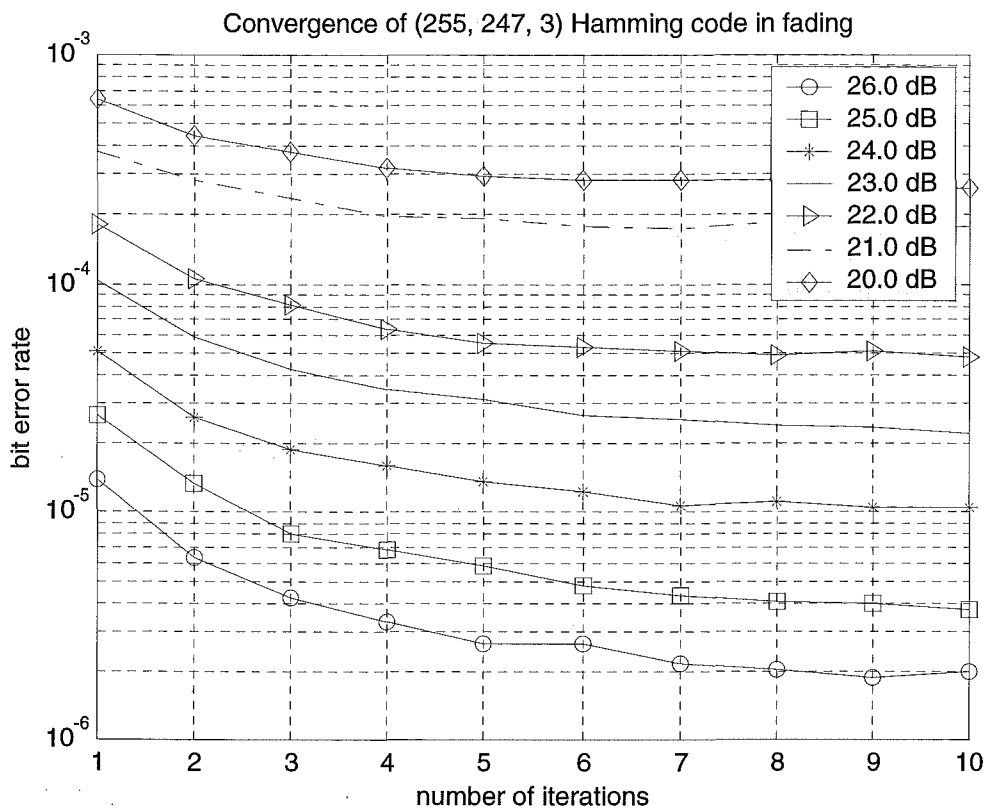


Figure 23 : Convergence behaviour of MAP-SPC decoding of the (255, 247, 3) Hamming code in the Rayleigh fading channel.

## 2.8 Summary

In this chapter, an iterative decoding technique based on MAP decoding of single parity check codes is applied to SISO decoding of systematic binary algebraic block codes. The MAP-SPC scheme performs very well compared to hard decision syndrome decoding and soft decision brute force decoding. The decoding complexity of this scheme grows linearly instead of exponentially with increasing block length. For codes such as Hamming codes, only 1 MAP-SPC decoder is needed to perform the whole decoding process. The component MAP decoders are extremely simple to implement. It can be further simplified by using the approximated Log-Likelihood Algebra (LLA) [30] for implementation on fixed point DSPs (refer to Appendix I for details).

In theory, this technique can be applied to any systematic block code. In practical, the achievable performance when applied to different codes will depend on the sparsity of the generator matrix. A generator matrix with high density will introduce high correlations, which will cause the decoder to converge very quickly to a suboptimal level. On the other hand, a sparse code will introduce less correlations, and error performance is likely to improve further with increasing number of iterations. This technique is potentially good for application to sparse codes such as Low Density Parity Check codes.

In general, the performance of this decoding strategy is expected to lie between those of ML soft decision decoding and hard syndrome decoding. The additional complexity of the MAP-SPC technique over hard algebraic decoding may or may not be worth the effort in the AWGN channel. On the other hand, a 5 dB gain at  $10^{-4}$  in the fading channel is achieved by adopting the MAP-SPC technique. This is a significant gain, and is well worth the extra effort. It is well known that the first few dB of gain is simple to achieve. After that, it becomes more difficult to improve performance. Depending on the application, the last minor gains may or may not be of practical interests. With this technique, there is an option to avoid the exponential complexity of a ML soft decoding algorithm at the cost of losing the last minor amount of gain.

It is obvious that this technique is suboptimal; concatenated iterative decoding is inherently suboptimal. Despite this suboptimality, this decoding strategy is a strong candidate for SISO decoding of long block codes, a feat not computationally practical for either brute force or trellis-based methods. This has a potential application in the decoding of concatenated block codes.

# CHAPTER 3 : DESIGN, ANALYSIS AND PERFORMANCE OF CONCATENATED SINGLE PARITY CHECK (SPC) CODES

## 3.1 Introduction

Single parity check (SPC) codes are some of the simplest and weakest algebraic codes in existence. A simple code is inherently simple to decode. Despite its simplicity, it has been shown to produce high performance at low complexity. This chapter presents two concatenated SPC coding schemes to attack the error floor, block length and code rate problems encountered in previous efforts as outlined in Chapter 1. The two schemes are the multiple parallel and the multiple serially concatenated SPC codes. The dimension of the codes is increased to improve the error performance. The error floor is also pushed further down as the dimensionality is increased. A method of incrementing the number of dimensions without changing the code rate and block length requirements is presented. Analytical bounds for these codes fixed at a rate of  $\frac{3}{4}$  and a data block lengths of 900 bits are derived to estimate the asymptotic performance in the AWGN and independent Rayleigh fading channels. An improved decoder structure for serially concatenated codes is also presented.

## 3.2 Multiple Parallel Concatenated SPC Codes

### 3.2.1 Encoder Structure

An  $M$  parallel concatenated SPC code consists of  $M$  SPC encoders, separated by  $M-1$  interleavers. Figure 24 shows the general encoder structure for multiple parallel concatenated single parity check codes (M-PC-SPC). The constituent interleavers can be of any type. In this work, random interleavers are used. The number of parallel concatenations is increased to improve performance. With an input block length of  $K = kM$  bits and output block length of  $N$  bits, the overall code rate of  $k/n$  is retained by selecting the  $(k^*M)/(k^*M+1)$  SPC as component codes.

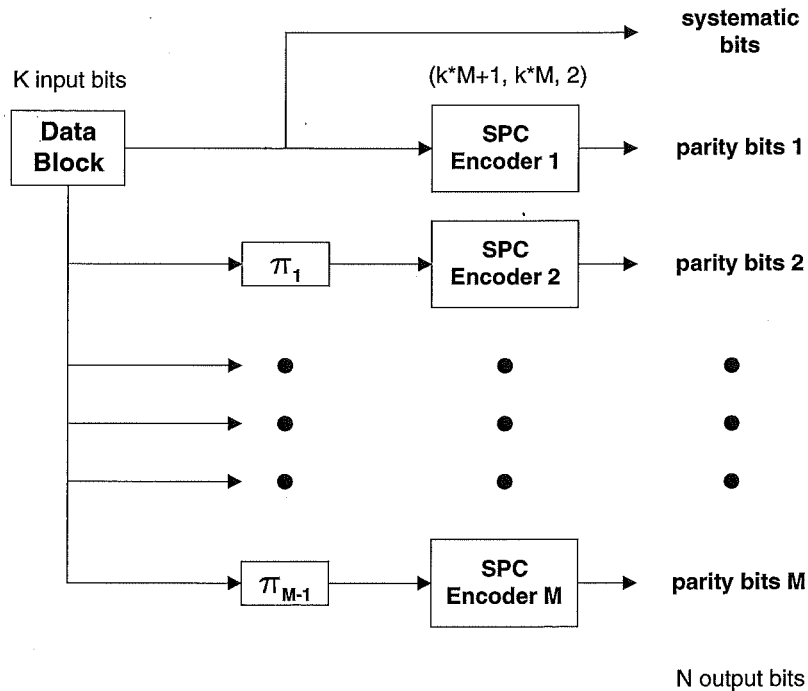


Figure 24 : General encoder structure for Multiple Parallel Concatenated Single Parity Check Codes (M-PC-SPC).

The following example shows how a rate  $\frac{3}{4}$  3 parallel concatenated SPC (3-PC-SPC) code with a data block length of 900 bits is constructed. The numerator of the overall code rate is multiplied by the number of parallel concatenations,  $M$ . In this example, the targeted code rate is  $\frac{3}{4}$ . Both the numerator of the targeted code rate and  $M$  are

equal to 3, so the component SPC is a  $(3*3)/(3*3+1)$  SPC code. As a result, the 3-PC-SPC code is composed of 3 (10, 9, 2) SPC component codes.

This technique can be extended to any code rate and almost any data block size. The only requirement is that the data block size has to be an integer multiple of the component SPC code's input word length. In the example, any data size that is an integer multiple of 9 can be used.

### 3.2.2 Decoder Structure and Decoding Algorithm

Figure 25 shows the decoder structure of a 3-PC-SPC code. The component soft-in-soft-out (SISO) decoder is shown in Figure 26. Each component decoder accepts soft information (LLR) from the demodulation process. These soft informations are combined with a priori information to generate extrinsic information for each data bit. The generated extrinsic information is then used by other component decoders as a priori information. There is no self-feedback of extrinsic information, meaning that extrinsic information generated by decoder 1 is used only by decoders 2 and 3. Although not explicitly shown in Figure 25, all soft informations are properly interleaved and deinterleaved before being used.

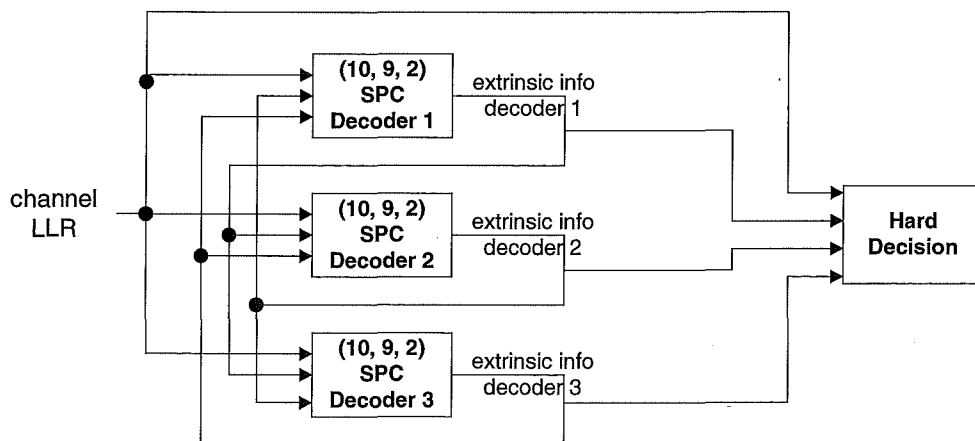


Figure 25 : Decoder structure for the 3-PC-SPC code.

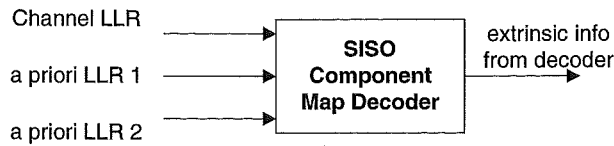


Figure 26 : SISO component MAP unit for each decoder.

The SISO component decoding units perform symbol-by-symbol MAP decoding of SPC codes. The MAP algorithm for SPC codes is shown in Appendix I.

### 3.2.3 Analytical Bounds

This section provides analytical estimates for the code performances at high SNR. It is not our intention to tackle this difficult bounding problem with rigour here. The analytical bounds employ the Input Redundancy Weight Enumerating Function (IRWEF) based on the work of [32]. The bounds are not very tight, particularly at very low SNR, because the decoding technique is suboptimal whereas the bounds assume ML decoding. Also, due to the computational complexity, only part of the codes' weight distributions are taken into account. Nevertheless, the work here provides good estimates of where the error floors are, and provides sufficient guidelines for the purpose of practical systems design. Performance bounds for the codes at an input length of 900 bits, output length of 1200 bits, and a code rate of  $\frac{3}{4}$  are shown here.

In [53], BER bounds for parallel concatenated SPC codes and zigzag codes were presented. They have used essentially the same approach as the method presented in this section to increase the dimensionality without changing the code rate or block length. The work in this section is a direct extension of [55].

### 3.2.3.1 The Union Bound

In [32], the Input Redundancy Weight Enumerating Function (IRWEF) for a  $(n, k)$  linear block code is defined as

$$A^C(W, Z) = \sum_{w,j} A_{w,j} W^w Z^j$$

where  $A_{w,j}$  denotes the (integer) number of codewords generated by an input information word of Hamming weight  $w$ , whose parity check bits have Hamming weight  $j$ , so that the overall Hamming weight is  $w + j$ .  $W$  and  $Z$  are symbolic variables. Under the uniform error property of a linear block code, the word and bit error probability performance of the code can be evaluated under the assumption that the all zero codeword,  $x_0$ , was transmitted. The pairwise error event  $e_{0h}(w)$  is then defined as the event in which the likelihood of a codeword with weight  $h$  and generated by an information word of weight  $w$  is greater than that of the all zero codeword  $x_0$ . Using the union bound, the bit error probability under ML soft decoding for BPSK transmission can then be upper bounded as [32]

$$P_b(e) \leq \sum_h D_h P[e_{0h}(w)]$$

where  $D_h$  is derived from the IRWEF as

$$D_h = \sum_{j+w=h} \frac{w}{k} A_{w,j}$$

Clearly, 2 terms have to be computed for the upper bound, namely, the pairwise error event probability and the term  $D_h$ .

### 3.2.3.2 Pairwise Error Event Probability

The pairwise error event probability is dependent on the channel. For the AWGN channel, it is equal to [25]

$$P[e_{oh}(w)] = \frac{1}{2} \operatorname{erfc} \left( \sqrt{\frac{hR_c E_b}{N_0}} \right)$$

where  $R_c = k/n$  is the code rate. For the independent fading channel, it is approximated as [56]

$$P[e_{oh}(w)] \leq \frac{1}{2} \left( 1 - \left[ \frac{R_c \frac{E_b}{N_0}}{1 + R_c \frac{E_b}{N_0}} \right]^{1/2} \right) \left( \frac{1}{1 + R_c \frac{E_b}{N_0}} \right)^{h-1}$$

### 3.2.3.3 The $D_h$ Term

The  $D_h$  term can be extracted from the IRWEF of the code. Therefore, the final piece of computation required is the derivation of the IRWEF for M-PC-SPC codes. This derivation is extended to higher dimensionalities ( $> 3$  dimensions) based on the work of [32]. The extension is a simple and straightforward task. The IRWEF computation is included in Appendix II.

### 3.2.4 Bounds Compared to Simulations Results

The bounds for the M-SPC-SPC codes in the AWGN and independent fading channels using BPSK are presented here using only partial IRWEFs. As mentioned earlier, evaluating the complete IRWEF of the M-PC-SPC codes at an input data block length of 900 bits for 2 to 6 dimensions is an almost computationally impossible

task. For practical reasons, only a limited number of terms of the IRWEF is computed. Here, the partial IRWEF of the M-PC-SPC codes are computed using the first 22 terms of the IRWEF of the component codes.

Figure 27 compares the bounds for 2, 3, 4, 5 and 6-PC-SPC codes with the simulation results in the AWGN channel. Figure 28 shows the bounds for the same codes in the independent fading channel. The bounds obtained for all the codes provide good estimates in both channels at high SNR. It is interesting to note that both the simulations and bounds indicate that, as the dimensionality of the codes increases from 4 to 5, the error floors are lowered by more than 1 order of magnitude in both channels ( $\approx 10^{-4}$  to  $< 10^{-5}$  in AWGN at about 3.3 dB, and  $> 10^{-5}$  to  $\approx 10^{-6}$  in fading at about 9 dB). As the dimensionality increases from 5 to 6, the error floor is lowered by almost 2 orders of magnitude in both channels ( $< 10^{-5}$  to  $\approx 10^{-7}$  in AWGN at about 3.5 to 4 dB, and  $\approx 10^{-6}$  to  $\approx 10^{-8}$  in fading at about 9 to 11 dB). In higher dimensionalities, the error floor improvement is achieved at the expense of the waterfall region.

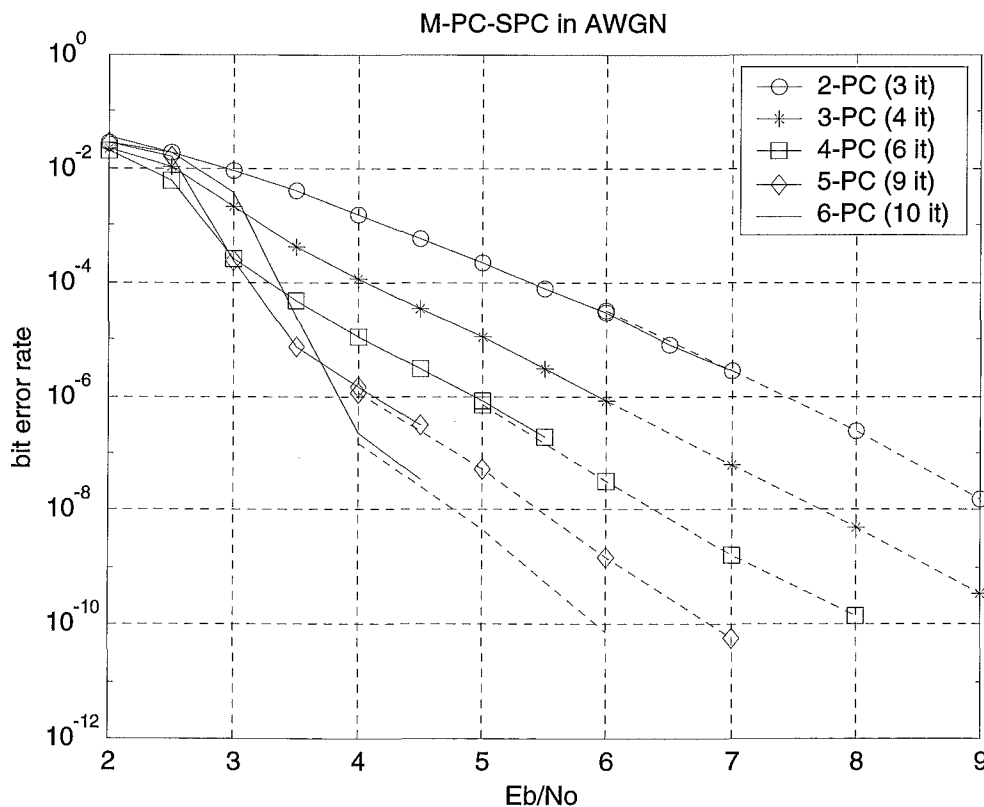


Figure 27 : Bounds for 2, 3, 4, 5 and 6-PC-SPC codes with the simulation results in the AWGN channel. Solid lines indicate simulation results whereas bounds are denoted by dashed lines.

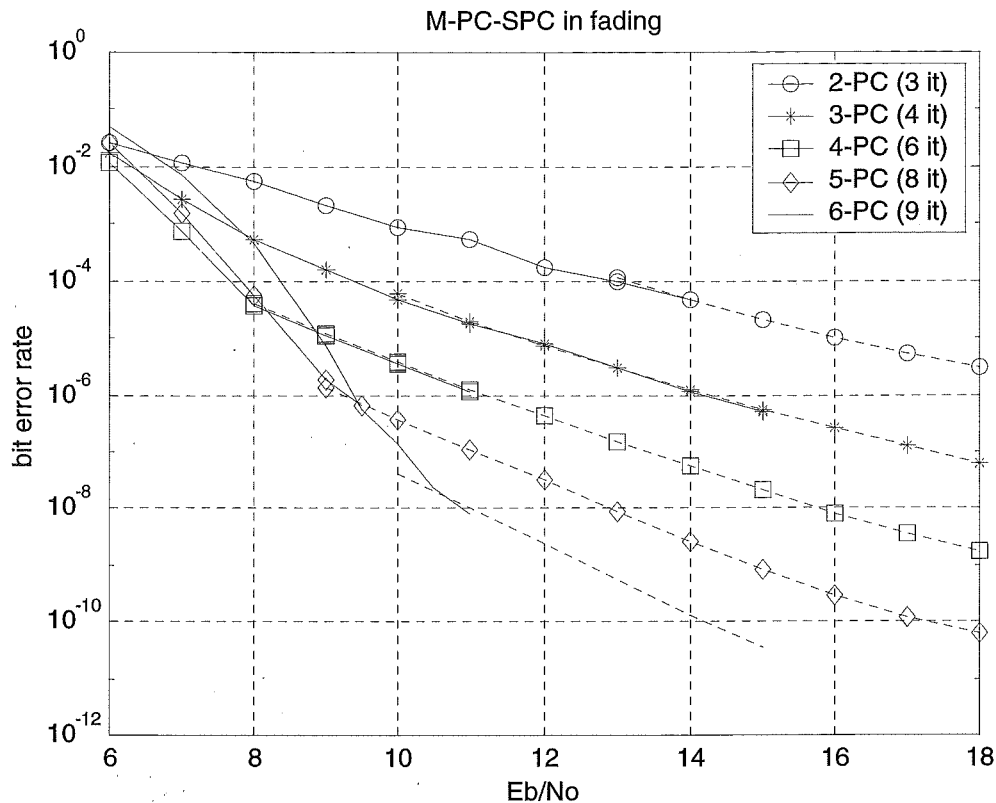


Figure 28 : Bounds for 2, 3, 4, 5 and 6-PC-SPC codes with the simulation results in the fading channel. Solid lines indicate simulation results whereas bounds are denoted by dashed lines.

### 3.3 Multiple Serially Concatenated SPC Codes

The same method applied to the construction of multiple parallel concatenated SPC codes can also be applied to the multiple serial concatenation structure.

#### 3.3.1 Encoder Structure

Figure 29 shows the general encoder structure for multiple serially concatenated single parity check (M-SC-SPC) codes. With  $M$  serial concatenations, there are  $M$  encoders, separated by  $M-1$  interleavers. As with the parallel concatenated SPC codes, the constituent interleavers can be of any type. In this investigation, random interleavers were used. In order to retain the overall code parameters (code rate  $k/n$ ,

input block length  $K$ , output block length  $N$ ), the component code rates were carefully chosen as shown in Figure 29.

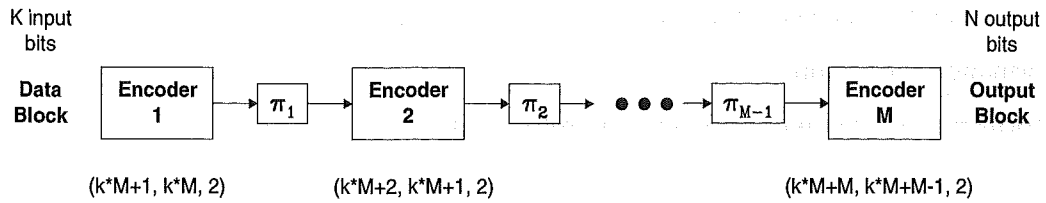


Figure 29 : General encoder structure for Multiple Serially Concatenated Single Parity Check Codes (M-SC-SPC).

The following example shows how a rate  $\frac{3}{4}$  3-SC-SPC code is constructed. The numerator and denominator of the target code rate are multiplied by the number of serial concatenations,  $M$ . In this case, the numerator of the code rate is 3, while its denominator is 4, and  $M=3$ , so the result is  $\frac{9}{12}$ . The following component codes are then used in the design :

Outer code :  $(10, 9, 2)$  SPC code

Middle code :  $(11, 10, 2)$  SPC code

Inner code :  $(12, 11, 2)$  SPC code

The input data block length is very flexible. The only requirement is that the data block size has to be an integer multiple of the outer code's input word length. In the example, any data size that is an integer multiple of 9 can be used.

### 3.3.2 Decoder Structure and Decoding Algorithm

In this section, an improved iterative decoder structure for multiple serially concatenated codes (SCC) is presented.

### 3.3.2.1 The Suboptimum Decoder Structure

The idea behind iterative decoding is the exchange of soft (extrinsic) information among decoders. As a general rule, self-feedback is avoided as it produces inferior performance and in some cases, causes the decoding algorithm to diverge (performance worsen with increasing number of iterations). There is little work in the literature that touches on the iterative decoder structure of multiple SCCs. The only significant work is that of [27] where the structure for 3 dimensional SCCs was presented. This structure was extended from that originally developed for 2 dimensional SCCs [25].

Figure 30 shows this suboptimum iterative decoder structure extended to the 4 dimensional SCC. Although not explicitly shown in the figure, all soft information are properly interleaved/deinterleaved before being used. The details of the SISO component MAP unit for the inner decoder is shown in Figure 31. Based on Figure 30, the following observations are made :

- Soft information from one decoder is only shared with immediate subsequent and previous decoders. Soft information from the mid3 decoder is fed back to the inner decoder and fed forward to the mid2 decoder. The mid3 decoder accepts soft information from the inner and mid2 decoder. There is no sharing of soft information between the mid3 decoder and the outer decoder.
- The first (inner) and last (outer) decoders only receive soft information from one source each – mid3 decoder and mid2 decoder respectively.
- The first (inner) and last (outer) decoders only feed soft information to 1 other decoder – mid3 decoder and mid2 decoder respectively

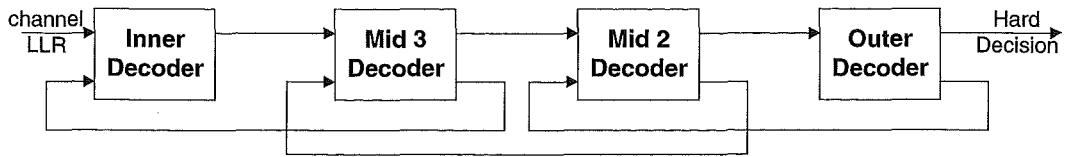


Figure 30 : Suboptimum iterative decoder structure for the 4 dimensional serially concatenated code extended from the work of [27].

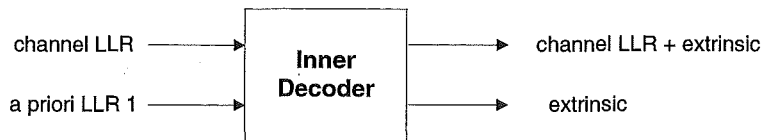


Figure 31 : SISO component MAP unit for the inner decoder.

### 3.3.2.2 An Improved Decoder Structure

The key to a complete iterative decoder is to maximize the sharing of soft information among component decoders. According to this criteria, the iterative decoder structure should have as much information sharing as possible among decoders. In multiple parallel concatenated decoding structures [21], soft information gleaned from one decoder is shared with all other decoders. Here, a similar structure for decoding multiple SCCs is proposed. The proposed iterative decoder structure is shown in Figure 32. Details of the SISO component MAP unit for the inner decoder is shown in Figure 33.

In Figure 32, soft information from every decoder is shared with all other decoders. The inner and outer decoders no longer receive soft information from only 1 decoder. Their soft informations are also shared with all other decoders. This iterative decoder structure maximises the sharing of soft information and therefore, meets the criteria for a complete iterative decoder as defined. This improved decoder structure is very similar to the decoder structure for multi-dimensional parallel concatenated codes. The complexity of the improved decoder is slightly higher than that of the suboptimum decoder due to the extra addition operations required to combine the extrinsic informations. We note here that for 2 dimensional SCCs, the iterative

decoder structure presented in [25] shares soft information among all the decoders and therefore, is the same as the proposed decoder structure.

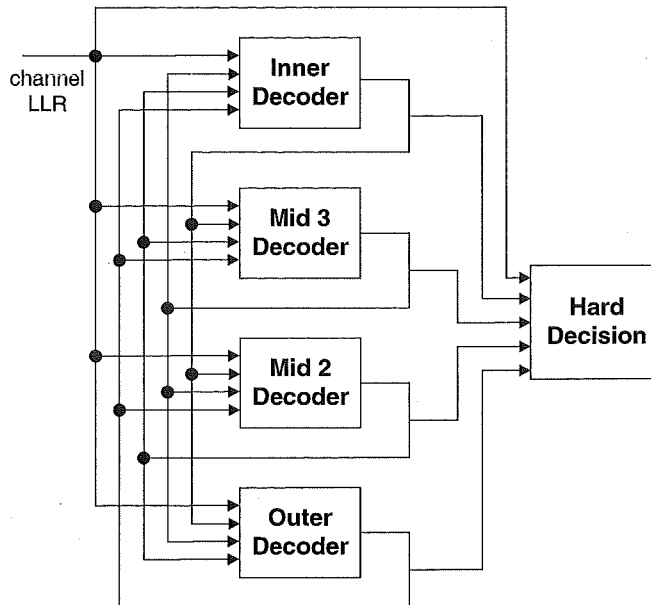


Figure 32 : The proposed iterative decoder structure for the 4 dimensional serially concatenated code.

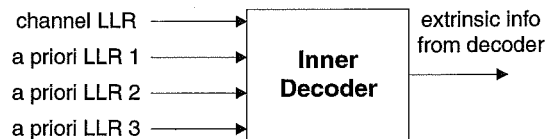


Figure 33 : SISO component MAP unit for the inner decoder.

### 3.3.2.3 Comparing the Suboptimum and Improved Decoder Structure

The performance of the suboptimum and improved iterative decoder structures are compared using the 4 dimensional serially concatenated single parity check (4-SC-SPC) code. Figure 34 compares their performances in the AWGN and independent fading channels using coherently demodulated BPSK. For a fair comparison, all results are obtained using identical parameters. They have identical code rates, block lengths and interleavers. The only difference is the iterative decoder structure. After 5

iterations, the proposed decoder gains approximately 0.5 dB in the AWGN channel. In the fading channel, the performance is about 0.9 dB better.

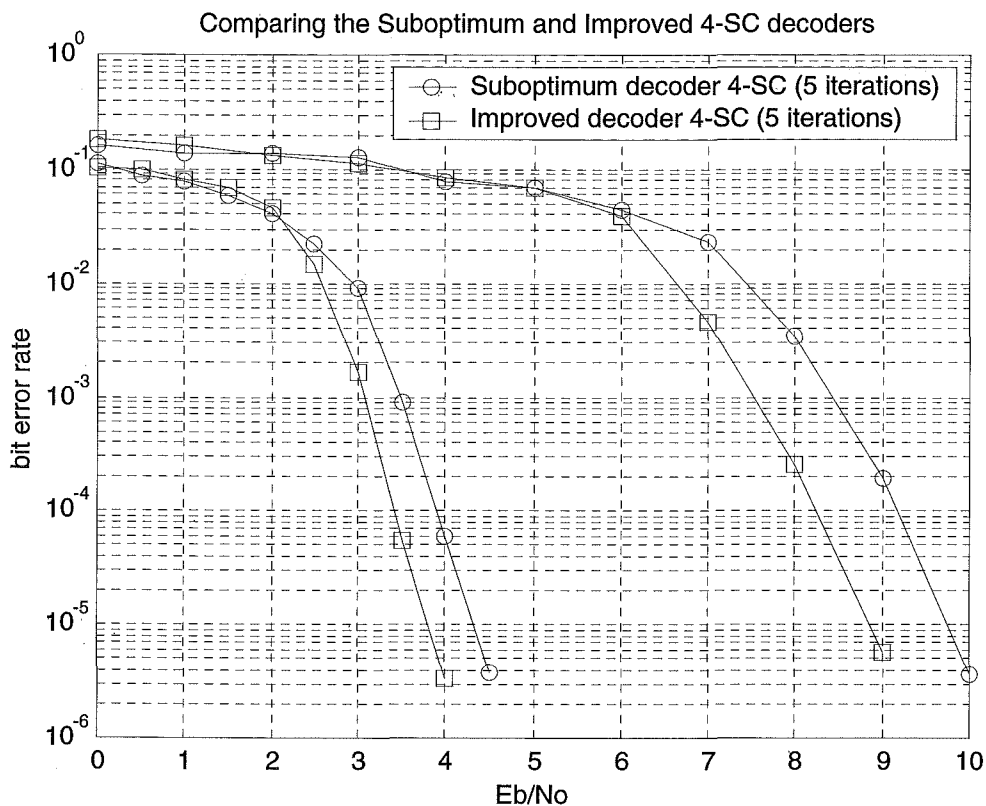


Figure 34 : Comparison of the suboptimum and improved decoders for the 4 dimensional serially concatenated single parity check (4-SC-SPC) code in the AWGN (curves on the left) and fading (curves on the right) channels.

#### 3.3.2.4 Generalisations of the Improved Decoder Structure

Results here show that the proposed iterative decoder structure produces superior performance for the decoding of multiple serially concatenated single parity check codes. In principle, this iterative decoder structure can be applied to any multiple serially concatenated block code. It can also be applied to multiple serially concatenated convolutional codes, since all terminated convolutional codes are essentially block codes.

In theory, this decoder structure is applicable to multi-dimensional product codes. A product code can be considered as a special case of a serially concatenated code with a stricter interleaver constraint. It requires parity bits to be interleaved separately from data bits. On the other hand, serially concatenated codes interleave data bits together with the parity bits. Based on this subtle difference, applying this decoder structure to the decoding of multi-dimensional product codes should also produce some performance improvements.

### 3.4.3 Analytical Bounds

This section provides an analytical estimate of code performance at very high SNR. As for the case of parallel concatenated SPC codes, the aim of this work is to produce asymptotic estimates due to computational difficulties as previous stated. The analytical bounds presented here employ the Input Output Weight Enumerating Function (IOWEF) based on the work of [25] and [27]. The bounds are not very tight, particularly at very low SNR. Also, due to the computational complexity, only part of the code weight distributions are taken into account. The performance bounds for the 2, 3, 4, 5 and 6-SC SPC codes at an input length of 900 bits, output length of 1200 bits, and a code rate of  $\frac{3}{4}$  are shown here.

#### 3.4.3.1 The Union Bound

In [25], the Input Output Weight Enumerating Function (IOWEF) of a  $(n, k)$  linear block code is defined as

$$A(W, H) = \sum_{w=0}^k \sum_{h=0}^n A_{w,h} W^w H^h = \sum_{w=0}^k W^w A(w, H)$$

where  $A_{w,h}$  represents the number of codewords with weight  $h$  generated by information words of weight  $w$ .  $W$  and  $H$  are symbolic variables. The Conditional Weight Enumerating Function (CWEF) is implicitly defined within the IOWEF as

$$A(w, H) = \sum_{h=0}^n A_{w,h} H^h$$

It is the function that enumerates the weight distribution of the codewords generated by information words of a given weight  $w$ . By using the uniform error property of a linear block code, the word and bit error probability performance of the code can be evaluated under the assumption that the all zero codeword,  $x_0$ , was transmitted. Using this assumption, the pairwise error event  $e_{oh}(w)$  is defined as the event in which the likelihood of a codeword with weight  $h$  and generated by an information word of weight  $w$  is higher than that of the all zero codeword  $x_0$ . Using the union bound, the bit error probability under ML soft decoding for BPSK transmission can then be upper bounded as [25]

$$P_b(e) \leq \sum_{h=1}^n \sum_{w=1}^k \frac{w}{k} A_{w,h} P[e_{oh}(w)]$$

Defining the bit error multiplicity as

$$B_h = \sum_{w=1}^k \frac{w}{k} A_{w,h}$$

results in

$$P_b(e) \leq \sum_{h=1}^n B_h P[e_{oh}(w)]$$

Thus, 2 terms have to be computed for the upper bound, the pairwise error event probability and the bit error multiplicity. The pairwise error event probability is identical to those described in section 3.1.3.2.

### 3.4.3.2 Bit Error Multiplicity

The bit error multiplicity can be extracted from the CWEF, which in turn is extracted from the IOWEF of the code. The IOWEF derivation is extended to higher dimensionalities ( $> 3$  dimensions) based on [25] [27]. The extension is a simple and straightforward task. The IOWEF computation is shown in Appendix III.

### 3.4.4 Bounds Compared to Simulations Results

The bounds for the 2, 3 and 4-SC-SPC codes in the AWGN and independent fading channels using BPSK are presented here using the partial CWEFs. For practical reasons, the partial CWEF of the M-SC-SPC codes are computed using the first 25 terms of the CWEF of the component codes.

Figure 35 shows the bounds for 2, 3 and 4-SC-SPC codes compared to simulation results for the AWGN channel. Figure 36 shows the bounds for the same codes for the independent fading channel. At high SNR, the bounds obtained for the 2, 3 and 4-SC-SPC codes are quite good for both channels. We note that, as the dimensionality of the code increases from 3 to 4, the simulations and bounds indicate that the error floors are lowered by approximately 2 orders of magnitude in the AWGN channel ( $\approx 10^{-4}$  to  $\approx 10^{-6}$  at about 4 dB). For the fading channel, the floor is lowered by more than 1 order of magnitude ( $> 10^{-5}$  to  $< 10^{-7}$  in fading at about 11 dB). The performance in the waterfall region is also improved.

Analytical bounds for the 5 and 6-SC SPC codes in the AWGN and fading channels are compared in Figure 37 and Figure 38 respectively. The bounds are very loose at low SNR because insufficient terms were evaluated, mainly due to the computational complexity involved. However, they provide some approximation for the asymptotic performance. Simulation results show that the error floor is not present at error rates above  $10^{-6}$ . The bounds suggest that the error floors are pushed to very low error rates ( $< 10^{-9}$ ).

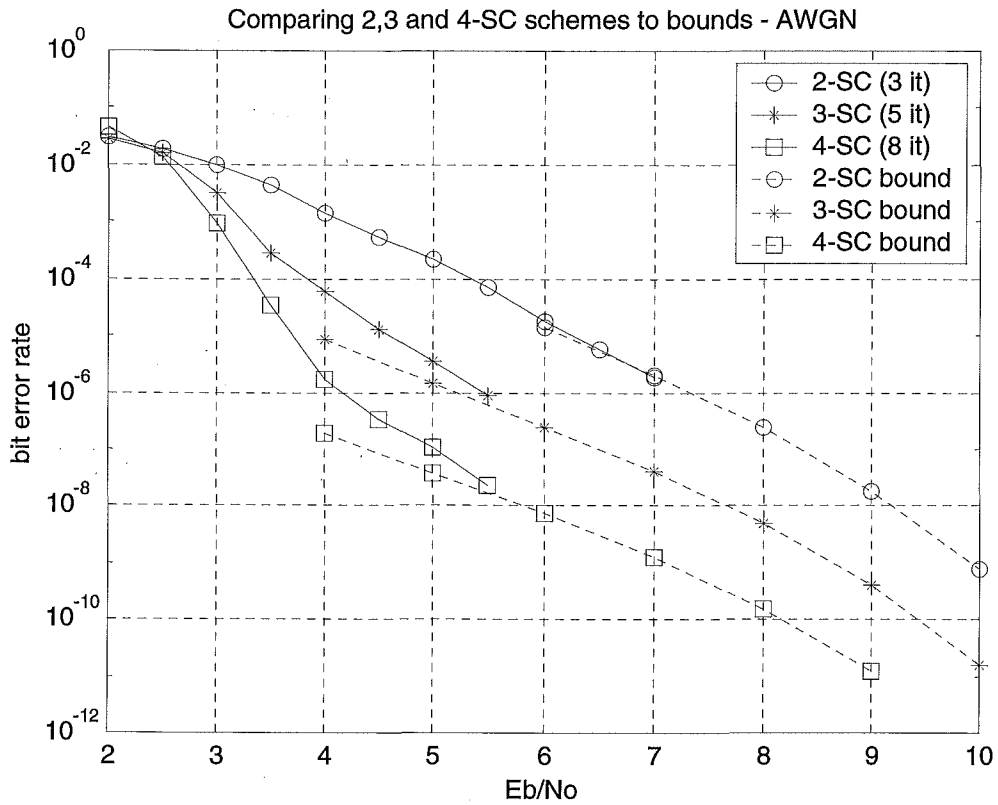


Figure 35 : Bounds for 2, 3 and 4-SC-SPC codes with the simulation results in the AWGN channel.

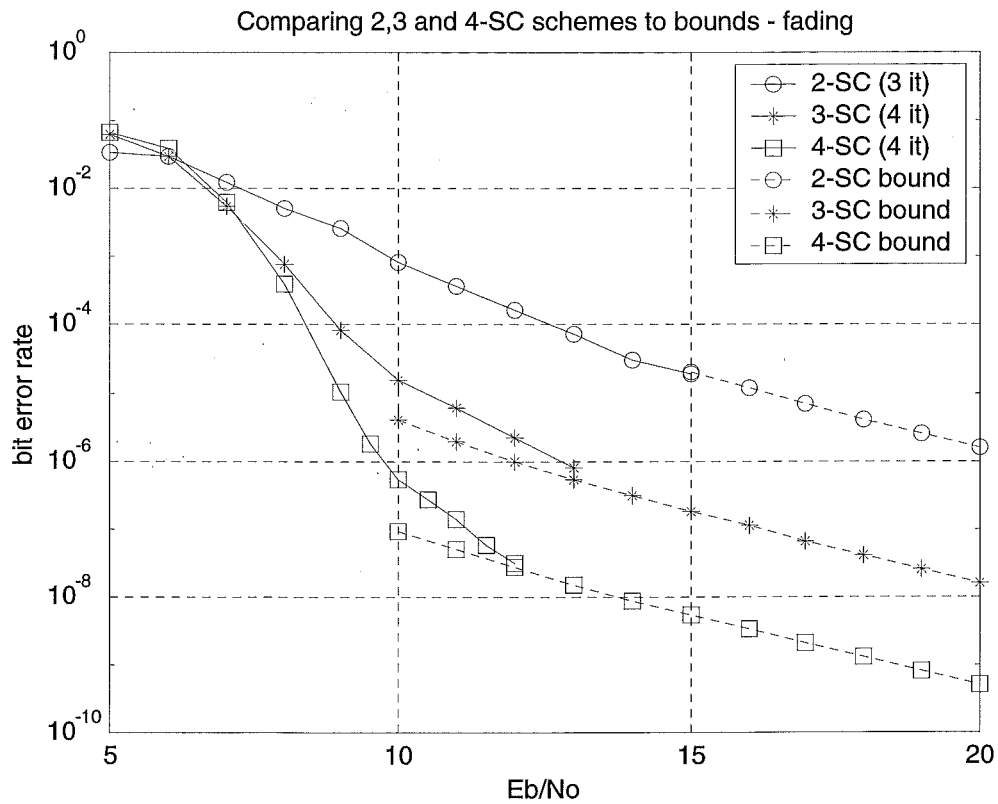


Figure 36 : Bounds for 2, 3 and 4-SC-SPC codes with the simulation results in the fading channel.

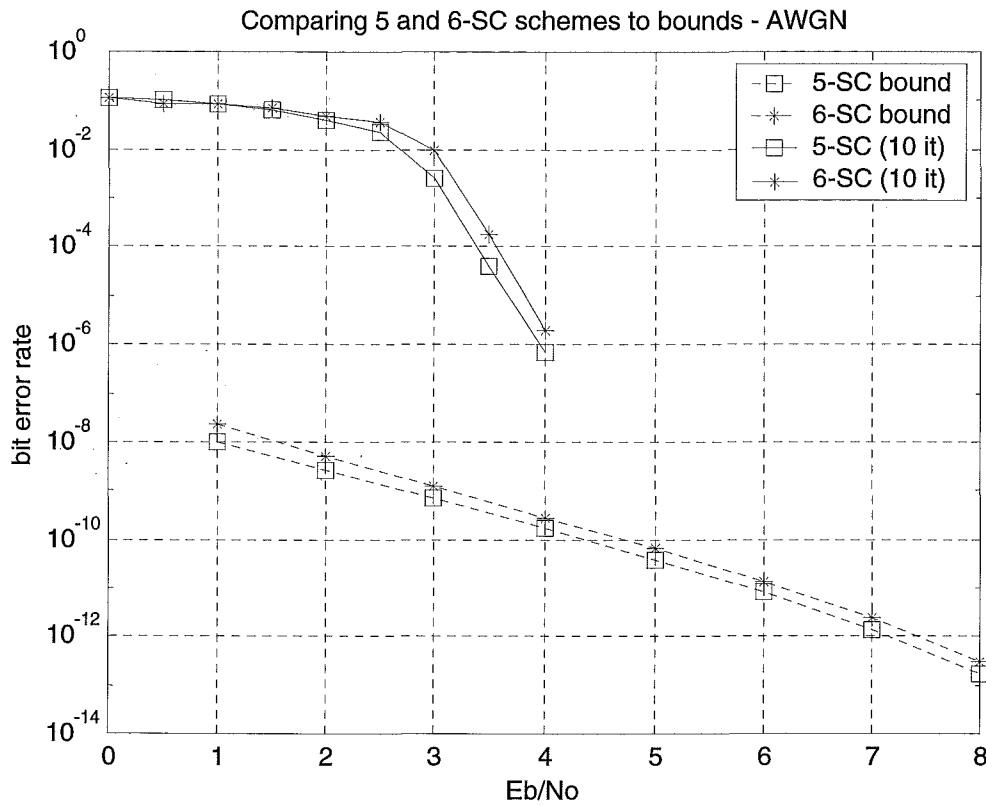


Figure 37 : Bounds (dashed lines) for 5 and 6-SC-SPC codes with the simulation results (solid lines) in the AWGN channel.

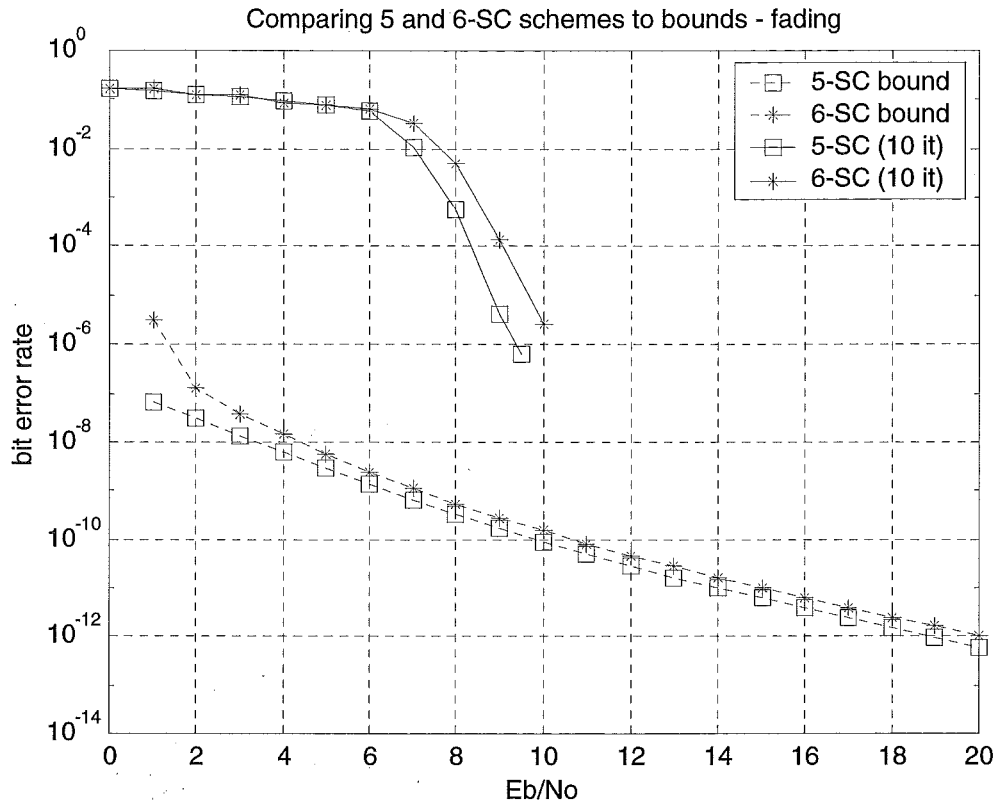


Figure 38 : Bounds (dashed lines) for 5 and 6-SC-SPC codes with the simulation results (solid lines) in the fading channel.

### 3.5 Summary

In this chapter, it has been shown that, by increasing the dimensionality, the error floors of multiple parallel and multiple serially concatenated SPC codes are lowered. At the same time, the bit error performance in the waterfall region improves. All these gains are achieved without changing the rate and block length of the code because the component SPC codes are properly chosen. The input data block length is flexible. For multiple parallel concatenated SPC codes, the size needs only be an integer multiple of the input word length of the constituent SPC encoders. For multiple serially concatenated SPC codes, the data block must be an integer multiple of the outer encoder's input word length. This flexibility opens up these coding schemes to a wide range of practical applications.

Analytical bounds are presented to estimate the performance of concatenated SPC codes at high SNRs. Due to computational complexity, only the partial weights of the concatenated codes are considered. The non tightness of the bound for parallel concatenated codes can be overcome by the simple method proposed in [125]. Simulation results for low to medium SNRs are presented to complement the asymptotic estimates of the bounds. Together, they provide sufficient guidelines for practical systems design.

More investigations on concatenated SPC codes will be presented in chapter 5 where the performance between the parallel and serial schemes are compared, the decoding complexities are estimated and the convergence of the decoding algorithms are discussed.

An improved iterative decoder structure for multiple serially concatenated codes is also presented. The decoder maximizes the sharing of soft information among all decoders to produce superior performance compared to the previously used decoder. The decoder structure is only applicable to systematic codes. Although only results for single parity check codes are presented here, the proposed iterative decoder structure is applicable to other component codes, and also product codes. It is very likely that if the improved iterative decoder is employed, there may still be some potential performance gains at low SNR for the works published in [27] and [43].

The first part of the document  
 discusses the importance of  
 maintaining accurate records  
 and the role of the  
 auditor in this process.  
 It also covers the  
 various methods used to  
 collect and analyze data.  
 The second part of the  
 document focuses on the  
 specific techniques used to  
 identify and measure  
 the risk of fraud.  
 This includes a detailed  
 discussion of the  
 various types of fraud  
 and the methods used to  
 detect them. The  
 document concludes with  
 a summary of the key  
 findings and a list of  
 recommendations for  
 improving the audit  
 process.

## CHAPTER 4 : CODED MODULATION

### 4.1 Introduction

Coded modulation has come a long way since the days of Ungerboeck. Traditionally, coded modulation treats coding and modulation as a single process by employing techniques such as set partitioning of the signal constellation [57]. Set partitioning has been successfully extended using multilevel codes with multistage decoding (MLC/MSD) [58] [59]. Until this day, this coded modulation structure still reigns as the best in the AWGN channel [60] [54]. However, its performance in the Rayleigh fading channel is not as good. Zehavi is arguably the first to recognise the advantages of separating coding and modulation for application to the Rayleigh fading channel [61] [62]. Coding and modulation were separated by performing bit interleaving before mapping the coded bits onto the signal constellation. His work was generalised to Bit Interleaved Coded Modulation (BICM) by Caire et. al. in [63]. Along the way, a few publications have also emerged in the literature with similar ideas [64] [65], [66]. Consistently, the superiority of separating coding and modulation in the Rayleigh fading channel is reported. In this chapter, an overview of key developments in coded modulation is presented. Strong emphasis is placed on the structure of the coded modulation schemes rather than the error correction scheme employed.

## 4.2 Coding and Modulation Combined

### 4.2.1 Trellis Coded Modulation and Ungerboeck's Codes

Convolutional codes [67] and the Viterbi algorithm [68] played key roles lead to the advancement and widespread use of combined coding and modulation. At one stage convolutional codes were considered as the most powerful practical codes.

Convolutional codes are more flexible in block length and code rates compared to block codes such as Hamming codes (pre-fixed block length). The Viterbi algorithm provided a way of implementing tractable maximum likelihood soft decision decoding of convolutional codes.

In [57], Ungerboeck was first to combine convolutional codes with multilevel signal constellations, forming Trellis Coded Modulation (TCM) [69], [70]. The significance of Ungerboeck's contribution lies in the use of larger signal constellations to cater for the redundant bits from the error correction codes such that bandwidth efficiency is not sacrificed. Designed for the AWGN channel, TCM employs set partitioning to progressively increase the minimum Euclidean distance between successive subsets. Set partitioning for 16-QAM is shown in Figure 39. The subsets resulting from successive partitioning have increasing intra-subset distance. Because the final subset has a very large intra-subset distance, uncoded bits can be used to select the signal points within this subset. This technique is referred to as Ungerboeck codes [71]. Figure 40 shows the structure of a 16-QAM Ungerboeck code with a bandwidth efficiency of 3 bit/s/Hz. In principle, a rate  $\frac{3}{4}$  convolutional code can also be used to achieve better gain since there are no parallel transitions, though this comes at the expense of increased decoding complexity.

TCM using signal constellations of higher dimensions are found in [69] and [70]. Schemes using signal constellations derived from lattice theory are presented in [72], [73], [74], [75] and [76].

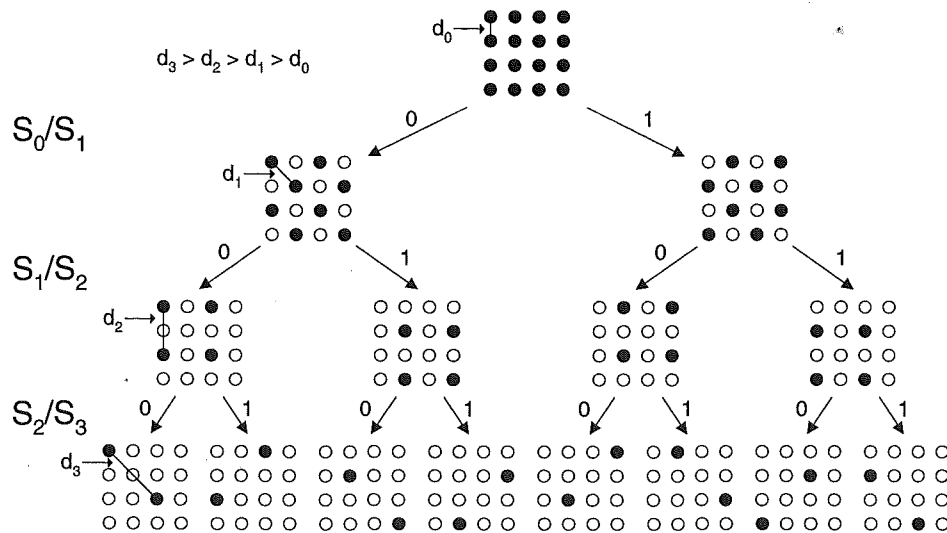


Figure 39 : Set partitioning for a 16-QAM signal constellation.

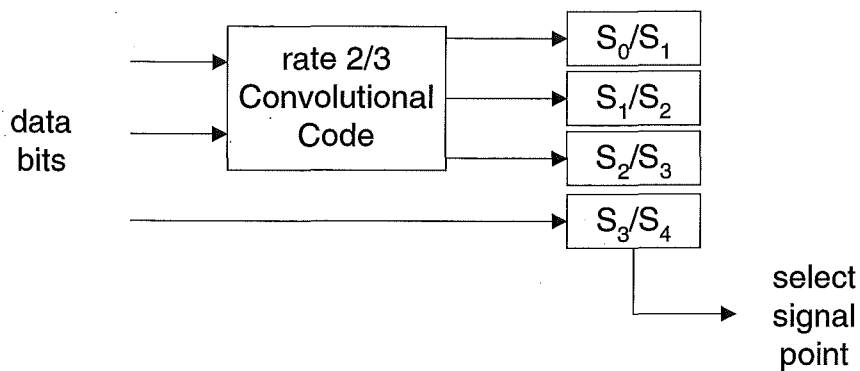


Figure 40 : The structure of a 16-QAM Ungerboeck code with a bandwidth efficiency of 3 bits/s/Hz.

#### 4.2.2 Trellis Coded Modulation for the Rayleigh/Rician Fading Channels

Trellis coded modulation schemes using MPSK modulation were extended to Rayleigh/Rician fading channels by Divsalar and Simon. In [77] the performance criteria were identified. They showed that substantial performance improvement can be achieved using simple TCM schemes combined with interleaving/deinterleaving. Interleaving plays the role of a zero redundancy code that “randomizes” the distribution of the errors, breaking up bursts and destroying the memory of the channel. In [78], optimum code design techniques using set partitioning were

presented. Multiple symbols were associated to a trellis branch to form multiple trellis coded modulation (MTCM). It was shown that MTCM is capable of achieving larger diversities than conventional trellis coded modulation. Other TCM efforts for fading channels can be found in [79] and [80].

#### 4.2.3 Multilevel Codes with Multistage Decoding (MLC/MSD)

Multilevel codes were originally invented by Imai and Hirakawa [81] in 1977. Unfortunately, in the early days, this powerful coding structure failed to find much use in practical applications, partly due to the fact that the multiple error correction codes require multiple decoders at the receiver, which was seen as a implementation disadvantage. Also, in [81], only algebraic decoding was considered.

##### 4.2.3.1 Based on Euclidean Distance

In 1989, Pottie and Taylor [58] applied multilevel codes to set partitions, resulting in a multilevel partition code, shown in Figure 41. The multistage decoder for this code is shown in Figure 42. At about the same time, this idea was also proposed by [59]. As with TCM, the multilevel partition code maximises the minimum Euclidean distance of successive partitions. The result is a very powerful reduced complexity coding structure. A multilevel concatenated partition code was also proposed to produce better performance [82]. This structure is shown in Figure 43. One work employing this structure is found in [83].

In [84] and [85], multilevel codes for the Rayleigh fading channel were presented. Multilevel codes over geometrically uniform partitions in the Rayleigh fading channel was investigated in [86].

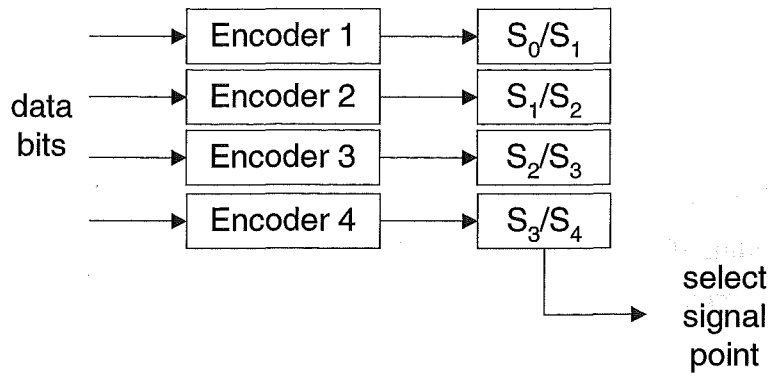


Figure 41 : Multilevel code with set partitioning (multilevel partition code).

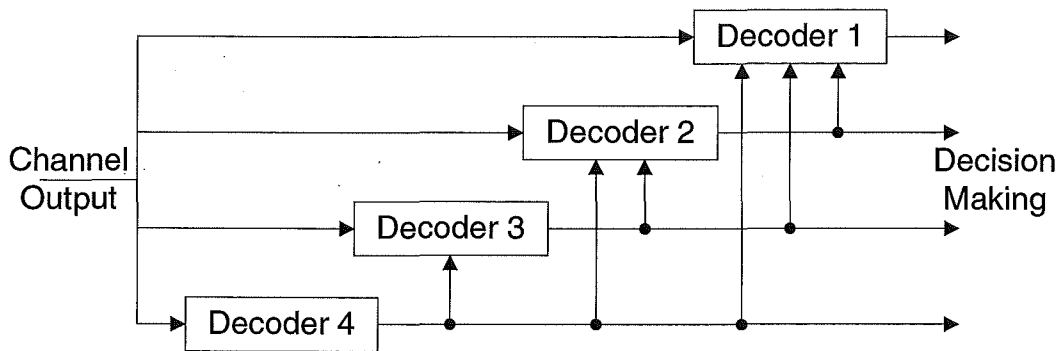


Figure 42 : Multistage decoder (MSD) for a multilevel partition code.

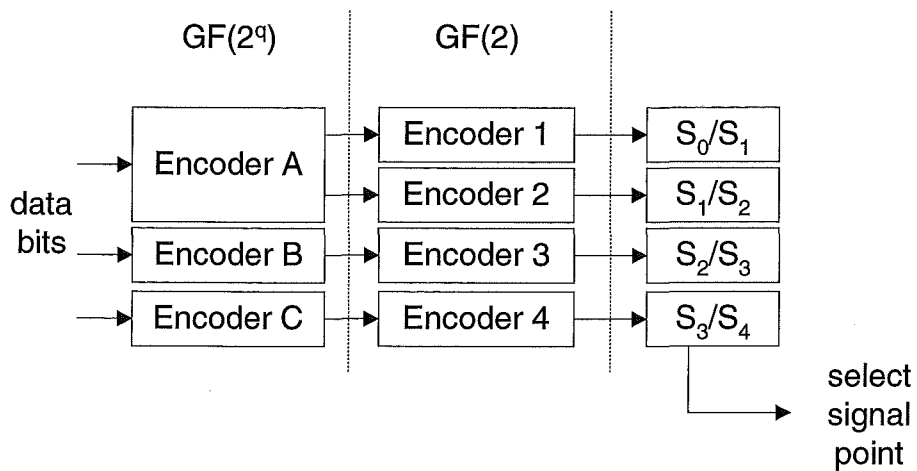


Figure 43 : Multilevel concatenated partition code.

#### 4.2.3.2 Based on Equivalent Channel Capacities

Huber et. al. [87], [88], [89], [90] and Kofman et. al. [91], [92], independently proved that the capacity of a modulation scheme can be achieved by multilevel codes with multistage decoding if and only if the individual rates of the component codes are properly chosen. This was proven using the chain rule for mutual information [93] [94]. The chain rule provides a model with virtually independent parallel channels for each address bit at the different partitioning levels, called equivalent channels. The equivalent channel represents the channel as “seen” by each partition/encoder. The information theoretic parameters of these channels lead to theoretical statements and practical rules for designing and constructing coded modulation schemes [90]. Figure 44 shows the structure of this coding scheme. In the figure,  $r_k$  denotes the code rate of encoder  $k$ , and  $C_k$  denotes the channel capacity of the respective equivalent channels.

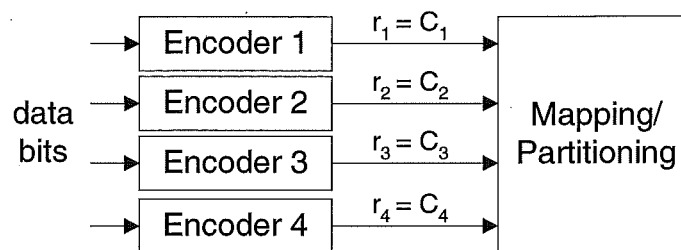


Figure 44 : Multilevel codes designed with equivalent channel capacities.

### 4.3 Coding and Modulation Separated

#### 4.3.1 I-Q Trellis Coded Modulation

This form of TCM is the first small step towards the departure from Ungerboeck's paradigm. I-Q TCM involves splitting a 2 dimensional modulation scheme into 2 independent 1 dimensional modulations, represented by the in-phase and quadrature components. This is shown in Figure 45.

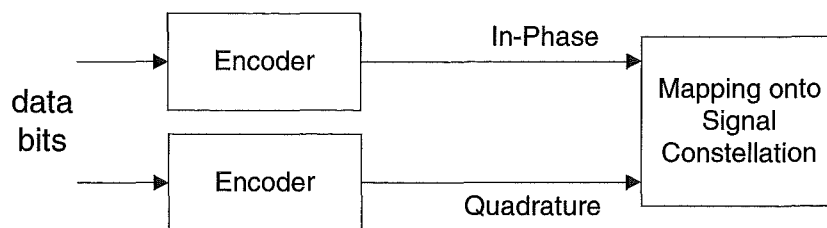


Figure 45 : Structure of an I-Q TCM scheme.

The idea of I-Q TCM first appeared in “pragmatic” TCM design by Viterbi et. al. [95]. Their scheme used 2 off-the-shelf rate  $\frac{1}{2}$  64-state encoders to encode the in-phase and quadrature components of a QAM constellation. This approach results in quadrupling the QAM constellation over what is required over uncoded transmission. For example, to achieve a bandwidth efficiency of 2 bits/s/Hz, 16-QAM is required for the pragmatic scheme compared to 4-PSK for the uncoded scheme. In [96], Heegard et. al. uses off-the-shelf convolutional codes with QAM modulation and demonstrated how coded QAM modulation can be implemented using QPSK-based coded modulation. This was shown to eliminate the need to quadruple the signal constellation size. In [97], the I-Q approach was used for transmitting 2 bits/s/Hz on the Rician fading satellite channel. In [98], the performance of I-Q TCM with 2 parallel 4-state encoders was compared the that of an 8-state 8-PSK trellis code. A large coding gain in the Rayleigh fading channel is achieved by using IQ-TCM. In [64], generalisation of these previous works are presented for spectral efficiencies of 1, 2 and 3 bits/s/Hz. Comparison to conventional TCM using convolutional codes of different constraint lengths show that I-Q TCM schemes offer a significant performance advantage in the Rayleigh fading channel.

#### 4.3.2 Zehavi’s Bit Interleaving Coded Modulation (Multiple Interleavers)

Bit interleaved coded modulation as we know it today was originally proposed by Zehavi in [61]. In the paper, Zehavi constructed a coded modulation scheme employing a rate  $\frac{2}{3}$  convolutional code with 8-PSK. The novelty of his work lies in the use of 3 bit interleavers instead of 1 symbol interleaver prior to mapping the coded bits to modulation symbols. The symbol interleaver and bit interleaver schemes are shown in Figure 46 and Figure 47 respectively. His work has shown that, compared to

symbol interleaving, bit interleaving produces superior performance in the Rayleigh fading channel because the diversity of the coded modulation scheme is increased. His work was extended by Kofman [62], [92] to multilevel codes designed using equivalent channel capacities, shown in Figure 48. Each equivalent channel is encoded by a separate encoder.

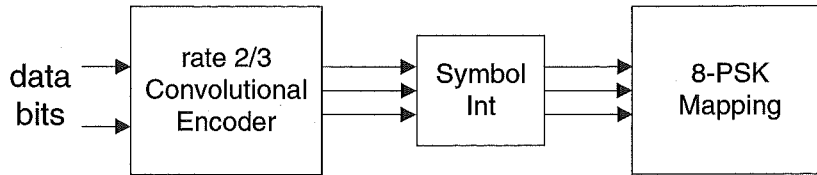


Figure 46 : Conventional coded modulation with symbol interleaving.

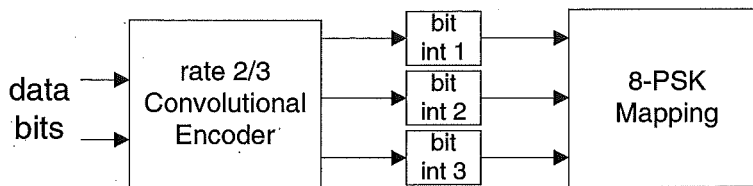


Figure 47 : Zehavi's coded modulation design using 3 bit interleavers.

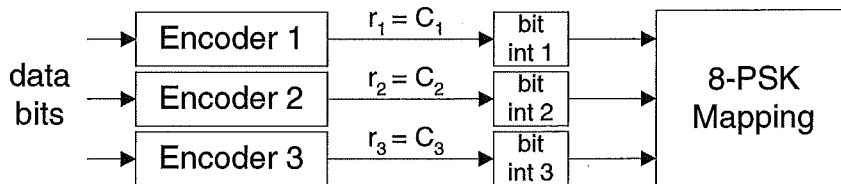


Figure 48 : Kofman's extension of Zehavi's work to multilevel codes.

### 4.3.3 Channel Symbol Expansion Diversity (CSED)

In [99], [100], [65], channel symbol expansion diversity (CSED) was proposed. Traditionally, in order to achieve the same bandwidth efficiency as an uncoded system, a 2-fold signal constellation expansion is used to offset for the redundant bits due to coding. For example, to achieve 2 bits/s/Hz, a typical uncoded system uses 4-PSK whereas Ungerboeck's approach would employ 8-PSK with a rate 2/3 code.

Hansson's proposal employs a 4-fold signal constellation expansion<sup>5</sup>. In his work, 16-QAM was used with a rate 2/4 code to achieve a bandwidth efficiency of 2 bits/s/Hz. Zehavi's bit interleaving was also used in his scheme to increase the code diversity. Hansson's results show that, in the Rayleigh fading channel, the 4-fold expansion scheme performs better than the 2-fold expansion scheme due to the increased code diversity of the rate 2/4 code.

#### 4.3.4 Multilevel Codes with Independent Decoding on Levels (MLC/IDL)

The multistage decoder for multilevel codes designed using the equivalent channel capacities method was shown to be the optimum decoder structure [87] [88].

Unfortunately, the optimality only applies to the asymptotic case (i.e. optimum for codes of infinite length). For finite codeword lengths, there is inherent error propagation in the multistage decoder which may lead to a significant performance degradation. In [66], an alternative decoding structure for multilevel codes was proposed to overcome the error propagation problem. Independent decoding on levels (also known as parallel decoding of levels) avoids the error propagation by treating each level separately. The decoder structure is shown in Figure 49.

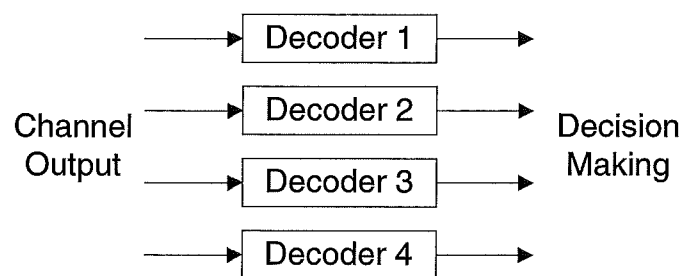


Figure 49 : The decoder structure for multilevel codes with independent decoding on levels (MLC/IDL).

---

<sup>5</sup> Note that this idea can be traced back to earlier pragmatic I-Q TCM efforts such as the work of Viterbi [95]. The subtle difference is that Viterbi used 2 encoders whereas Hansson used only 1 encoder.

Although the MLC/IDL scheme in [66] uses symbol interleaving instead of bit interleaving, an analogous effect to bit interleaving is achieved. This is because each level is comprised of a different encoder and at the decoder, the separate decoders in each level produces the independence effect similar to a bit interleaving scheme. Schramm demonstrated via simulations that MLC/IDL produces the best overall performance when compared to MLC/MSD in both the AWGN and Rayleigh fading channels. A variant of multilevel coding based on Multiple Classes of Levels was considered for an evolved GSM and IS-136 system in [101].

#### 4.3.5 Caire's Bit Interleaved Coded Modulation (Single Interleaver)

Zehavi's multiple interleaver bit interleaving scheme was generalised by Caire et. al. in [102], [63]. Instead of using separate bit interleavers for the encoder output, all the bit interleaving is performed by only 1 bit interleaver, resulting in Bit Interleaved Coded Modulation (BICM). A BICM scheme using a rate  $\frac{3}{4}$  convolutional code with 16-QAM is shown in Figure 50. Using a single interleaver, the BICM scheme can be modelled using the equivalent parallel channel model shown in Figure 51 [63]. Extensive analysis performed in [63] shows the superiority of BICM in the Rayleigh fading channel. The work of [90] mentions the similarities between BICM and MLC/IDL.

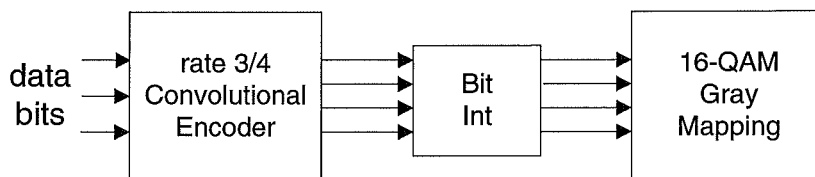


Figure 50 : Caire's single interleaver bit interleaving scheme, generalised from Zehavi's multiple interleaver scheme.

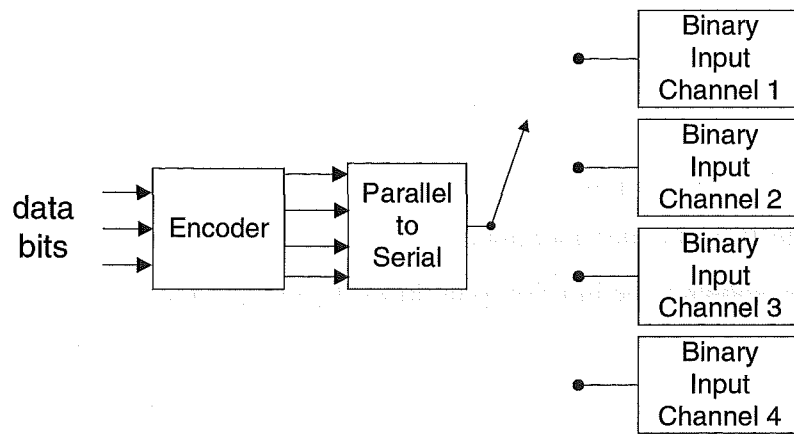


Figure 51 : Equivalent parallel channel model for a 16-QAM BICM scheme.

#### 4.4 Coded Modulation Employing Turbo Codes

Since the invention of Turbo codes, there have been numerous efforts to incorporate Turbo codes into coded modulation. The first attempt to employ Turbo codes in a pragmatic approach to TCM was the work of [18]. Soon after that, Turbo codes were applied as component codes in multilevel codes [103]. Using the equivalent channel capacity technique applied to multilevel codes with multistage decoding, the performance of 8-PSK, 16-QAM, 32-QAM and 64-QAM in the AWGN was shown to be less than 1 dB away from the AWGN channel capacity using blocklengths of 20,000 bits. The work of [104] and [105] introduced the idea of iterative multistage decoding. Turbo Trellis Coded Modulation (TTCM) schemes were proposed in [106], [107], [108], [109], [110]. Parallel and serial concatenated TCM schemes were reported in [111] and [112] respectively. More recent implementations of turbo codes with bit interleaved coded modulation are found in [113], [114], [115], [60], and [116].

## 4.5 Summary

An overview of key developments in coded modulation has been presented in this chapter. Bit interleaved coded modulation (BICM) is a relatively new scheme. While BICM has been shown to be inferior to multilevel coding in the AWGN channel [90], various works in the literature consistently suggest that separating coding and modulation increases the code diversity effect, and therefore, it is advantageous in the Rayleigh fading channel [61] [60]. Because the channels encountered in practical mobile systems are mostly of the Rayleigh type, it is suggested that BICM may be a practical solution. As the primary of interests of this thesis is the Rayleigh fading channel, the work in subsequent chapters employs BICM with simple concatenated coding schemes.

# **CHAPTER 5 : PERFORMANCE OF CONCATENATED SINGLE PARITY CHECK CODES WITH BIT INTERLEAVED CODED MODULATION**

## **5.1 Introduction**

In this chapter, all the codes designed in Chapter 3 are extended to BICM. The error performance of Symbol Interleaved Coded Modulation (SICM) and Bit Interleaved Coded Modulation (BICM) are compared in the independent Rayleigh fading channel. The performance of all the parallel and serially concatenated SPC codes are compared using BICM, and then benchmarked against the best schemes in the literature. Decoding complexity estimates are provided for both schemes. Convergence of the decoding algorithms is also discussed.

## **5.2 System Model**

Figure 52 shows the system model being considered. All the channel coding schemes used in this chapter have the same input data block of 900 bits and output block length

of 1200 bits, resulting in an overall code rate of  $\frac{3}{4}$ . For BICM, a random bit interleaver precedes the mapping process order to scramble the bit mappings onto the channel symbols. For SICM, this bit interleaving process is omitted. The AWGN and the independent Rayleigh fading channels are considered here. At the receiver, we have assumed that coherent demodulation is performed with the presence of perfect channel state information. After computing the metrics, the minimum metrics are selected and then deinterleaved to reverse the effect of the bit interleaving. The decoder accepts the deinterleaved metrics and starts the decoding process. The MAP algorithm for SPC codes in Appendix I is used.

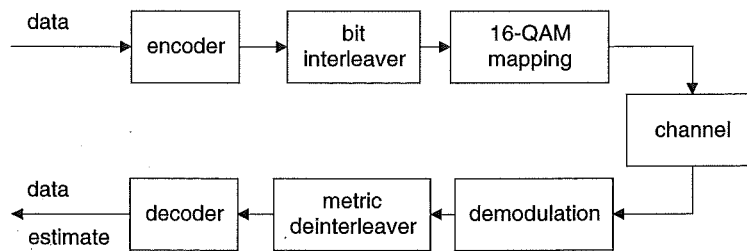


Figure 52 : System model .

The coded bits are transmitted using Gray mapped 16-QAM as in Figure 53. In both the AWGN and Rayleigh fading channels, the demodulation process is performed by treating 16-QAM as 2 independent 4-ASK channels [117] as shown in Figure 54. Two separate sets of the metric are computed. The first set is computed using the real part of the received sample and the 4 amplitude levels of the in-phase channel, whereas the second set is computed using the imaginary part of the received sample and the 4 amplitude levels of the quadrature channel. With 16-QAM, the received sample is compared to all 16 symbols on the signal constellation. With 4-ASK, the received sample is compared to 4 symbols on each 4-ASK channel, which sums up to a total of 8 symbols because there are 2 channels (in-phase and quadrature). This reflects a 50% saving in demodulation complexity <sup>6</sup>. The squared Euclidean distance metric for 4-ASK is 1 dimensional whereas the metric is 2 dimensional for 16-QAM. This results in a further reduction in demodulation complexity. Overall, the total complexity of the

<sup>6</sup> By demodulation complexity, we are referring to the complexity of the entire metric computation process.

demodulation process is less than half of the demodulation complexity of standard 16-QAM.

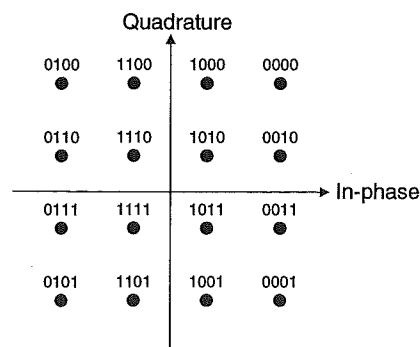


Figure 53 : Gray mapped 16-QAM signal constellation.

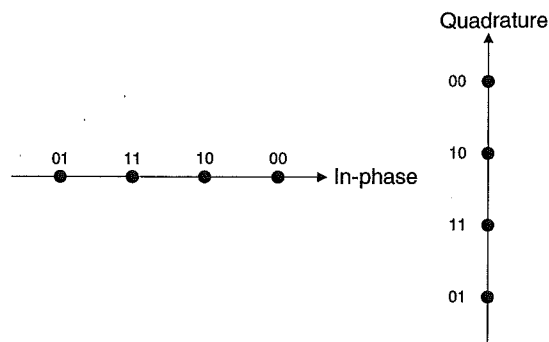


Figure 54 : Splitting the gray mapped 16-QAM constellation into 2 independent gray mapped 4-ASK constellations.

## 5.3 BICM versus SICM

### 5.3.1 Equivalent Parallel Channel Model

In [63], the concept of an equivalent parallel channel model for BICM systems was presented. This is shown in Figure 55 for the Gray mapped 16-QAM signal constellation. For 16-QAM, each signal point represents 4 bits. Each bit position sees a slightly different channel. Both BICM and SICM can be represented using the parallel channel model of Figure 55. The only difference is that in SICM, each bit

position is fixed to 1 of the 4 parallel channels, whereas in BICM, consecutive bits hop randomly among all parallel channels as determined by the random bit interleaver. The correlation effect caused by the modulation process through the use of a fixed channel (ie SICM) is broken by channel hopping, thereby increasing the code diversity.

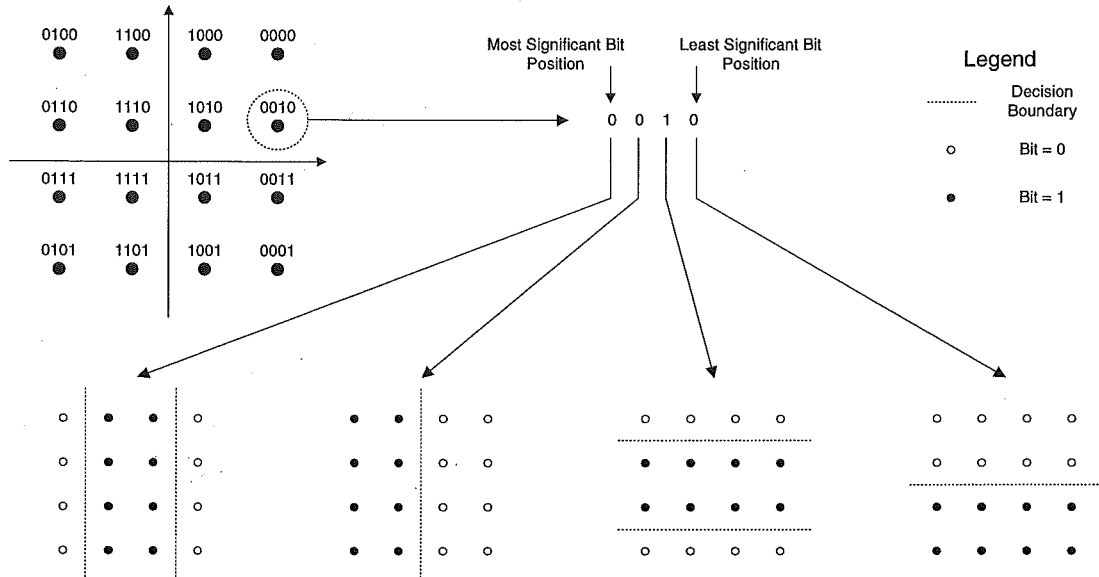


Figure 55 : The equivalent parallel channel model for a Gray mapped 16-QAM signal constellation.

### 5.3.2 Performance Comparison

The channel codes used in the SICM and BICM comparisons are the 3 and 4 dimensional parallel concatenated (3-, 4-PC) single parity check (SPC) codes. The code structures are shown in Figure 56 and Figure 57 respectively. Random interleavers are used in the encoders.

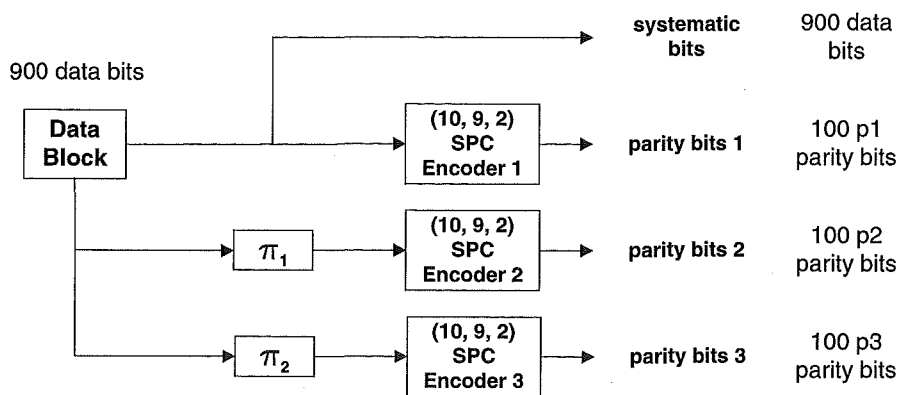


Figure 56 : Encoder structure 3-PC-SPC.

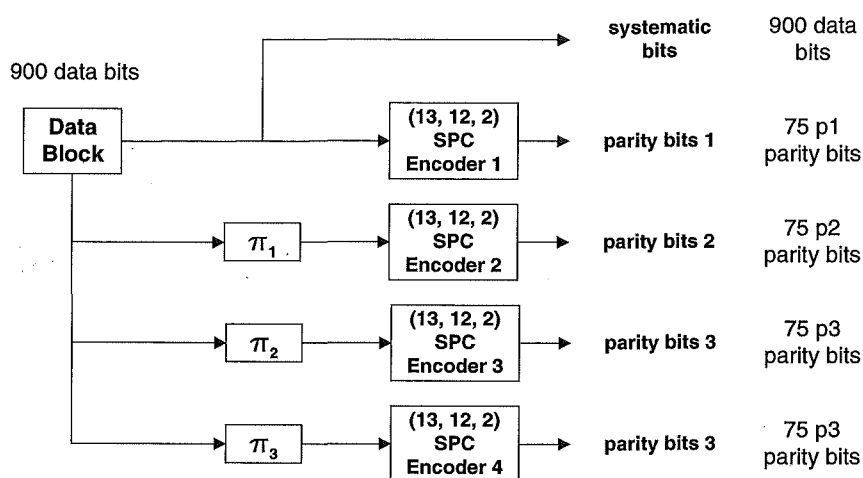


Figure 57 : Encoder structure for 4-PC-SPC.

Figure 58 compares the performance of SICM and BICM in the Rayleigh fading channel with 16-QAM using the 3-PC SPC code. At low SNR, BICM gains about 0.6 dB over SICM. However, at high SNR, the gap increases significantly to more than 4 dB at  $5 \times 10^{-6}$ . A closer look at the code structure of the 3-PC-SPC code structure employed in the simulation reveals that this huge gain is not entirely contributed by the BICM interleaver. It was discovered that bad random interleavers used for the 3-PC-SPC code structure was the primary reason. Thus, good interleaver design is essential in designing codes for the fading channel.

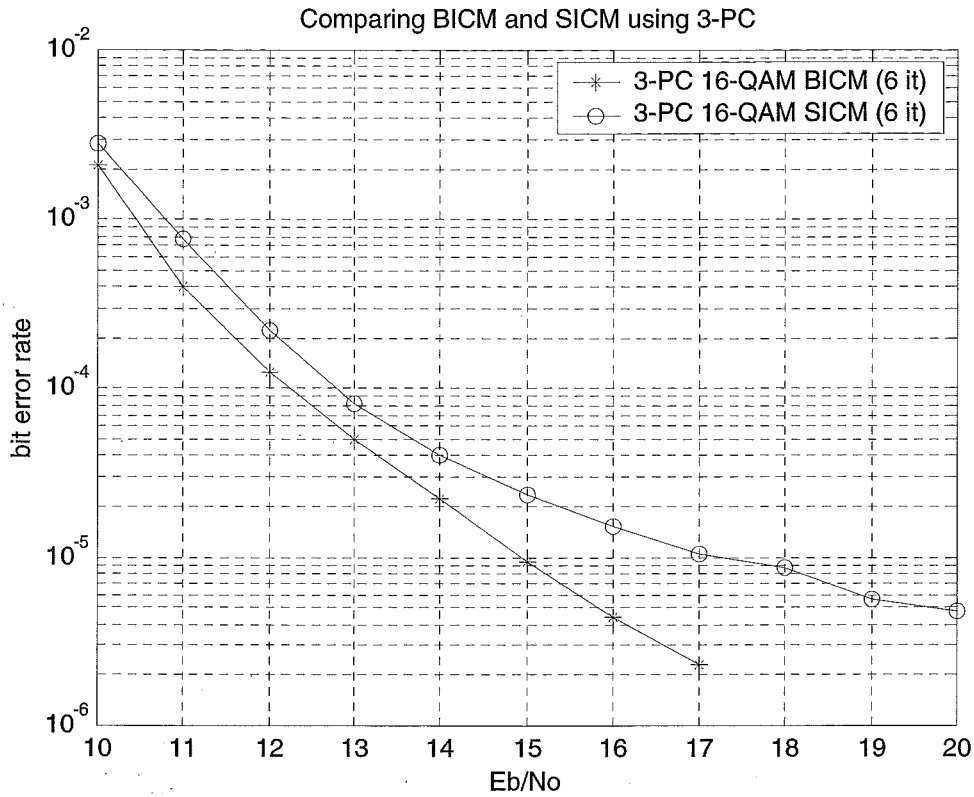


Figure 58 : Comparing SICM with BICM in the fading channel using 3-PC-SPC.

To show this effect, better random interleavers are used. The better random interleaver is generated by “random luck” without any particular care in design. Figure 59 shows the performance of SICM and BICM using better random interleavers. It is observed that the flooring effect seen previously for the SICM case is not present. This implies that that BICM’s superiority over SICM is largely dependent on the type of channel coding employed. If the channel coding scheme has properly designed bit interleaving, then the resultant gap between SICM and BICM will be small. This marginal gain is also reported in [66]. Although the gain is marginal, BICM appears to always be better than SICM in the fading channel. These results also imply that BICM is capable of compensating to some extent for a badly designed channel coding scheme (i.e. poor random interleaver).

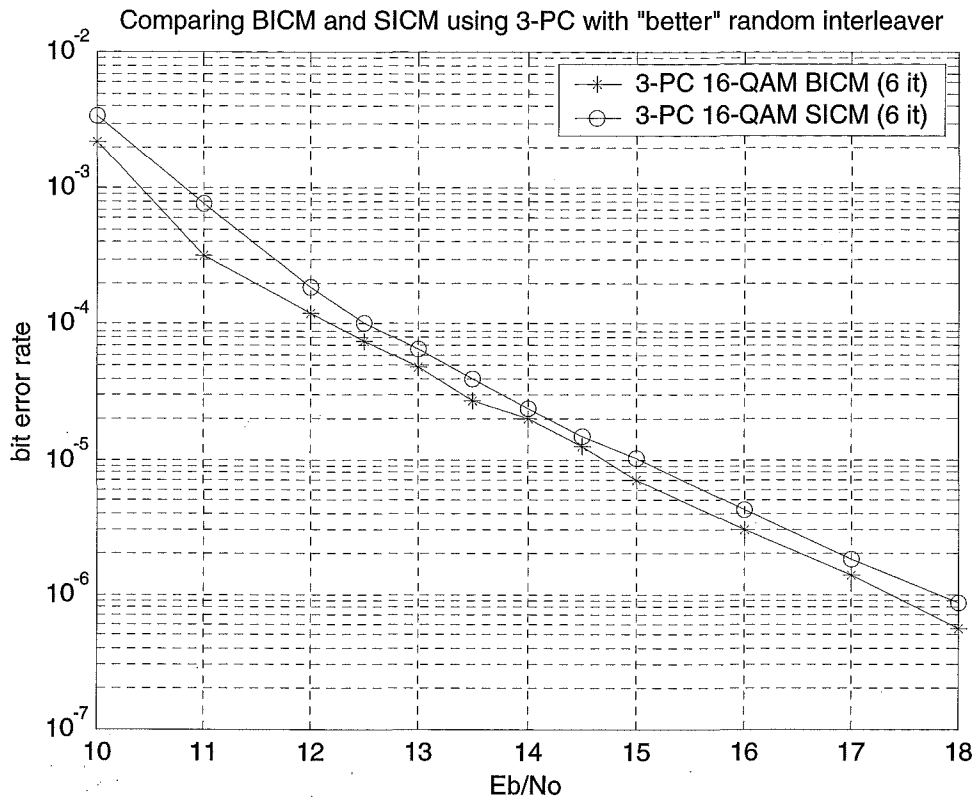


Figure 59 : Comparing SICM and BICM in the fading channel using 3-PC-SPC with “better” random interleaver.

#### 5.4 Performance of Multiple Parallel Concatenated SPC Codes

In this section, simulation results for  $M = 2, 3, 4, 5$  and 6 dimensional PC-SPC structures are presented. The component codes for each scheme and the minimum Hamming distance of the overall code are summarised in the Table 4.

Figure 60 shows the performance of these codes in the AWGN channel. The number of decoding iterations used in each curve represents the near-best performance, where further iterations result in little or no gain. In general, the curves show performance improvements and the lowering of error floors with an increasing number of parallel concatenations. By increasing the number of parallel concatenations, the minimum Hamming distance of the code improves, and therefore, the error floor effect is gradually lowered. The 4-PC scheme is the best scheme at  $10^{-4}$ . At  $10^{-5}$ , 5-PC gives

the best performance. At  $10^{-6}$  and beyond, the 6-PC scheme yields the best performance. The improved error floor performance comes at the expense of the waterfall region.

M-PC-SPC Coding Scheme	Component SPC Code	Minimum Hamming Distance
2-PC-SPC	(7, 6, 2)	3
3-PC-SPC	(10, 9, 2)	4
4-PC-SPC	(13, 12, 2)	5
5-PC-SPC	(16, 15, 2)	6
6-PC-SPC	(19, 18, 2)	7

Table 4 : M-PC-SPC schemes being investigated.

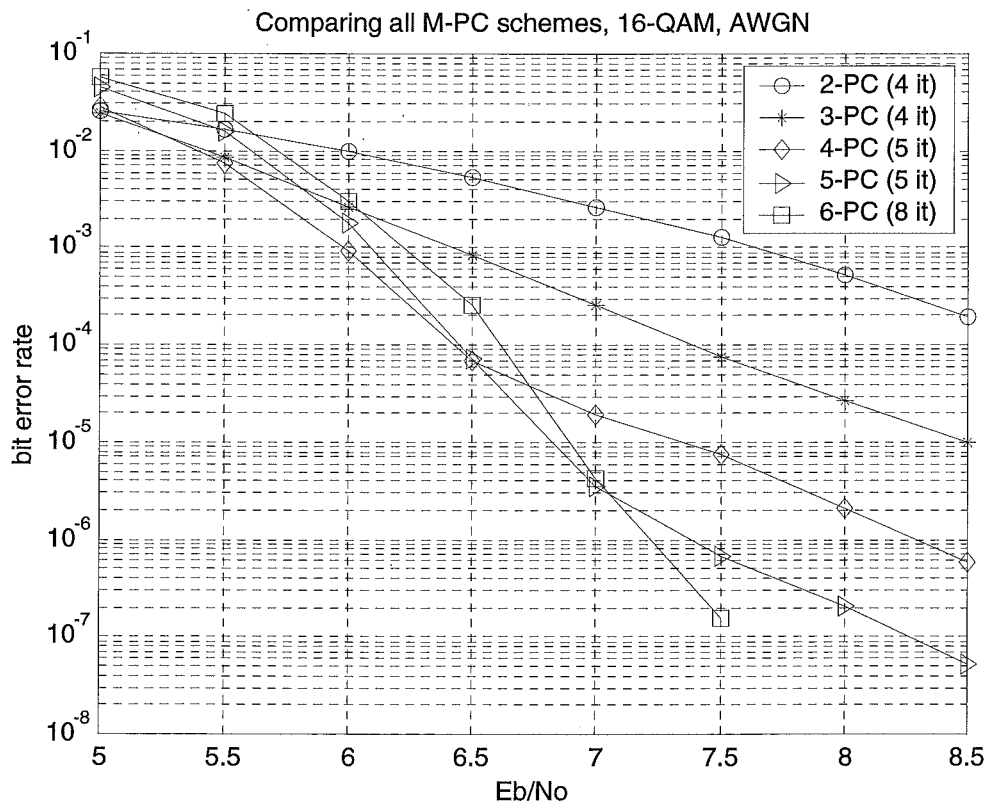


Figure 60 : Performance of 2, 3, 4, 5 and 6-PC-SPC using 16QAM in the AWGN channel. Based on [63], the channel capacity and cutoff rate for 3 bits/sec/Hz using 16-QAM BICM over the AWGN channel is about 4.5 dB and 6.7 dB respectively.

Figure 61 shows the performance of the same codes in the Rayleigh fading channel. There is clear evidence of an increasing diversity effect as the number of

concatenations increases. Again, this is due to the increasing minimum Hamming distance. Because the minimum Hamming distance of the M-PC-SPC code is equal to  $M+1$ , the slope of the BER curve steepens with increasing  $M$  prior to the floor effect.

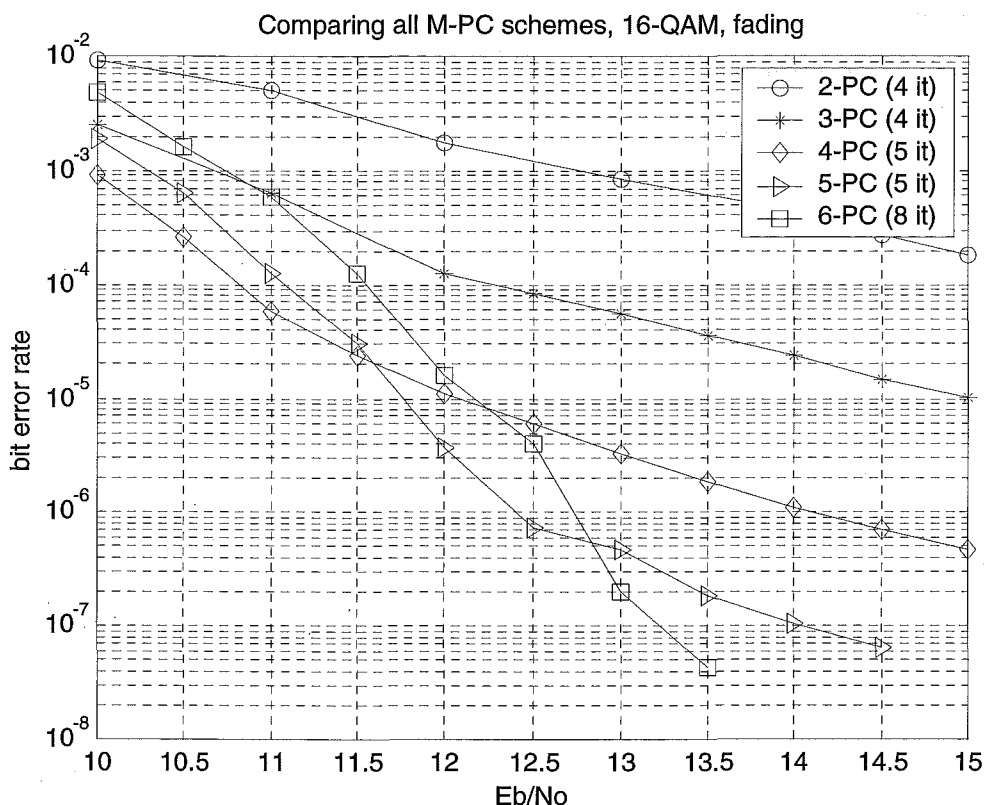


Figure 61 : Performance of 2, 3, 4, 5 and 6-PC-SPC using 16-QAM in the independent fading channel. Based on [63], the channel capacity and cutoff rate for 3 bits/sec/Hz using 16-QAM BICM over the Rayleigh fading channel is about 7.7 dB and 10.7 dB respectively.

### 5.5 Performance of Multiple Serially Concatenated SPC Codes

Simulation results for  $M = 2, 3, 4, 5$  and  $6$  are presented here. As with the parallel concatenated SPC codes, all M-SC-SPC codes are designed with an input data block length of 900 bits and an output code length of 1200 bits, resulting in an overall code rate of  $\frac{3}{4}$ . The component codes for each scheme are shown in Table 5.

Figure 62 shows the performance of 2, 3, 4, 5, and 6-SC-SPC using 16-QAM BICM codes over the AWGN channel. Again, graphs are plotted using the near best number of decoding iterations. The figures show improved performance at low bit error rates

with increasing dimensionality. Above  $10^{-5}$ , the 4-SC-SPC code is the best scheme. Below that, 5-SC-SPC is the superior scheme. The performance of the same codes in the independent fading channel is shown in Figure 63. A similar trend in performance improvements is observed as the dimensionality increases. Again, the improved performance in the error floor region comes at the expense of the waterfall region. The 4-SC-SPC code is the best scheme above  $10^{-6}$ . Below that level, the 5-SC-SPC code is the best. 6-SC is expected to dominate only at very low bit error rates.

M-SC-SPC Coding Scheme	Component SPC Code
2-PC-SPC	(7, 6, 2)
3-PC-SPC	(10, 9, 2)
4-PC-SPC	(13, 12, 2)
5-PC-SPC	(16, 15, 2)
6-PC-SPC	(19, 18, 2)

Table 5 : M-SC-SPC schemes considered.

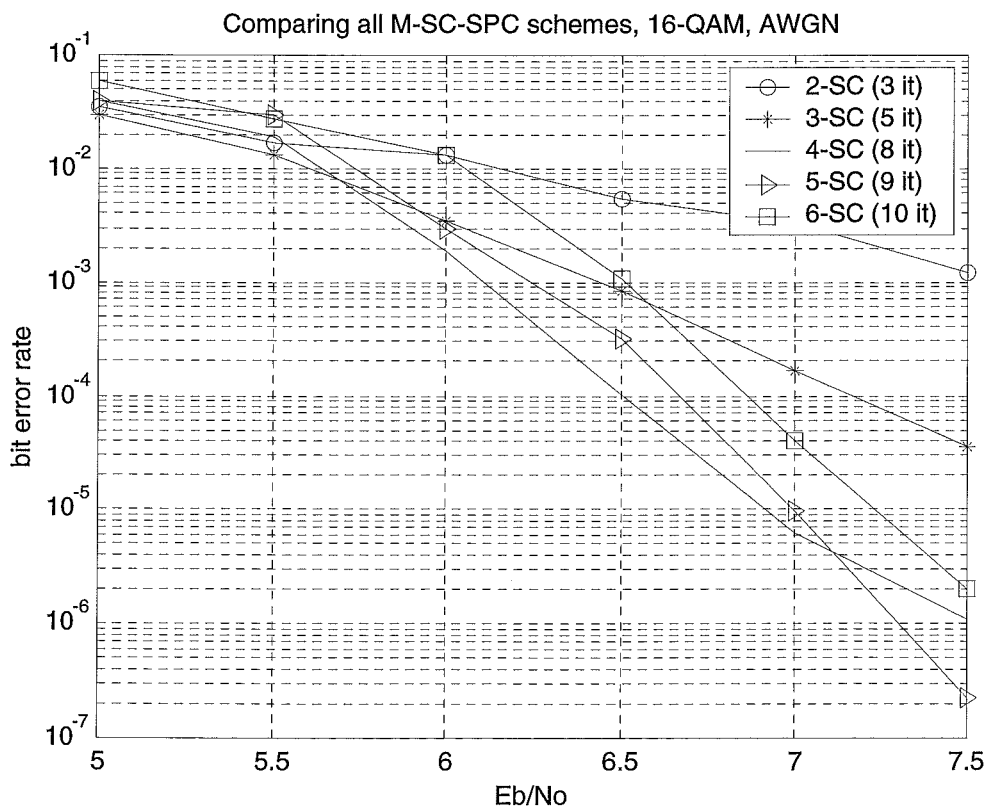


Figure 62 : 2, 3, 4, 5 and 6-SC-SPC codes using 16-QAM in the AWGN channel.

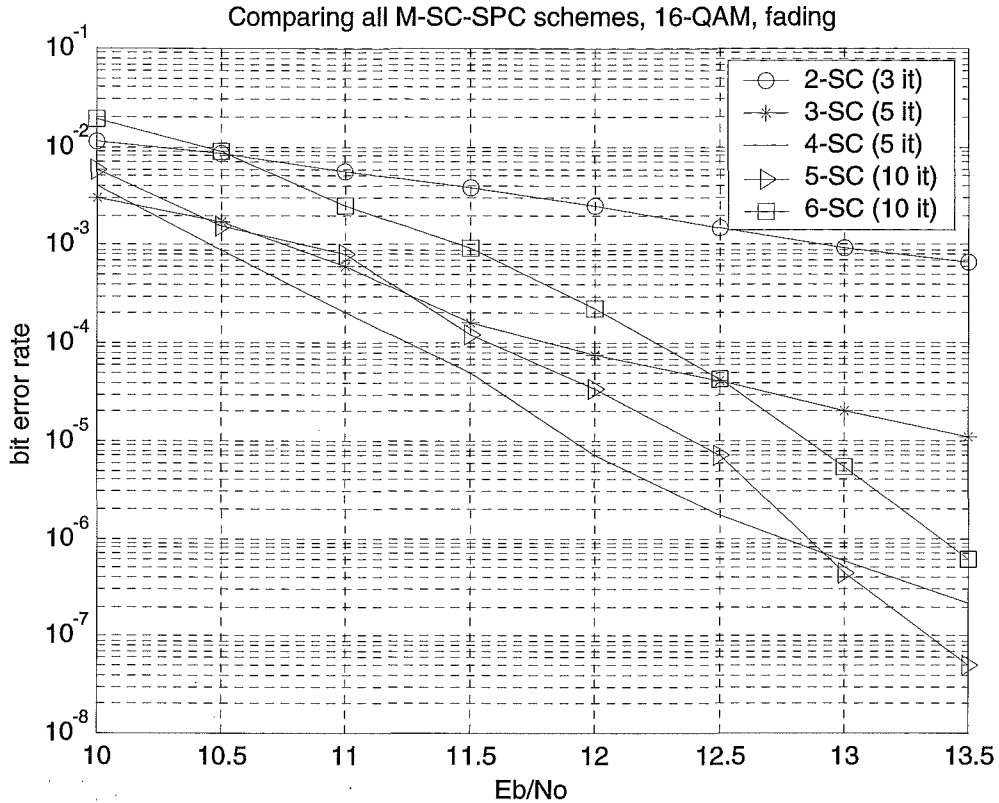


Figure 63 : 2, 3, 4, 5 and 6-SC SPC codes using 16-QAM in the independent fading channel

## 5.6 Performance Comparison and Benchmark

Table 6 compares the performance of parallel and serially concatenated SPC codes against the best schemes available in the literature at  $10^{-4}$ . The 4-PC and 4-SC code are used for comparison since they achieve the best BER performance at  $10^{-4}$  among all the parallel and serially concatenated SPC codes considered. All schemes have identical code parameters; code rate is  $\frac{3}{4}$ , data block length is 900 bits and the modulation scheme is 16-QAM. From Table 6, the 4-PC code is the best among all the codes in the fading channel. In the AWGN channel, it is second only to the AWGN multilevel 16-state Turbo code. The inferior performance of BICM compared to MLC/MSD is as predicted by [90]. It outperforms the 16-state BICM Turbo code by 0.1 dB in both channels. Moreover, this is achieved with only 5 iterations

compared to 6 iterations for the Turbo code. There is a gain of about 0.3 dB and 0.5 dB over the 4-SC code in the AWGN and fading channels respectively. Both the 4-PC and 4-SC codes scheme perform better than the best 64-state multilevel convolutional codes in both channels.

	Fading Channel	AWGN Channel
Best 64-state punctured convolutional codes with MLC/MSD designed for fading channel [101]	12.2 dB	8.2 dB
Best 64-state punctured convolutional codes with MLC/MSD designed for AWGN channel [101]	> 14.0 dB	7.0 dB
16-state Turbo codes with MLC/MSD designed for AWGN channel – 6 iterations [60]	12.1 dB	6.0 dB
16-state Turbo codes with BICM – 6 iterations [60]	10.9 dB	6.5 dB
4-SC-SPC code – 5 iterations	11.3 dB	6.7 dB
4-PC-SPC code – 5 iterations	10.8 dB	6.4 dB

Table 6 : Performance comparison of the best schemes in literature at BER =  $10^{-4}$ .

Figure 64 compares the performance of 3-PC, 4-PC with 3-SC and 4-SC at a wider range of bit error rates in the fading channel. The performance curves show that 3-PC is slightly superior to 3-SC above  $10^{-3}$ . However, as the bit error rate moves below  $10^{-4}$ , 3-SC becomes superior. Above  $10^{-5}$ , the 4-PC is the better scheme. However, as the error rates decrease further, the 4-PC scheme hits an error floor before the 4-SC scheme does. Below  $10^{-5}$ , the superiority of 4-SC is not matched by the 4-PC scheme.

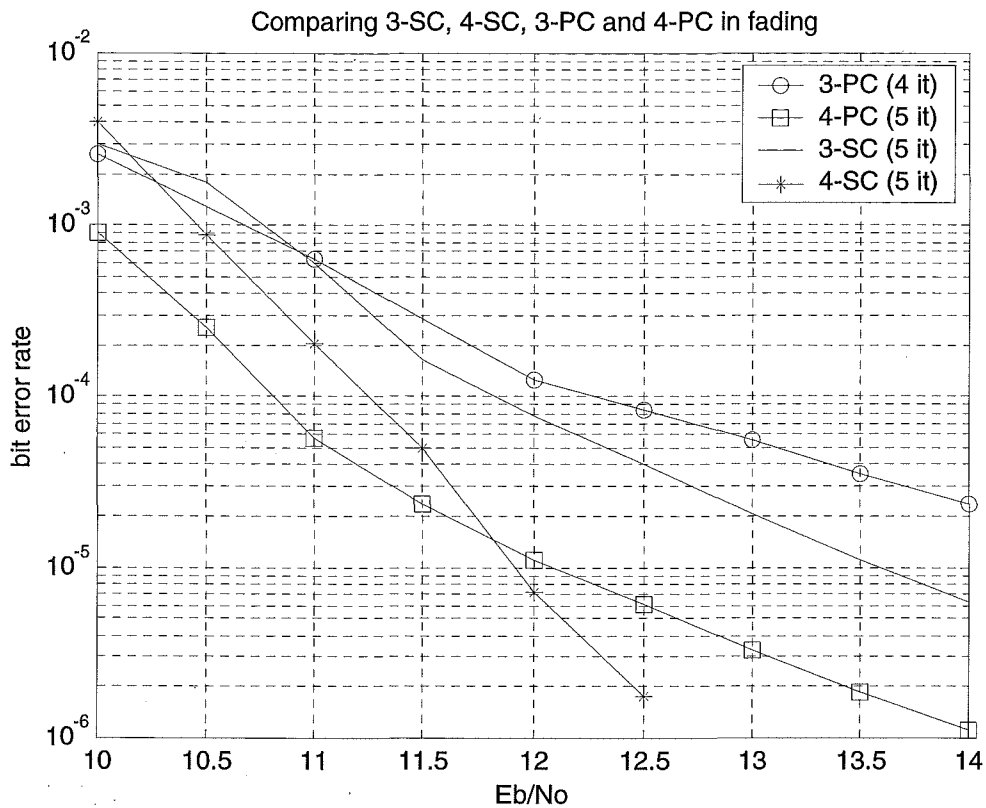


Figure 64 : Comparison of 3-SC, 4-SC, 3-PC and 4-PC in the Rayleigh fading channel.

## 5.7 Decoding Complexity

The decoding complexity of any decoding algorithm varies with different implementation methods and trade-offs. In this section, a rough estimate of the decoding complexity for the 4-PC-SPC code is provided. The complexity is compared to those of Turbo codes and convolutional codes.

An approximate per-data-bit Viterbi decoding complexity of a rate  $\frac{1}{2}$  convolutional code is given by [15]

$$C_{\text{conv}} = 3S$$

where  $S$  represents the number of states in the trellis. In [15], the Log-MAP decoding complexity of the rate 1/3 Turbo code was estimated <sup>7</sup>. Here, the per-data-bit Log-MAP decoding complexity of the Turbo code is approximated using only the dominant factor

$$C_{\text{Turbo}} = 18SI$$

where  $S$  represents the number of states of the component convolutional codes and  $I$  represents the number of decoding iterations. The complexity figures reflect the approximate number of comparison, multiplication and addition operations. This can be used to compare the decoding delays when implemented on a DSP. We note here that operations required for interleaving/deinterleaving of LLRs and other housekeeping operations are not included in this comparison.

The decoding complexity of the 4-SC-SPC code is estimated to be about 33 operations per data bit per iteration. After 5 iterations, the total decoding complexity is 165 operations. A 64-state convolutional code requires a total of 192 operations, whereas the 16-state Turbo code (iterated 5 times) requires 1440 operations. The 4-SC-SPC code is slightly less complex than the 64-state convolutional code. Compared to the 16-state Turbo codes, it is about 9 times less complex.

The decoding complexity of concatenated SPC codes is roughly proportional to the length of their component SPC codes. In comparison to the 4-SC code, the 4-PC code is about 10% less complex because of shorter component SPC codes – (13, 12, 2), (14, 13, 2), (15, 14, 2) and (16, 15, 2) SPC codes for the 4-SC code as compared to four (13, 12, 2) SPC codes for the 4-parallel concatenated SPC code. Using the 4-SC scheme as a baseline for comparisons, the 4-PC scheme requires about 30 operations per data bit per iteration. This is approximately 10 times less complex than the 16-state Turbo code.

---

<sup>7</sup> The Turbo code considered in [60] is basically a rate 1/3 scheme, with appropriate puncturing to give the targeted code rate. A punctured trellis has the same trellis complexity as a non-punctured trellis. Therefore, we can estimate the decoding complexity of a punctured Turbo code using the rate 1/3 Turbo code.

## 5.8 Convergence of the Decoding Algorithm

The performance curves presented in previous figures represent the near-best achievable performances respectively. This means that further decoding iterations will result in only slightly better performances. Figure 65 shows the convergence characteristics of the decoding algorithm for the 4-PC code in the fading channel. The convergence is smooth and does not exhibit any instability. Smooth convergence is obtained in all parallel concatenated SPC codes investigated in this work. It is observed that the optimum number of iterations varies with SNR. At 10.0 dB, there are still small gains obtained if the decoding is pushed beyond 5 iterations. However, at 15.0 dB, there is virtually nothing to be gained beyond 3-4 iterations. Fast and stable convergence are both very desirable properties.

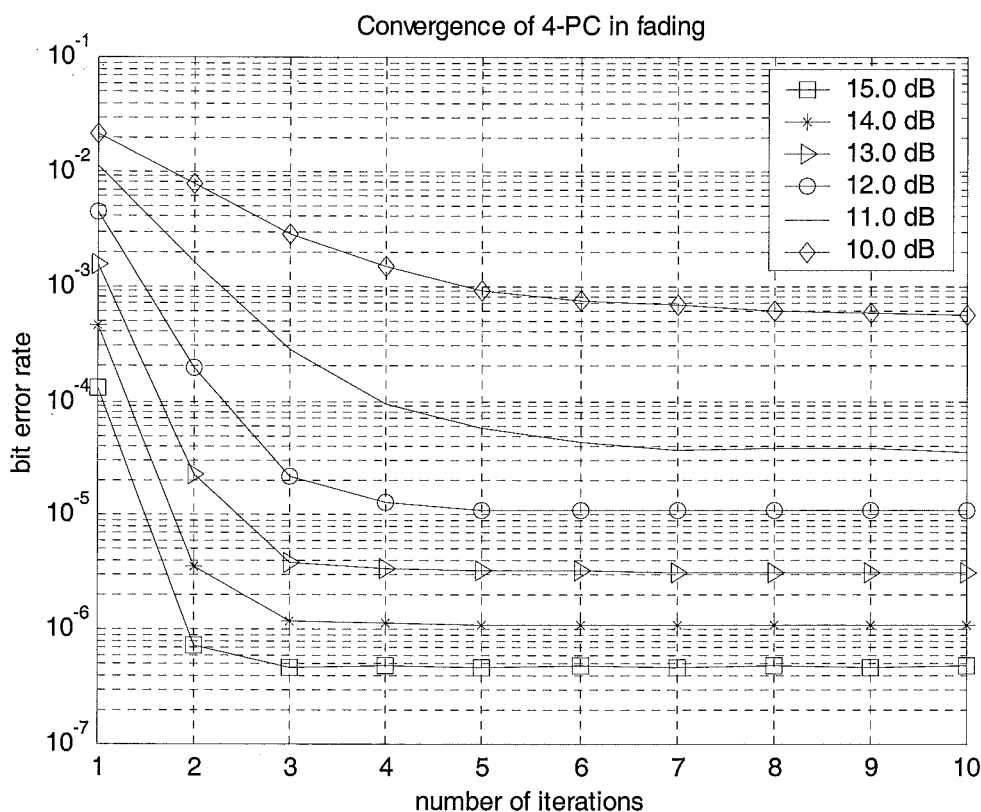


Figure 65 : Convergence characteristics of the decoding algorithm of 4-PC in the fading channel.

M-SC-SPC codes show negligible or no convergence problems in the AWGN channel. However, in the fading channel, some convergence problems begin to surface for 4, 5 and 6-SC-SPC codes. Based on our simulations, the most severe case appears to be the 4-SC-SPC, shown in Figure 66. It is observed that the bit error rate may get worse as the number of iterations is increased. The decoding algorithm starts to exhibit some instability below  $10^{-5}$  at around 12.0 dB after 9 iterations. We note that if the suboptimum decoder structure for serially concatenated codes is used, simulation results have shown that the convergence problem becomes more severe. This behaviour is not likely to be contributed by numerical problems within the simulation setup, otherwise, it would have been noted in all other results. The convergence behaviours are not yet understood at this time.

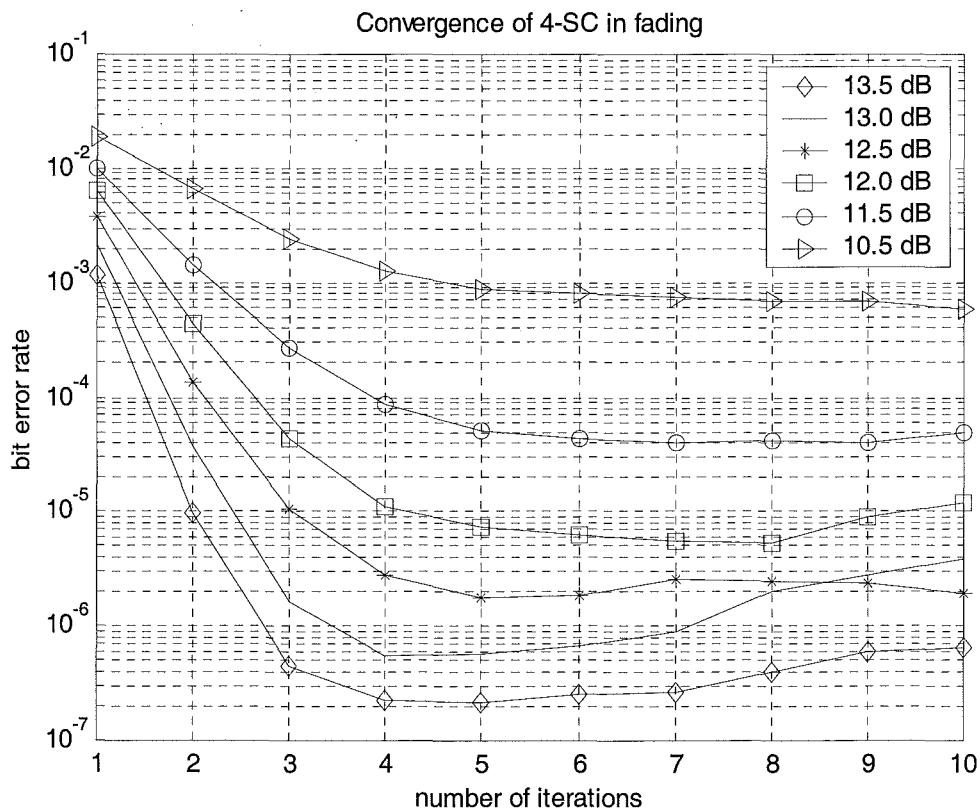


Figure 66 : Convergence of the 4-SC-SPC code in the fading channel using the improved decoder structure.

## 5.9 Summary

The performances of SICM and BICM are compared in the independent Rayleigh fading channel. Simulation results here show that the superiority of BICM over SICM is dependent on the type of channel coding employed. Nevertheless, results show that the extra interleaving provided by the BICM produces an error performance that is always better than SICM in the independent Rayleigh fading channel. BICM is not as sensitive to the code (interleaver) design compared to SICM. Also, BICM is capable of partially compensating for badly designed interleavers within the code structure. With proper code design, particularly combined with Multilevel Codes, the gain of BICM over SICM is marginal.

The performance of concatenated SPC codes compares very favourably to other schemes in the literature. At  $10^{-4}$ , the 4-PC code outperforms the best multilevel convolutional codes and is only inferior to the AWGN multilevel 16-state Turbo codes in the AWGN channel. Based on the work in this chapter, it can be concluded that there is no single concatenated SPC coding scheme that offers the best performance for every bit error rate. The parallel codes are superior at medium to low BER. Beyond that, they start to encounter error floors and the serial codes begin to show superiority.

Decoding complexity estimates for concatenated SPC codes are provided. Based on the estimates, concatenated SPC codes are shown to have significant complexity advantages over Turbo codes. The decoding algorithm for concatenated SPC codes exhibits fast convergence. Convergence is smooth for all parallel concatenated codes investigated. However, in the fading channel, 4, 5, and 6-SC SPC codes exhibit some instabilities. One interesting observation is that the decoding algorithm converges properly up to the first 5 iterations. Therefore, a simple solution to the convergence problem is to limit the decoding to 5 iterations. Even if there is no convergence problem, it would be wise to stop decoding at about 4-5 iterations because additional iterations produce only slight improvement in performance.

1900  
1901  
1902

# CHAPTER 6 : A GENERALISED PERFORMANCE BOUNDING TECHNIQUE FOR BICM SYSTEMS IN THE RICIAN FADING CHANNEL

## 6.1 Introduction

In [63], Caire et. al. presented a comprehensive analysis of BICM in the AWGN and the Rician fading channel. Asymptotic bounds for BICM schemes in the independent Rayleigh fading channel were derived using the BICM Expurgated bound. In this chapter, a generalised performance bounding technique for BICM systems in the Rician fading channel is presented. By using the difference between the BICM Expurgated bounds, it is possible to accurately estimate the error performance of coded BICM systems with larger signal constellations using only the error performance of a BPSK system employing the same channel coding scheme in the same channel. Also, this method is shown to be valid for a wide range of SNR, and to be independent of the type of channel coding scheme and code rate employed. Our work implies that, in the Rician fading channel, analytical bounds for any coding scheme derived for the BPSK system can be easily applied to BICM systems with larger signal constellations in the same channel. In fact, the difference in error

performance is merely a translation factor along the SNR (per bit) axis of the bit error rate vs SNR (per bit) plot. Simulation results are presented to verify the analysis.

As an introduction to the derivation, Sections 6.1 and 6.2 are directly referenced from [63]. The authors of [63] have performed a comprehensive bounding effort for BICM systems. Sufficient details are provided here to follow the derivations. The interested reader is directed to [63] for a more rigorous treatment. Our derivation begins in section 6.3.

## 6.2 BICM Expurgated Bound

In [63], the BICM union bound on the bit error probability is defined as

$$P_{ub} \leq m^{-d} \sum_{\underline{S}} 2^{-d} \sum_{\underline{U}} 2^{-d(m-1)} \sum_{\underline{x} \in X_{\underline{c}}^{\underline{S}}} \sum_{\underline{z} \in X_{\underline{\hat{c}}}^{\underline{S}}} P(\underline{x} \rightarrow \underline{z}) \dots (1)$$

where

$\underline{x}$  denotes the transmitted sequence

$\underline{z}$  denotes the erroneous sequence

$P(\underline{x} \rightarrow \underline{z})$  is the pairwise error probability between the two signal sequences  $\underline{x}$  and  $\underline{z}$

$m$  denotes the number of information bits represented by a signal point on the constellation

$d$  denotes the Hamming distance of the error event

$X$  denotes the choice of signal constellation and

$$X_{\underline{c}}^{\underline{S}} = X_{c_1}^{i_1} \times \dots \times X_{c_k}^{i_k} \times \dots \times X_{c_d}^{i_d}$$

$$X_{\underline{\hat{c}}}^{\underline{S}} = X_{\hat{c}_1}^{i_1} \times \dots \times X_{\hat{c}_k}^{i_k} \times \dots \times X_{\hat{c}_d}^{i_d}$$

denote the sequence (Cartesian product) of signal subsets selected by the bits  $c_k$  of  $\underline{c}$  (correct subsets) and  $\hat{c}_k$  of  $\underline{\hat{c}}$  (complementary subsets) given the label positions  $S_k = i_k$  and the labelling map selected by  $U_k$ .

$\underline{S}$  and  $\underline{U}$  range over all the possible  $m^d$  and  $2^d$  sequences of the bit positions of the signal points and constellation mapping respectively.

This bound is very loose. To get a tighter bound, it is expurgated to produce the BICM Expurgated bound

$$P_{ex} \leq m^{-d} \sum_{\underline{s}} 2^{-d} \sum_{\underline{u}} 2^{-d(m-1)} \sum_{\underline{x} \in X_{\underline{z}}^{\underline{s}}} P(\underline{x} \rightarrow \underline{\hat{z}}) \quad \dots (2)$$

where  $\underline{\hat{z}}$  is the unique nearest neighbour of  $\underline{x}$  in  $X_{\underline{z}}^{\underline{s}}$ .

The BICM Expurgated bound is similar in form to the BICM union bound, but it includes only one (the nearest) error event  $(\underline{x} \rightarrow \underline{\hat{z}})$  for each possible transmitted sequence  $\underline{x}$ , rather than all the possible  $2^{d(m-1)}$  error events  $(\underline{x} \rightarrow \underline{z})$ , for all  $\underline{z} \in X_{\underline{z}}^{\underline{s}}$ . It has been shown [63] to provide a tighter approximation to the probability of error. To obtain a computationally efficient form of the BICM expurgated bound, the Laplace-transform approach is used. Using this approach, the expurgated bound is approximated by the Chernoff bound [63] as

$$P_{ex} \leq \min_{0 < \alpha < \alpha_2} [\psi_{ex}(\alpha)]^d \quad \dots (3)$$

where

$$\psi_{ex}(s) = \frac{1}{m2^m} \sum_{i=1}^m \sum_{b=0}^1 \sum_{\underline{x} \in X_b^i} \Phi_{\Delta(x, \hat{z})}(s)$$

and

$$\Phi_{\Delta(x, \hat{z})}(s) = \frac{\exp\left(-\frac{s(1-s\sigma^2)K|x-\hat{z}|^2/(K+1)}{1+s(1-s\sigma^2)|x-\hat{z}|^2/(K+1)}\right)}{1+s(1-s\sigma^2)|x-\hat{z}|^2/(K+1)}$$

$\Phi_{\Delta}(s) = E[e^{-s\Delta}]$  denotes the Laplace transform of the pdf of  $\Delta$ , where  $\Delta$  is a continuous real random variable which takes on values over the whole real line.

$\Delta(x, \hat{z}) = \log p_\theta(y | x) - \log p_\theta(y | \hat{z})$  denotes the metric difference relative to the components  $x$  and  $\hat{z}$  of the sequences  $\underline{x}$  and  $\underline{\hat{z}}$ .

$\underline{y}$  denotes the channel output sequence (i.e. received sequence)

$\theta$  denotes the fade sample

$K$  is the Rician parameter

$\sigma^2$  is the noise variance

### 6.3 Asymptotic Approximation by Caire et. al.

In [63], the BICM Expurgated bound was derived for performance at high SNR in the Rician fading channel ( $K < \infty$ ). From equation (61) of [63],

$$\min_{0 < \alpha < \alpha_2} \Phi_{\Delta(\underline{x}, \hat{z})}(\alpha) = \prod_{k=1}^d \frac{\exp\left(-\frac{K |x_k - \hat{z}_k|^2 / (4\sigma^2(K+1))}{1 + |x_k - \hat{z}_k|^2 / (4\sigma^2(K+1))}\right)}{1 + |x_k - \hat{z}_k|^2 / (4\sigma^2(K+1))} \dots (4)$$

Using (4), the authors of [63] chose  $\sigma$  to be sufficiently small that for all  $k$ ,

$$1 \ll |x_k - \hat{z}_k|^2 / (4\sigma^2(K+1)) \dots (5)$$

Substituting (5) into (4) results in

$$\min_{0 < \alpha < \alpha_2} \Phi_{\Delta(\underline{x}, \hat{z})}(\alpha) \cong \prod_{k=1}^d \frac{\exp(-K)}{|x_k - \hat{z}_k|^2 / (4\sigma^2(K+1))} \dots (6)$$

The BICM expurgated bound can then be made approximately equal to

$$\begin{aligned}
P_{ex} &\leq \min_{0 < \alpha < \alpha_2} [\psi_{ex}(\alpha)]^d \\
&= \frac{1}{m2^m} \sum_{i=1}^m \sum_{b=0}^1 \sum_{x \in X_b^i} \min_{\alpha < \alpha_2} \Phi_{\Delta(x, \hat{z})}(\alpha) \\
&\approx \left( \frac{4(K+1)e^{-K}}{d_h^2 / \sigma^2} \right)^d \quad \dots(7)
\end{aligned}$$

where

$$d_h^2 = \left( \frac{1}{m2^m} \sum_{i=1}^m \sum_{b=0}^1 \sum_{x \in X_b^i} \frac{1}{|x - \hat{z}|^2} \right)^{-1}$$

and  $d_h^2$  is the harmonic mean of the minimum squared Euclidean distance between complementary subsets of the signal constellation X.

Equation (7) is valid for the Rician fading channel at high SNR. For the Rayleigh fading channel ( $K = 0$ ), it is simplified to

$$P_{ex} \approx \left( \frac{4}{d_h^2 / \sigma^2} \right)^d \quad \dots (8)$$

The SNR is equal to

$$SNR = \frac{1}{\sigma^2} = \frac{RE_b}{N_0} \quad \dots (9)$$

By taking into account the channel coding scheme and taking the  $\log_{10}$ , (8) results in equation (65) of [63] as

$$\log_{10} P_{ex} \approx -\frac{d}{10} \left[ \left( Rd_h^2 \right)_{dB} + \left( \frac{E_b}{N_0} \right)_{dB} \right] + d \log_{10} 4 \quad \dots (10)$$

where  $R$  denotes the spectral efficiency (bits/symbol).

The second term on the right hand side is the constant in equation (65) of [63]. Based on this derivation, the bound is applicable to Rayleigh fading channel but only at high SNR.

#### 6.4 Adding a Twist to the BICM Expurgated Bound

Our approach is focused on applying the BICM expurgated bound to a wider range of SNR in the Rician fading channel. Starting from equation (4), we introduce a constraint such that for all  $k$ ,

$$1 = Y (|x_k - \hat{z}_k|^2 / 4\sigma^2) \dots (11)$$

where  $Y$  is a scaling factor such that for high SNR,  $Y \ll 1$  and for low SNR,  $Y \gg 1$ . The variable  $Y$  is introduced to avoid making a high SNR assumption. Substituting equation (11) into (4) results in

$$\begin{aligned} \min_{0 < \alpha < \alpha_2} \Phi_{\Delta(\underline{x}, \hat{\underline{z}})}(\alpha) &= \prod_{k=1}^d \frac{\exp\left(-\frac{K |x_k - \hat{z}_k|^2 / (4\sigma^2 (K+1))}{[Y+1] |x_k - \hat{z}_k|^2 / (4\sigma^2 (K+1))}\right)}{[Y+1] |x_k - \hat{z}_k|^2 / (4\sigma^2 (K+1))} \\ &= \prod_{k=1}^d \frac{\exp\left(-\frac{K}{(Y+1)}\right)}{[Y+1] |x_k - \hat{z}_k|^2 / (4\sigma^2 (K+1))} \\ &= \prod_{k=1}^d \frac{\exp\left(-\frac{K}{(V)}\right)}{[V] |x_k - \hat{z}_k|^2 / (4\sigma^2 (K+1))} \dots (12) \end{aligned}$$

where we have set  $Y + 1 = V$ . Using equation (12), the BICM expurgated bound then becomes

$$\begin{aligned}
P_{ex} &\leq \min_{0 < \alpha < \alpha_2} [\psi_{ex}(\alpha)]^d \\
&= \frac{1}{m2^m} \sum_{i=1}^m \sum_{b=0}^1 \sum_{x \in X_b^i} \min_{0 < \alpha < \alpha_2} \Phi_{\Delta(x, \hat{z})}(\alpha) \\
&= \left( \frac{4(K+1)e^{-\frac{K}{V}}}{Vd_h^2 / \sigma^2} \right)^d \quad \dots(13)
\end{aligned}$$

This is in the same form as (7), though there is an extra scaling factor V in (13).

However, unlike (7), we have not made any high SNR assumptions to get to (13).

Substituting equation (9) into (13) and taking the  $\log_{10}$ , we get

$$\log_{10} P_{ex} \approx -\frac{d}{10} \left[ (V)_{dB} + (Rd_h^2)_{dB} + \left( \frac{E_b}{N_0} \right)_{dB} \right] + d \log_{10} \left[ 4(K+1)e^{-\frac{K}{V}} \right] \quad \dots (14)$$

For the Rayleigh fading channel, K is set equal to zero such that (14) becomes

$$\log_{10} P_{ex} \approx -\frac{d}{10} \left[ (V)_{dB} + (Rd_h^2)_{dB} + \left( \frac{E_b}{N_0} \right)_{dB} \right] + d \log_{10} 4 \quad \dots (15)$$

Again, (15) is in the same form as that of [63], apart from the additional scaling factor V. By including V, the BICM expurgated bound is simplified without making the high SNR assumption. Equation (15), by itself, is not of much use, mainly because V is a function of SNR. Rearranging equation (15) for a given value of  $P_{ex}$  results in

$$\left( \frac{E_b}{N_0} \right)_{dB} \approx -\frac{10}{d} \log_{10} P_{ex} + 10 \log_{10} 4 - (Rd_h^2)_{dB} - (V)_{dB} \quad \dots (16)$$

In order to make (16) useful, the relative difference in the required energy per bit between 2 BICM systems (of different signal constellation sizes but with the same channel coding and code rate) is computed instead of the absolute value. This is

means that when comparing 2 different constellations, (16) will have to be computed for each of the constellations. In addition, we introduce the constraint that the value of  $V$  ( $V = Y + 1$ ) is the same for all signal constellations. This is justifiable because in (11),  $Y$  is a function only of SNR and the Euclidean distance between the transmitted and erroneous sequences. If each signal constellation is normalised using the appropriate energy value (SNR) such that the minimum Euclidean distances between signal points are equal, then  $V$  is independent of the signal constellation employed. Comparing 2 BICM constellations, say 4-PSK and 16-QAM, the difference in required energy per bit (in dB) is computed as

$$SNR_{gap} = \left( \frac{E_b}{N_0} \right)_{dB(16-QAM)} - \left( \frac{E_b}{N_0} \right)_{dB(4-PSK)} \quad \dots (17)$$

Performing the comparison at the same but arbitrary bit error rate,  $P_{ex}$ , (17) reduces to

$$SNR_{gap} = (Rd_h^2)_{dB(4-PSK)} - (Rd_h^2)_{dB(16-QAM)} \quad \dots (18)$$

where  $P_{ex}$ , the constant term and the SNR dependent  $V$  terms cancel out. The minimum distance of the channel coding scheme,  $d$ , disappears as well. In (18),  $R$ , the rate in bits/symbol, can be represented by

$$R = \frac{k}{n} m \quad \dots (19)$$

where  $k/n$  is the code rate, and  $m$  is the number of bits represented by each signal point. Because it was stated earlier that both BICM systems have the same code rate, substituting (19) into (18) results in

$$SNR_{gap} = (md_h^2)_{dB(4-PSK)} - (md_h^2)_{dB(16-QAM)} \quad \dots (20)$$

where the code rate is cancelled out due to the use of dB units.

Equation (20) is interpreted as the gap in average energy per bit between 2 BICM schemes compared at fixed bit error rate. Because the gap is not a function of  $P_{ex}$ , (i.e.,  $P_{ex}$  is not present in (20)), the  $\text{SNR}_{\text{gap}}$  is constant across all bit error rates. The value of this gap is in fact, equal to that presented for the high SNR (asymptotic) performance in [63]. The gaps with respect to 4-PSK for common signal constellations are reproduced here from [63] in Table 7. The  $d_h^2$  values for each signal constellation as computed in [63] are also shown. The  $E_b/N_0$  gap for 8-QAM was not given in [63].

Signal Constellation	$d_h^2$	$E_b/N_0$ gap (dB)
4-PSK (Gray)	2	0
8-PSK (Gray)	0.7644	2.4
8-QAM (quasi-Gray)	0.96	-
16-QAM (Gray)	0.4923	3.07
32-QAM (quasi-Gray)	0.2788	4.57
64-QAM (Gray)	0.1442	6.65
128-QAM (quasi-Gray)	0.077	8.7
256-QAM (Gray)	0.043	10.65

Table 7 : Values for  $d_h^2$  and the gap in  $E_b/N_0$ , reproduced from [63].

The SNR gap in (20) is not a function of  $d$  and  $k/n$ . This implies that the gap is applicable to any channel coding scheme at any code rate. Due to the definition of the BICM Expurgated bound, only 1 error event for each transmitted sequence was taken into account. This is reflected by taking into account only the minimum Hamming distance of the code. At first look, this is not an accurate representation for the exact performance of the channel coding scheme because the whole distance distribution of the code is not included. However, if every Hamming distance coefficient is taken into account, they will all be cancelled out after taking the difference of the SNR values. Therefore, by this argument, it is shown the SNR gap is not dependent on the code distance properties, making it independent of the type of channel coding scheme used and also of the code rate.

## 6.5 Verifications via Simulations

Based on Table 7, a gap of 3.07 dB is expected when the error performance of coded 16-QAM BICM is compared to that of coded 4-PSK BICM. When compared to coded 64-QAM BICM, a gap of 6.65 dB is expected. Simulation results are presented to verify the accuracy of these estimates. Figure 67 shows simulation results for BPSK<sup>8</sup>, 16-QAM and 64-QAM using the 4-PC-SPC code. The 4-PC BPSK bound was computed based on the work in Chapter 3. It is used to represent the asymptotic performance of the BPSK scheme (below  $10^{-6}$ ). It is observed that all 3 curves have the same slope and the same shape. The error floors occur at almost the same bit error rate. The gap between the BPSK and the 16-QAM curves is about 3 dB at all bit error rates. The gap between BPSK and 64-QAM is about 6.6 dB at all bit error rates.

To show more clearly the gap between each set of curves, Figure 67 is replotted in Figure 68, taking into account the SNR gap. The BPSK curves are shifted to the right by the appropriate SNR gaps (3.07 dB and 6.65 dB for 16-QAM and 64-QAM respectively). Based on Figure 68, the shifted (translated) BPSK curves match the 16-QAM and 64-QAM curves very well. As mentioned previously, the asymptotic performance of the BPSK scheme was represented using its bound. From the comparison to the large constellations, it is explicitly shown that the bound for coded BPSK is applicable to the large constellation schemes.

---

<sup>8</sup> After taking into account the complex dimension, coded 4-PSK BICM is the same as coded BPSK. Therefore, the comparison using BPSK can be made.

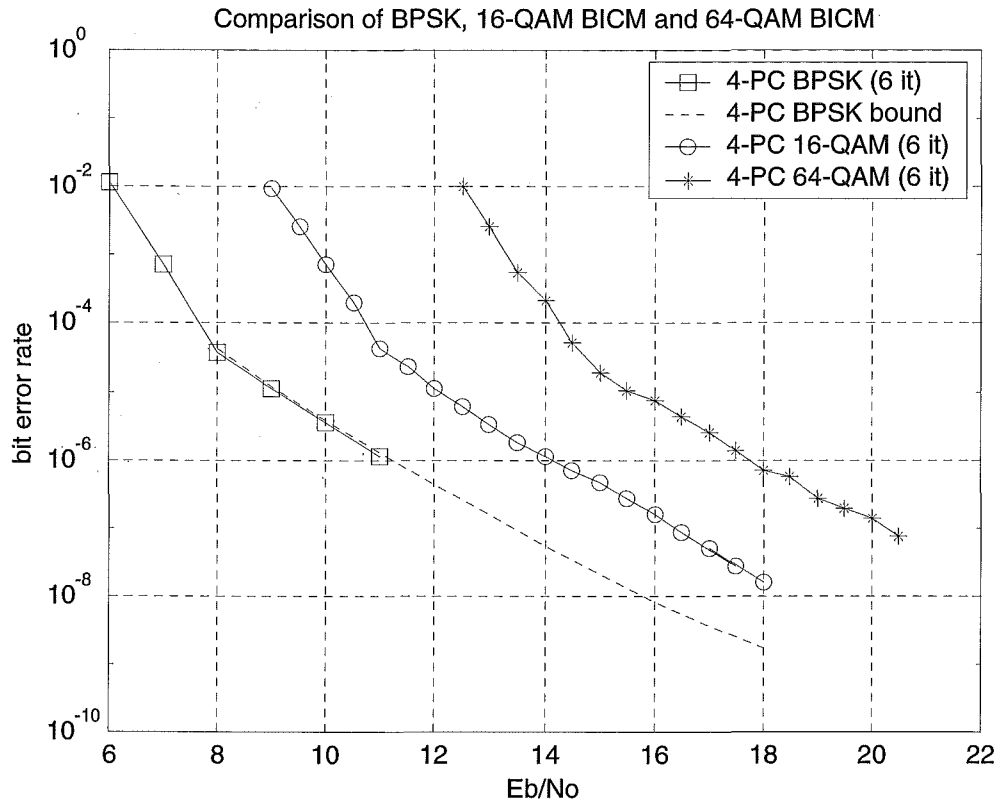


Figure 67 : The performance of BPSK, 16-QAM and 64-QAM in the Rayleigh fading channel using the 4-PC-SPC code.

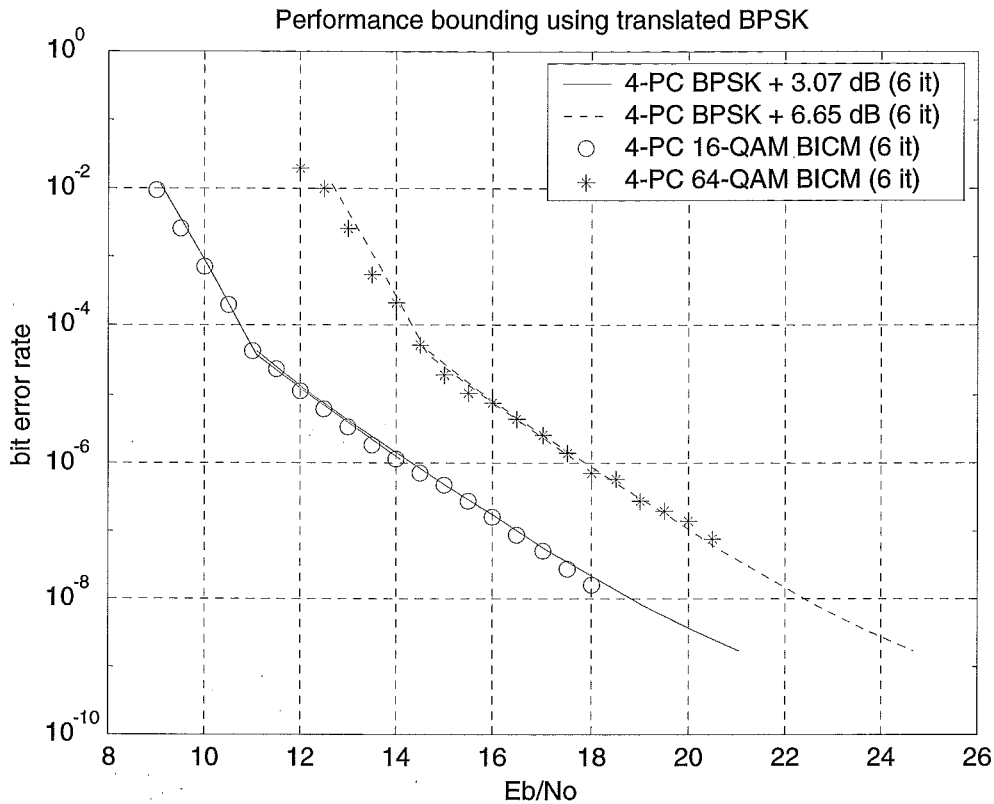


Figure 68 : Using the translated BPSK to bound the performance of 16-QAM and 64-QAM in the Rayleigh fading channel.

Apart from the simulation results presented here, we have also simulated the performance of BICM systems in the independent Rayleigh fading channel using 2, 3, 4, 5, and 6 dimensional serially concatenated SPC codes, and 2, 3, 5 and 6 dimensional parallel concatenated SPC codes. All the results (not presented here) verify the 3.07 dB gap between the BPSK and 16-QAM performance. They imply that the gap is independent of the type of channel coding employed. It is noted here that an independent set of simulation results in [63] also verifies our analysis. In Figure 12 of [63], the simulated results of the error performances for the optimal 64-state rate  $\frac{1}{2}$  convolutional codes are plotted for a range of different signal constellations. After allowing for some tolerances in the simulation results, the SNR gaps are consistent with values in Table 7 over a wide range of SNR, although, this observation was not reported by the authors of [63].

## 6.6 Extension to the Rician Fading Channel

The BICM Expurgated bound based on the work of [63] was derived for the Rician fading channel for all  $K < \infty$ . Therefore, using the bounding method presented here, we can extend our derivation to the Rician fading channel for a wide range of SNR. Starting from (14), reproduced here for convenience

$$\log_{10} P_{ex} \approx -\frac{d}{10} \left[ (V)_{dB} + (Rd_h^2)_{dB} + \left( \frac{E_b}{N_0} \right)_{dB} \right] + d \log_{10} \left[ 4(K+1)e^{-\frac{K}{V}} \right] \quad \dots (21)$$

After rearranging (21), we get

$$\left( \frac{E_b}{N_0} \right)_{dB} \approx -\frac{10}{d} \log_{10} P_{ex} + 10 \log_{10} \left[ 4(K+1)e^{-\frac{K}{V}} \right] - (Rd_h^2)_{dB} - (V)_{dB} \quad \dots (22)$$

From (22), it is observed that the Rician parameter,  $K$ , is isolated in one term of (22). This means that when computing the SNR gap, the  $K$  factor will also be cancelled out. Comparing 4-PSK with 16-QAM, we arrive at an equation identical to (20), reproduced here as

$$\text{SNR}_{\text{gap}} = (md_h^2)_{dB(4-PSK)} - (md_h^2)_{dB(16-QAM)} \quad \dots (23)$$

Equation (23) implies that the SNR gap between 2 BICM schemes in the Rician fading channel for all  $K < \infty$  is the same as the gap in the Rayleigh fading channel.

In Figure 69, the performance of the BPSK, 16-QAM and 64-QAM with the 4-PC-SPC code is simulated in the Rician fading channel ( $K = 5$  dB) to verify this. Figure 69 is replotted in Figure 70 with the BPSK curves properly translated (3.07 dB for 16-QAM and 6.65 dB for 64-QAM). For a wide range of SNR, the curves agree with the SNR gap as predicted.

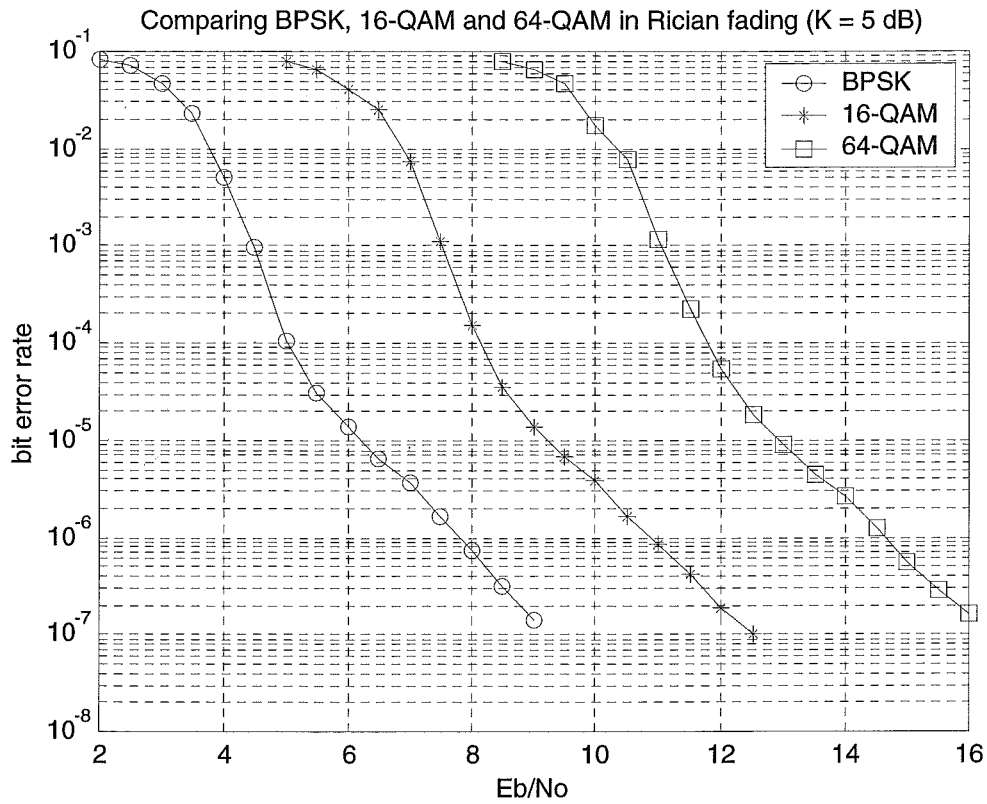


Figure 69 : The performance of BPSK, 16-QAM and 64-QAM with 4-PC-SPC in the Rician fading channel ( $K = 5$  dB).

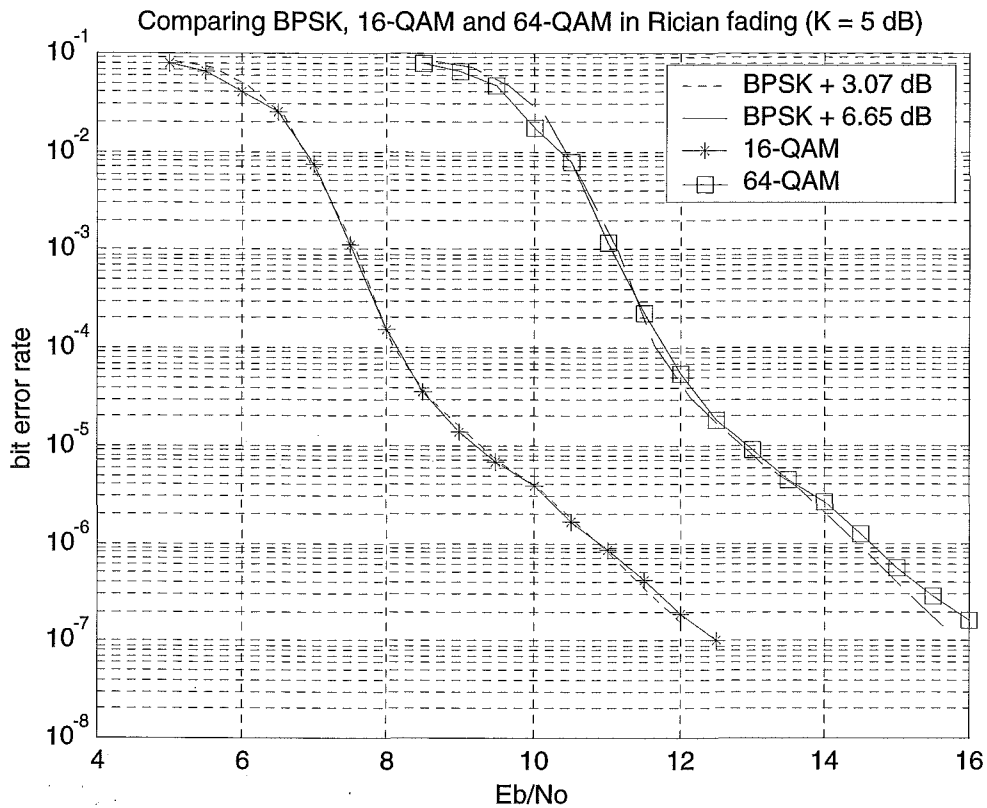


Figure 70 : Using the translated BPSK to bound the performance of 16-QAM and 64-QAM in the Rician fading channel ( $K = 5$  dB).

Unfortunately, there is a limitation to the accuracy of this elegant bounding technique. As  $K$  and the signal constellation size increase, the technique becomes less accurate. Figure 71 shows the performance of this bounding technique applied to the Rician fading channel with  $K = 10$  dB. A good approximation to the performance of 16-QAM is obtained. For 64-QAM, there is a 0.5 dB gap between the predicted performance and the actual performance at  $10^{-6}$ . The performance of the bounding technique for the Rician fading channel with  $K = 15$  dB is shown in Figure 72. Compared to the  $K = 10$  dB scenario, the prediction is slightly worse. In the limiting case of  $K$  equal to infinity, the Rician fading channel is transformed into the AWGN channel. This represents the worst case scenario of the bounding technique. Figure 73 shows the performance of this bounding technique applied to the AWGN channel. For 16-QAM, the translated BPSK performance still provides a reasonably good approximation. However, this technique becomes rather loose in the high SNR region when applied to 64-QAM. The looseness of this bounding technique is mainly due to

the fact that as the K factor increases, the channel behaves more like an AWGN channel, in which case the Q function is a better approximation to the pairwise error probability.

Despite the limitation of this bounding technique for high K values, it is still a useful tool. This technique provides an approximation to the performance of large constellation BICM systems. It is still effective when applied to smaller increments in signal constellation size. For example, BPSK provides a rather loose approximation to 64-QAM, but it provides a good approximation to 16-QAM even in the limiting case of K equal to infinity.

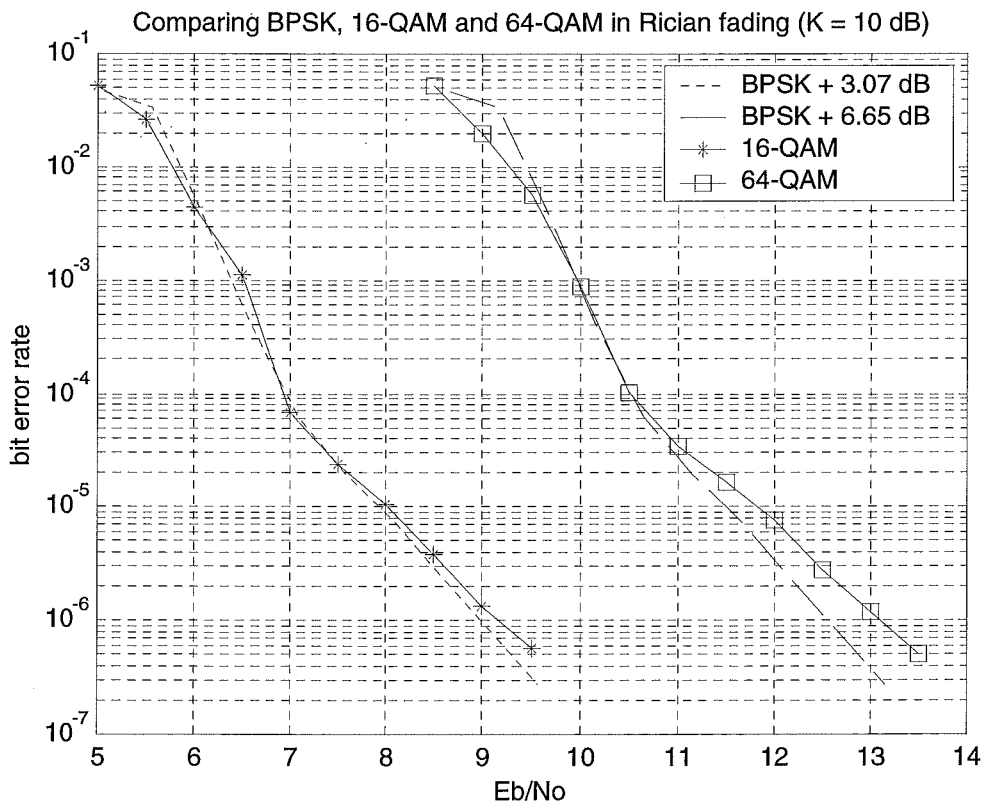


Figure 71 : Using the translated BPSK to bound the performance of 16-QAM and 64-QAM in the Rician fading channel ( $K = 10$  dB).

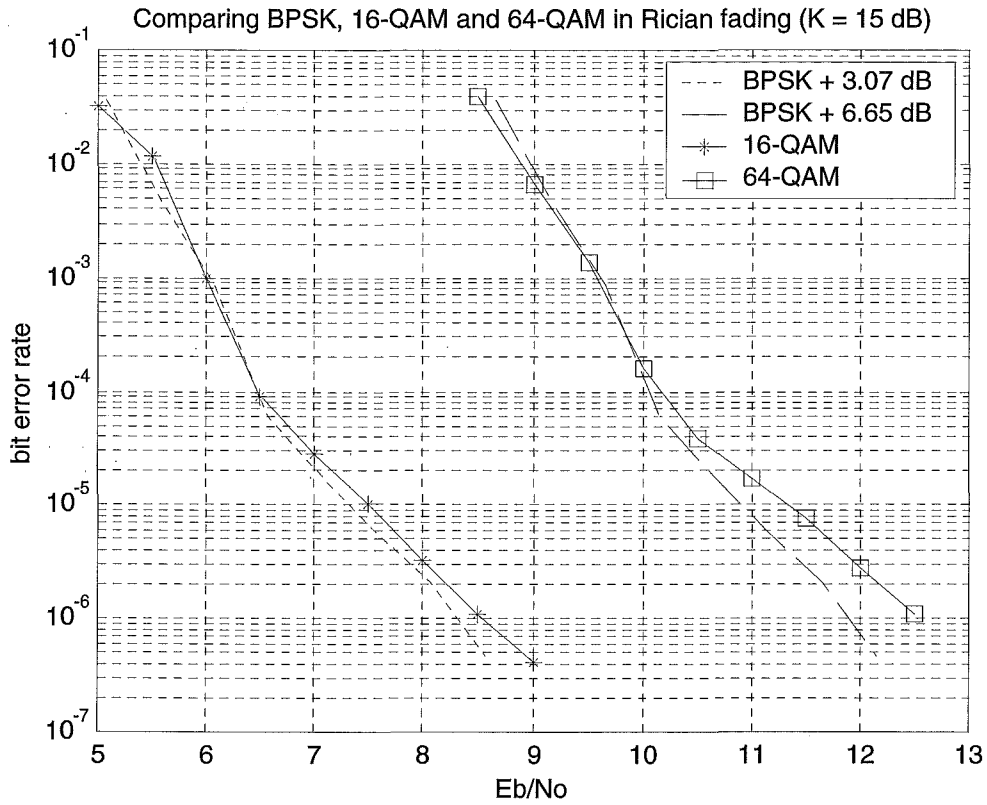


Figure 72 : Using the translated BPSK to bound the performance of 16-QAM and 64-QAM in the Rician fading channel ( $K = 15$  dB).

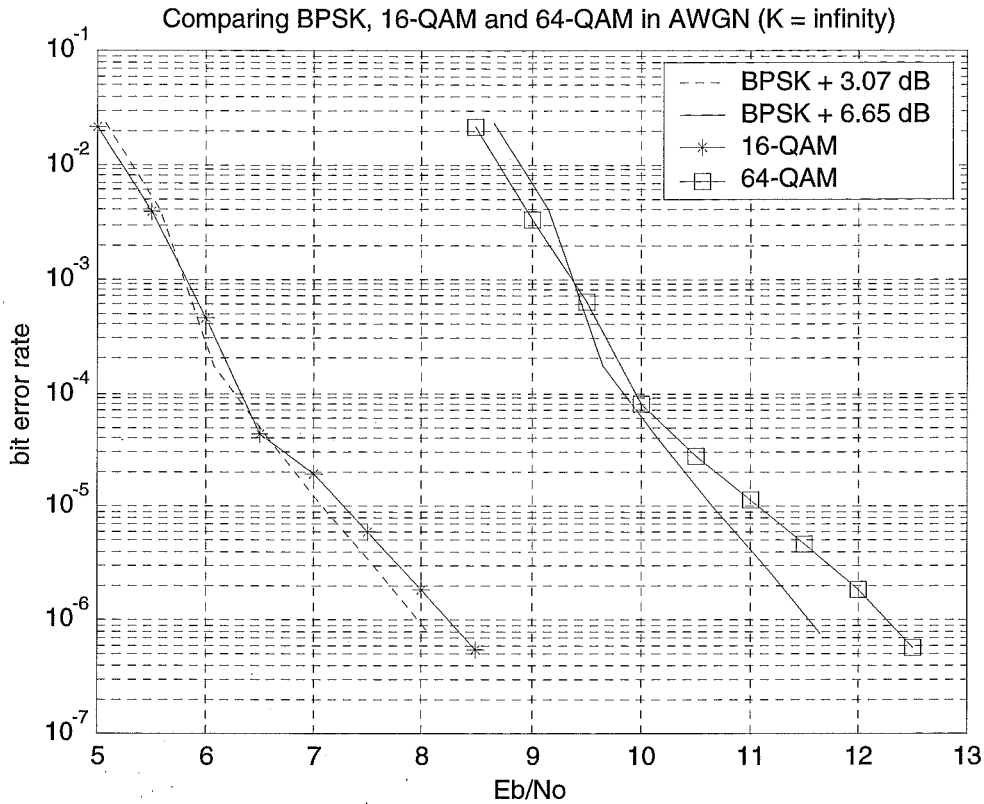


Figure 73 : Using the translated BPSK to bound the performance of 16-QAM and 64-QAM in the AWGN channel ( $K = \infty$ ).

## 6.7 Summary

Based on the work in [63], a link between the error performance of BPSK and large constellation BICM systems in the Rician fading channel has been successfully established. For the Rician fading channel with low to moderate  $K$  values including the case of Rayleigh fading, the bit error rate performance is only a translation factor away from that of the BPSK scheme. This bounding method is independent of the type and rate of channel coding scheme. It is applicable to all common M-PSK and M-QAM signal constellations. Because the gain of BICM over SICM is marginal if the code (interleaver) is properly designed, this bounding technique can also be applied to some Gray-mapped SICM schemes. As  $K$  and the signal constellation size increase, this bounding method becomes less accurate.

This chapter is summarised by emphasizing 2 significant implications as a result of this work. Firstly, the difficult problem of performance bounding for large signal constellations in some Rician fading channel is made easy. Only bounds for BPSK performance are required. This greatly simplifies efforts to bound the performance of Turbo-type codes for large constellations such as those in [118]. Secondly, practical systems design becomes a simpler task. Spectrally efficient communications systems can be easily extended from the BPSK designs. The work here may also find use in adaptive coded modulation systems employing a wide range of signal constellations [119] and variable data rate communication systems.

1. The first part of the document  
 2. The second part of the document  
 3. The third part of the document  
 4. The fourth part of the document  
 5. The fifth part of the document

# CHAPTER 7 : CONCLUSIONS AND FUTURE WORK

## 7.1 Accomplishments

There has been much work performed by research groups worldwide with respect to the theoretical performance of various iterative channel coding schemes.

Comparatively, I believe that there is a lack of research interest focusing on practical coding schemes that are closer to ever being built and applied to real wireless communications systems.

The work performed here has been directed towards the theme of low complexity techniques, with strong emphasis on practicality of the techniques rather than maximum achievable theoretical performance. The accomplishments of this PhD research are summarised as follows :

- 1) Suboptimal SISO Decoding of Systematic Binary Algebraic Block Codes

This soft-in-soft-out decoding strategy simplifies the decoding problem in MAP SPC decoders. By taking a cue from the turbo codes, the concatenated iterative decoding strategy is used to attack this difficult problem of soft decision decoding. There is strong potential applications in the decoding of concatenated block codes.

## 2) Multiple Parallel Concatenated Single Parity Check Codes

This coding scheme offers excellent error performance at medium to low bit error rates. The rate and block length of these codes were designed with flexibility in mind. Combined with BICM, it is capable of operating under high bandwidth efficiency constraints. Although estimated to be approximately 10 times less complex, it is capable of outperforming 16-state Turbo codes in the independent fading channel.

## 3) Multiple Serially Concatenated Single Parity Check Codes

An improved decoder structure was developed for serially concatenated codes. This decoder structure maximises the sharing of extrinsic informations among decoders. In theory, this decoder structure can also be applied to the decoding of product codes. Multiple serially concatenated single parity check codes provide superior performances at low to very low bit error rates. It inherits all the practical merits of its parallel counterpart.

## 4) Bounds for Bit Interleaved Coded Modulation

A simple performance bounding method for the Rician fading channel was developed. This greatly simplifies the problem of bounding error performance for large signal constellation systems. Also, BPSK designs can be ported to larger signal constellations with ease.

## 7.2 Practical Applications

The superb performance of codes designed in this work is well suited for power efficient high data rate wireless communication systems. Combined with bit interleaved coded modulation (BICM), high bandwidth efficiency can be achieved.

These power and bandwidth efficiency advantages are very practical for future wireless and cellular systems.

Concatenated SPC codes have very low decoding complexities. A low decoding complexity translates to a low decoding delay. This can be exploited in 2 ways. Firstly, a low decoding delay makes the scheme a potential candidate for delay sensitive applications such as voice transmission. It is also suitable for very high rate ( $> 1$  Mbps) data communications systems. Secondly, given the same decoding delay budget, concatenated SPC codes can employ a larger block size (about 1 order of magnitude larger) than that of a Turbo decoder. Because the performance of iteratively decoded concatenated codes tends to improve with increasing block size, the gains from the increase in block size can potentially produce superior overall performance compared to a shorter block length Turbo code.

The MAP-SPC decoders for concatenated SPC codes are extremely simple to implement compared to Turbo codes and also convolutional codes. For parallel concatenated codes, there is only 1 MAP-SPC decoder required for each coding scheme. Both parallel and serially concatenated SPC codes allow for a gradual increase in decoding complexity to improve system performance. This offers a performance versus complexity tradeoff. Different schemes can be tailored to specific decoding budgets and performance requirements. This flexibility may prove to be advantageous in communications systems with a range of bit error rate requirements. For example, in cellular systems, 4-PC-SPC can be used for voice transmission ( $10^{-3}$  to  $10^{-4}$ ), whereas 5-PC-SPC can be used to cater for data transmission ( $< 10^{-6}$ ). There is no need to spend more decoding budget than necessary by over-designing the error correction capability.

### 7.3 Future Work

There are many possible directions to go from here. Some of these potential future works are listed as follows :

### 1) Behaviour of Iterative Decoding Algorithm

It was shown in Chapter 5 that the decoding algorithm for serially concatenated SPC codes does not always converge. This unstable nature is not understood yet. A possible place to start this investigation can be found in [120] and [126]. Also, the introduction of some form of adaptive scaling factor on the extrinsic informations should smooth the convergence of the decoding process.

### 2) Interleaver Design for Concatenated SPC Codes

It is widely known that error performance can be improved via proper interleaver designs. Interleaver design efforts can be directed to fine-tune the error performance of concatenated SPC codes with particular focus on shorter block lengths.

### 3) Finite Quantisation Effects

Simulations in this work are all performed using floating point precision. It will be interesting to see how sensitive the MAP SPC algorithm is to the effects of finite quantisation. This issue is critical for practical system implementations using fixed point DSPs. Also, the effect of using the approximated LLA instead of the exact LLA expression is worth some investigations.

### 4) Performance in Time-Selective and Frequency-Selective Channels

This work in this thesis only encompasses investigations under the 2 most basic channel models for wireless communications – the additive white gaussian noise channel and the independent Rayleigh fading channel. These channel models underestimate the complex problem of wireless communications. For the Rayleigh fading channel, investigations under time-selective (correlated fading) and imperfect channel estimation conditions are worth pursuing. There is also an opportunity to

work on combined equalisation and decoding strategies in the frequency-selective channel.

## 5) Bipartite Graphs

The concept of a single block code decomposed into several subcodes brings up the viewpoint of codes defined by bipartite graphs. Each subcode is defined by a set of parity nodes which check a certain subset of information bits. This view shares the non-interleaver based model as discussed in Chapter 2. It is potentially useful to study this model by linking it to recent works on bipartite graphs [35] [128].



# APPENDIX I : THE MAP ALGORITHM FOR SPC CODES

In MAP decoding, there are 3 parameters to be defined; the channel log-likelihood ratio (LLR), the a priori LLR and the extrinsic LLR. This section shows how each LLR is computed, and how they are used to perform MAP decoding of concatenated SPC codes [121].

## Log Likelihood Ratio

The decoding process starts by calculating the channel log likelihood ratio (LLR) for each received bit (This includes both the data bits and the parity bits). The LLR may be written as

$$\begin{aligned} L_c(d | r) &= \log_e \left[ \frac{P(d = 1 | r)}{P(d = 0 | r)} \right] = \log_e \left[ \frac{p(r | d = 1)P(d = 1)}{p(r | d = 0)P(d = 0)} \right] \\ &= \log_e \left[ \frac{p(r | d = 1)}{p(r | d = 0)} \right] + \log_e \left[ \frac{P(d = 1)}{P(d = 0)} \right] \end{aligned}$$

where  $r$  is the received metric, and  $d$  is the hypothesised transmitted data bit.

Assuming all bits are equally likely, the second term can be ignored. The first term can be simplified to

$$\log_e \left[ \frac{p(r | d = 1)}{p(r | d = 0)} \right] = \log_e \left[ \frac{\frac{1}{\sigma\sqrt{2\pi}} \exp\left(-\frac{(r - ax_1)^2}{2\sigma^2}\right)}{\frac{1}{\sigma\sqrt{2\pi}} \exp\left(-\frac{(r - ax_0)^2}{2\sigma^2}\right)} \right]$$

$$= \frac{1}{2\sigma^2} [(r - ax_0)^2 - (r - ax_1)^2]$$

where  $x_1$  is the hypothesis representing  $d = 1$ ,  $x_0$  is the hypothesis representing  $d = 0$ ,  $a$  represents the fade envelope and  $r$  is the received sample

Hard decisions are made using the following criteria - If the LLR is greater than zero, then a hard decision of binary 1 is made. If the LLR is less than zero, a hard decision of binary 0 is made. If the LLR is equal to zero, then a random guess is made.

### Log-Likelihood Algebra

For single parity check (SPC) codes, the parity bit is obtained by performing a mod 2 sum of all the data bits. For example

$$p = d_1 \oplus d_2$$

where  $p$  is the parity bit,  $d_1$  and  $d_2$  are the data bits and  $\oplus$  denotes mod 2 sum. The extrinsic LLR for  $d_1$  is obtained by performing the equivalent log-likelihood algebra (LLA) operations using  $p$  and  $d_2$ .

$$L_{ex}(d_1) = L(p \oplus d_2)$$

$$= \log_e \left[ \frac{e^{L(p)} + e^{L(d_2)}}{1 + e^{L(p)} e^{L(d_2)}} \right]$$

$$= -2 \tanh^{-1} \left( \frac{\tanh[L(p)] * \tanh[L(d_2)]}{2} \right)$$

This represents the exact implementation for the LLA operation. To avoid the use of the  $\log_e$  function or the tanh function, the LLA can be approximated by

$$L_{ex}(d_1) \approx (-1) \times \text{sign}[L(p)] \times \text{sign}[L(d_2)] \times \min[|L(p)|, |L(d_2)|]$$

For SPC codes of length  $(n, n-1, 2)$ , the exact LLA is generalised to

$$L_{ex}(d_j) = 2(-1)^n \tanh^{-1} \left( \frac{\tanh[L(p)]}{2} \prod_{l=1, l \neq j}^{n-1} \frac{\tanh[L(d_l)]}{2} \right)$$

where  $L(d_i)$  is the channel LLR for the data bits. For the approximate LLR, the expression is simplified to

$$L_{ex}(d_j) \approx (-1)^n \cdot \min_{l=1, \dots, (n-1), l \neq j} [ |L(p)|, |L(d_l)| ] \cdot \text{sign}[L(p)] \prod_{l=1, l \neq j}^{n-1} \text{sign}[L(d_l)]$$

There is a  $(-1)^n$  factor in the expression due to a different choice of null element. The work here has followed the convention in [121] as opposed to that of [30]. All simulations in this thesis are based on the exact LLA implementation.

## MAP Decoding of SPC codes

The iterative decoding process uses the extrinsic LLR obtained as the a priori LLR in successive iterations. The improved LLR of the data bits,  $L(\hat{d})$ , are obtained by summing the channel LLRs and the a priori LLRs.

$$L(\hat{d}) = L_c(d) + L_{ex}(d)$$

The following example shows how the iterative MAP decoding algorithm is applied to concatenated SPC codes. In this example, a very short 2 parallel concatenated SPC code is used. This code is shown in Figure 74.

d1	d2	p12
d3	d4	p34
p13	p24	

Figure 74 : 2 dimensional parallel concatenated SPC code.

Suppose the data block (1, 0, 0, 1) is to be encoded. This results in the following code

d1 = 1	d2 = 0	p12 = 1
d3 = 0	d4 = 1	p34 = 1
p13 = 1	p24 = 1	

The coded sequence is (1, 0, 0, 1, 1, 1, 1, 1). Using BPSK, the transmitted sequence is represented by (+1, -1, -1, +1, +1, +1, +1, +1) where +1 represents binary 1 and -1 represents binary 0. Assume that noise in the channel transforms the transmitted sequence into an erroneous sequence (0.75, 0.05, 0.10, 0.15, 1.25, 1.0, 3.0, 0.5) at the receiver. Computing the channel LLR results in

$L_c = 1.5$	$L_c = 0.1$	$L_c = 2.5$
$L_c = 0.2$	$L_c = 0.3$	$L_c = 2.0$
$L_c = 6.0$	$L_c = 1.0$	

If hard decisions are made using the channel LLRs, the estimated sequence will be (1, 1, 1, 1, 1, 1, 1, 1), which results in 2 bit errors.

In this example, each data bit has 2 a priori LLR sources; one from the horizontal parity bits and another from the vertical parity bits. MAP decoding is initiated by computing the a priori LLR for the data bits using one set of the parity bits, either horizontal or vertical. Here, we start decoding by arbitrarily choosing the horizontal parity bits, and for simplicity, we apply the approximated LLA expression.

For the horizontal decoding, only the horizontal LLRs are used

$L_c = 1.5$	$L_c = 0.1$	$L_c = 2.5$
$L_c = 0.2$	$L_c = 0.3$	$L_c = 2.0$

In the first iteration, there is no a priori information available yet, so, the extrinsic LLRs for the 4 data bits are computed as

$L_{ex} = -0.1$	$L_{ex} = -1.5$
$L_{ex} = -0.3$	$L_{ex} = -0.2$

Adding the extrinsic LLRs and the channel LLRs results in

1.4	-1.4
-0.1	0.1

In this example, although only the horizontal decoding has been performed, the errors are already corrected. It is easy to see that if hard decisions are made, then the estimated data bits will be equal to (1, 0, 0, 1). Note that the improved LLR of  $d_3$  and  $d_4$  are of low reliability values (both at 0.1). We will proceed with vertical decoding to show that further decoding can improve the reliability of the LLRs. The vertical decoding operates on the improved LLR for the data bits

1.4	-1.4
-0.1	0.1
6.0	1.0

Using this, the extrinsic LLRs are computed as

$L_{\text{ex}} = 0.1$	$L_{\text{ex}} = -0.1$
$L_{\text{ex}} = -1.4$	$L_{\text{ex}} = 1.0$

Summing the new channel LLRs and the vertical extrinsic LLRs results in

1.5	-1.5
-1.5	1.1

It is observed that after the vertical decoding, the reliabilities of the LLR for  $d_3$  and  $d_4$  are improved from  $-0.1$  and  $0.1$  to  $-1.5$  and  $1.1$  respectively. If another complete iteration is performed, the reliability of the LLRs will be improved further

2.6	-2.5
-2.5	2.5

In this example, only 1 complete iteration is required to correct all the bit errors. In a real system, more iterations are necessary to correct the errors.

## APPENDIX II : EXAMPLE OF IRWEF COMPUTATION

In this appendix, an example of the IRWEF (Input Redundancy Weight Enumerating Function) computation is presented. This example uses the 2 dimensional parallel concatenated (7, 4, 3) Hamming code [32]. This (n, k) encoder structure is shown in Figure 75, where n and k are the output and input block lengths respectively. First, the IRWEF for interleaver length  $N = 4$  (ie,  $g = 1$ ) is computed. After that, the computation is extended for any integer value of  $g$ <sup>9</sup>. Finally, the IRWEF is extended to higher dimensions (more parallel concatenated branches). The general expression for the IRWEF of component SPC codes is also presented.

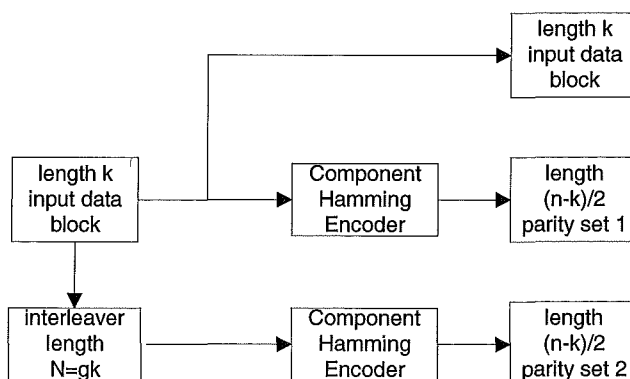


Figure 75 : Encoder structure for the 2 dimensional parallel concatenated Hamming code.

---

<sup>9</sup>  $g$  restricts the input data block length to be integer multiples of the component Hamming code's input word length.

For a systematic block code, the IRWEF is defined as

$$A^C(W, Z) = \sum_{w,j} A_{w,j} W^w Z^j$$

where  $A_{w,j}$  is the number of codewords generated by an information word of Hamming weight  $w$  whose parity check bits have Hamming weight  $j$ , so that the overall Hamming weight is  $w + j$ . The CWEF (Conditional Weight Enumerating Function),  $A_w^C(Z)$  is extracted from the IRWEF using the following relations

$$A^C(W, Z) = \sum_w W^w A_w^C(Z)$$

The IRWEF for the component (7, 4, 3) Hamming code is given by

$$A^C(W, Z) = 1 + W(3Z^2 + Z^3) + W^2(3Z + 3Z^2) + W^3(1 + 3Z) + W^4 Z^3$$

The corresponding CWEF is extracted from the IRWEF as

$$\begin{aligned} A_0^C(Z) &= 1 \\ A_1^C(Z) &= 3Z^2 + Z^3 \\ A_2^C(Z) &= 3Z + 3Z^2 \\ A_3^C(Z) &= 1 + 3Z \\ A_4^C(Z) &= Z^3 \end{aligned}$$

Using the CWEF of the component Hamming codes, the CWEF of the 2 dimensional parallel concatenated Hamming code  $A_w^{C_p}(Z)$  is computed as

$$A_w^{C_p}(Z) = \frac{A_w^C(Z) \cdot A_w^C(Z)}{\binom{k}{w}}$$

where  $\cdot$  denotes term by term multiplication. The IRWEF of the parallel concatenated Hamming code is

$$\begin{aligned} A^{C_p}(W, Z) &= \sum_{w=0}^k W^w A_w^{C_p}(Z) \\ &= 1 + W(2.25Z^4 + 1.5Z^5 + 0.25Z^6) + \\ &\quad W^2(1.5Z^2 + 3Z^3 + 1.5Z^4) + \\ &\quad W^3(0.25 + 1.5Z + 2.25Z^2) + W^4Z^6 \end{aligned}$$

Having obtained the IRWEF for the 2 dimensional parallel concatenated Hamming code, computation of the  $D_h$  term is straightforward.

### Larger Interleaver Sizes

For larger interleaver sizes (ie  $g > 1$ ), the IRWEF of the component Hamming codes must be raised to the power of  $g$ . To simplify the notation, let

$$A^{C^g}(W, Z) = [A^C(W, Z)]^g$$

The CWEF for the 2 dimensional parallel concatenated Hamming code with interleaver size  $N = gk$  is computed as

$$A_w^{C^g_p}(Z) = \frac{A_w^{C^g}(Z) \cdot A_w^{C^g}(Z)}{\binom{N}{w}}$$

### Higher Dimensions

In order to extend the IRWEF computation to higher dimensions, the only modification required is to add additional terms for the computation of the CWEF.

For 3 dimensions, the CWEF is computed as

$$A_w^{C_p^s}(Z) = \frac{A_w^{C^s}(Z) \cdot A_w^{C^s}(Z) \cdot A_w^{C^s}(Z)}{\binom{N}{w} \binom{N}{w}}$$

Generalizing this to M dimensions results in

$$A_w^{C_p^s}(Z) = \frac{\prod^M A_w^{C^s}(Z)}{\binom{N}{w}^{M-1}}$$

where the numerator denotes an M-fold component multiplication operation.

### IRWEF for SPC Codes

For a (n, n-1) SPC code, the IRWEF is obtained as

$$A^{C_{SPC}}(W, Z) = 1 + W \binom{n-1}{1} Z + W^2 \binom{n-1}{2} + \dots + W^s \binom{n-1}{s} Z^q + \dots + W^{n-1} Z^q$$

where

$$s = 1, 2, \dots, n-1$$

$$q = \begin{cases} 0 & \text{if } s \text{ is even} \\ 1 & \text{if } s \text{ is odd} \end{cases}$$

## APPENDIX III : EXAMPLE OF IOWEF COMPUTATION

In this section, an example of the IOWEF (Input Output Weight Enumerating Function) computation is presented. This example uses the serially concatenated block code with a  $(4, 3, 2)$  SPC code as the outer code and a  $(7, 4, 3)$  Hamming code as the inner code [25]. The  $(n, k)$  encoder structure is shown in Figure 76, where  $n$  and  $k$  are the output and input block lengths respectively. First, the IOWEF for interleaver length  $N = 4$  (ie,  $g = 1$ ) is computed. After that, the computation is extended for any integer value of  $g$ . Finally, the IOWEF is extended to higher dimensions (more serial concatenations) [27]. The general expression of the IOWEF of the component SPC codes is also presented.

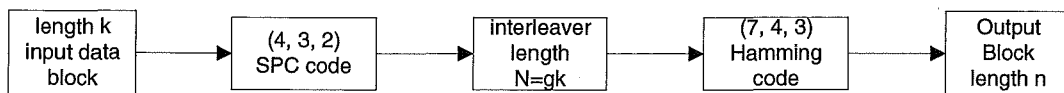


Figure 76 : Serially Concatenated Block Code using the  $(4, 3, 2)$  SPC code and  $(7, 4, 3)$  Hamming code.

For a systematic block code, the IOWEF is defined as

$$\begin{aligned} A(W, H) &= \sum_{w=0}^k \sum_{h=0}^n A_{w,h} W^w H^h \\ &= \sum_{w=0}^k W^w A(w, H) \end{aligned}$$

where  $A_{w,h}$  represents the number of codewords with weight  $h$  generated by information words of weight  $w$ . The CWEF (conditional weight enumerating function) is defined implicitly in the IOWEF

$$A(w, H) = \sum_{h=0}^n A_{w,h} H^h$$

The CWEF is the function that enumerates the weight distribution of codewords generated by information words of a give weight  $w$ . For the SCBC depicted in Figure 76, the IOWEF of the outer (4, 3, 2) SPC code,  $C_o$ , is

$$A^{C_o}(W, L) = 1 + W(3L^2) + W^2(3L^2) + W^3(L^4)$$

For the inner (7, 4, 3) Hamming code,  $C_i$ , the IOWEF is

$$A^{C_i}(L, H) = 1 + L(3H^3 + H^4) + L^2(3H^3 + 3H^4) + L^3(H^3 + 3H^4) + L^4H^7$$

The CWEF of both codes are computed as

$$A^{C_o}(W, 0) = 1$$

$$A^{C_o}(W, 1) = 0$$

$$A^{C_o}(W, 2) = 3W + 3W^2$$

$$A^{C_o}(W, 3) = 0$$

$$A^{C_o}(W, 4) = W^3$$

$$A^{C_i}(0, H) = 1$$

$$A^{C_i}(1, H) = 3H^3 + H^4$$

$$A^{C_i}(2, H) = 3H^3 + 3H^4$$

$$A^{C_i}(3, H) = H^3 + 3H^4$$

$$A^{C_i}(4, H) = H^7$$

Using the CWEF of the component codes, the CWEF of the serially concatenated block code is computed as

$$A^{C_s}(w, H) = \sum_{l=0}^N \frac{A^{C_o}(w, l) \times A^{C_i}(l, H)}{\binom{N}{l}}$$

For this example, the IOWEF of the serially concatenated block code,  $C_s$ , is

$$\begin{aligned} A^{C_s}(W, H) &= \sum_{l=0}^N \frac{A^{C_o}(W, l) \times A^{C_i}(l, H)}{\binom{N}{l}} \\ &= \frac{1 \cdot 1}{1} + \frac{0 \cdot (3H^3 + H^4)}{4} + \frac{(3W + 3W^2) \cdot (3H^3 + 3H^4)}{6} + \\ &\quad \frac{0 \cdot (H^3 + 3H^4)}{4} + \frac{W^3 \cdot H^7}{1} \\ &= 1 + W(1.5H^3 + 1.5H^4) + W^2(1.5H^3 + 1.5H^4) + W^3H^7 \end{aligned}$$

From here onwards, the computation for the bit error multiplicity term is straightforward.

### Larger Interleaver Sizes

For larger interleaver sizes (ie  $g > 1$ ), the IOWEF of the component codes must be raised to the power of  $g$ . To simplify the notation, let

$$A^{C_o^g}(W, L) = [A^{C_o}(W, L)]^g$$

$$A^{C_i^g}(L, H) = [A^{C_i}(L, H)]^g$$

Using these, the CWEF of the serially concatenated block code,  $C_s^g$ , is obtained as

$$A^{C_s^g}(w, H) = \sum_{l=0}^N \frac{A_{w,l}^{C_o^g} \times A^{C_i^g}(l, H)}{\binom{N}{l}}$$

The IOWEF is

$$A^{C_s^g}(W, H) = \sum_{l=0}^N \frac{A^{C_o^g}(W, l) \times A^{C_i^g}(l, H)}{\binom{N}{l}}$$

### Higher Dimensions

In order to extend the IOWEF computation to higher dimensions, additional summation terms are required for the computation of the CWEF. The encoder structure for the 3 dimensional serially concatenated block code, also known as the double serially concatenated block code [27], is shown in Figure 77.

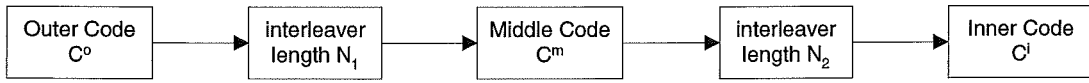


Figure 77 : Encoder structure for a 3 dimensional serially concatenated block code, also known as a double serially concatenated block code [27].

The CWEF is computed as

$$A^{C_s^g}(w, H) = \sum_{l_1=0}^{N_1} \sum_{l_2=0}^{N_2} \frac{A_{w,l_1}^{C_o^g} \times A_{l_1,l_2}^{C_m^g} \times A^{C_i^g}(l_2, H)}{\binom{N_1}{l_1} \binom{N_2}{l_2}}$$

The IOWEF is derived as

$$A^{C_s^g}(W, H) = \sum_{l_1=0}^{N_1} \sum_{l_2=0}^{N_2} \frac{A^{C_o^g}(W, l_1) \times A_{l_1,l_2}^{C_m^g} \times A^{C_i^g}(l_2, H)}{\binom{N_1}{l_1} \binom{N_2}{l_2}}$$

The computation complexity becomes large very quickly with increasing dimensionality, much more complex than the IRWEF evaluation for the parallel concatenated codes. For an M dimensional serially concatenated code, there are M-1 summations, with M terms in the numerator and M-1 terms in the denominator. In this work, up to 6 dimensions is used. For the 6 dimensional, code the CWEF is

$$A^{C_s^g}(w, H) = \sum_{l_1=0}^{N_1} \sum_{l_2=0}^{N_2} \sum_{l_3=0}^{N_3} \sum_{l_4=0}^{N_4} \sum_{l_5=0}^{N_5} \frac{A_{w,l_1}^{C_o^g} \times A_{l_1,l_2}^{C_{m2}^g} \times A_{l_2,l_3}^{C_{m3}^g} \times A_{l_3,l_4}^{C_{m4}^g} \times A_{l_4,l_5}^{C_{m5}^g} \times A^{C_i^g}(l_5, H)}{\binom{N_1}{l_1} \binom{N_2}{l_2} \binom{N_3}{l_3} \binom{N_4}{l_4} \binom{N_5}{l_5}}$$

and the IOWEF is

$$A^{C_s^g}(W, H) = \sum_{l_1=0}^{N_1} \sum_{l_2=0}^{N_2} \sum_{l_3=0}^{N_3} \sum_{l_4=0}^{N_4} \sum_{l_5=0}^{N_5} \frac{A_o^{C_g}(W, l_1) \times A_{l_1,l_2}^{C_{m2}^g} \times A_{l_2,l_3}^{C_{m3}^g} \times A_{l_3,l_4}^{C_{m4}^g} \times A_{l_4,l_5}^{C_{m5}^g} \times A^{C_i^g}(l_5, H)}{\binom{N_1}{l_1} \binom{N_2}{l_2} \binom{N_3}{l_3} \binom{N_4}{l_4} \binom{N_5}{l_5}}$$

where  $N_1, N_2, N_3, N_4,$  and  $N_5$  represent the length of the constituent interleavers, and  $C_o, C_{m2}, C_{m3}, C_{m4}, C_{m5},$  and  $C_i$  represent successive encoders in the concatenated structure.

### IOWEF for SPC Codes

For an  $(n, n-1)$  SPC code, the IOWEF is computed as

$$A^{C_{SPC}}(W, L) = 1 + W \binom{n-1}{1} L^2 + W^2 \binom{n-1}{2} L^2 + W^3 \binom{n-1}{3} L^4 + \dots + W^s \binom{n-1}{s} L^q + \dots + W^{n-1} L^q$$

where

$$s = 1, 2, \dots, n-1$$

$$q = \begin{cases} s & \text{if } s \text{ is even} \\ s+1 & \text{if } s \text{ is odd} \end{cases}$$



## REFERENCES

- [1] G. I. Zysman, J. A. Tarallo, R. E. Howard, J. Freidenfelds, R. A. Valenzuela & P. M. Mankiewich, "Technology Evolution for Mobile and Personal Communications", Bell Labs Technical Journal, January-March 2000, pp. 107-129.
- [2] J. F. Huber, D. Weiler & H. Brand, "UMTS, the Mobile Multimedia Vision for IMT-2000 : A Focus on Standardization", IEEE Communications Magazine, September 2000, pp. 129-136.
- [3] M. Zeng, A. Annamalai & V. K. Bhargava, "Recent Advances in Cellular Wireless Communications", IEEE Communications Magazine, September 1999, pp. 128-138.
- [4] C. E. Shannon, "A Mathematical Theory of Communication", Bell System Technical Journal, vol. 27, pp. 379-423, 623-656, July, October, 1948.
- [5] C. Berrou, A. Glavieux & P. Thitimajshima, "Near Shannon Limit Error – Correcting Coding and Decoding : Turbo Codes (1)", proceedings of IEEE International Communications Conference (ICC), May 1993, Geneva, Switzerland, pp. 1064-1070.
- [6] C. Berrou and A. Glavieux, "Near Optimum Error Correcting Coding and Decoding: Turbo Codes", IEEE Transactions on Communications, vol. 44, No. 10, October 1996, pp. 1261-1271.
- [7] G. Battail, "A Conceptual Framework for Understanding Turbo Codes", Journal on Selected Areas in Communications, vol. 16, No. 2, February

1998, pp. 245-254.

- [8] C. Heegard & S. B. Wicker, "Turbo Coding", Kluwer Academic Publishers, USA, 1999
- [9] L. R. Bahl, J. Cocke, F. Jelinek & J. Raviv, "Optimal Decoding of Linear Codes for Minimizing Symbol Error Rate", IEEE Transactions on Information Theory, March 1974, pp. 284-287.
- [10] P. Jung and M.M. NaBhan, "Comprehensive Comparison of Turbo-Code Decoders", proceedings of IEEE 45<sup>th</sup> Vehicular Technology Conference, vol. 2, pp. 624-628, 1995,
- [11] P. Jung, "Comparison of Turbo-Code Decoders Applied to Short Frame Transmission Systems", IEEE Journal on Selected Areas in Communications, vol. 14, No. 2, April 1996, pp.530-537.
- [12] S. Benedetto, G. Montorsi, D. Divsalar & F. Pollara, "Soft-Input Soft-Output Modules for the Construction and Distributed Iterative Decoding of Code Networks", European Transactions on Telecommunications (ETT), vol. 9, No. 2, March/April 1998, pp. 155-172.
- [13] A. J. Viterbi, "An Intuitive Justification and a Simplified Implementation of the MAP Decoder for Convolutional Codes", IEEE Journal on Selected Areas in Communications, vol. 16, No. 2, February 1998, pp.260-264.
- [14] V. Franz & J. B. Anderson, "Concatenated Decoding with a Reduced-Search BCJR Algorithm", IEEE Journal on Selected Areas in Communications, vol. 16, No. 2, February 1998, pp. 186-195.
- [15] H. Koorapaty, Y. E. Wang and K. Balachandran, "Performance of Turbo Codes with Short Frame Sizes", IEEE 47<sup>th</sup> Vehicular Technology Conference (VTC) 1997, vol. 1, pp. 329-333.
- [16] H. Herzberg, "Multilevel Turbo Coding with Short Interleavers", IEEE Journal on Selected Areas in Communications, vol. 16, No. 2, February 1998, pp.303-309.
- [17] S. Dolinar, D. Divsalar & F. Pollara, "Code Performance as a Function of Block Size", TMO Progress Report 42-133, May 15, 1998.
- [18] S. Le Goff, A. Glavieux & C. Berrou, "Turbo-Codes and High Spectral Efficiency Modulation, proceedings of IEEE International

- Communications Conference (ICC), May 1994, New Orleans, USA  
pp.645-649.
- [19] O. F. Acikel & W. E. Ryan, "Punctured Turbo-Codes for BPSK/QPSK Channels" IEEE Transactions on Communications, vol. 47, No. 9. September 1999, pp.1315-1323.
- [20] D. Divsalar & F. Pollara, "Multiple Turbo Codes for Deep-Space Communications", TDA Progress Report 42-121, May 15, 1995, pp. 66-77.
- [21] D. Divsalar & F. Pollara, "Multiple Turbo Codes", proceedings of IEEE Milcom Conference 1995, pp. 279-285.
- [22] D. Divsalar & F. Pollara, "Turbo Codes for PCS Applications", proceedings of IEEE International Communications Conference (ICC), June 1995, Seattle, Washington, USA.
- [23] D. Divsalar & F. Pollara, "On the Design of Turbo Codes", TDA Progress Report 42-123, November 15, 1995, pp. 99-121.
- [24] G. D. Forney, "Concatenated Codes", Cambridge, MA, MIT Press, 1966.
- [25] S. Benedetto, D. Divsalar, G. Montorsi & F. Pollara, "Serial Concatenation of Interleaved Codes : Performance Analysis, Design, and Iterative Decoding", IEEE Transactions on Information Theory, vol. 44, No. 3, May 1998, pp. 909-926.
- [26] S. Benedetto, D. Divsalar, G. Montorsi & F. Pollara, "A Soft-Input Soft-Output Maximim A Posteriori (MAP) Module to Decode Parallel and Serial Concatenated Codes", TDA Progress Report 42-127, November 15, 1996.
- [27] S. Benedetto, D. Divsalar, G. Montorsi & F. Pollara, "Analysis, Design, and Iterative Decoding of Double Serially Concatenated Codes with Interleavers", IEEE Journal on Selected Areas in Communications, vol. 16, No. 2, February 1998, pp. 231-244.
- [28] D. Divsalar & F. Pollara, "Hybrid Concatenated Codes and Iterative Decoding", TDA Progress Report 42-130, August 15, 1997, pp. 1-23.
- [29] D. Divsalar, & R. J. McEliece, "On the Design of Concatenated Coding Systems with Interleavers", TMO Progress Report, 42-134, August 15,

1998.

- [30] J. Hagenauer, E. Offer and L. Papke, "Iterative Decoding of Binary Block and Convolutional Codes", IEEE Transactions on Information Theory, vol. 42, No. 2, March 1996, pp. 429-445.
- [31] R. Lucas, M. Bossert and M. Breitbart, "On Iterative Soft-Decision Decoding of Linear Binary Block Codes and Product Codes", IEEE Journal on Selected Areas in Communications, vol. 16, No. 2, Feb. 1998, pp. 276-296.
- [32] S. Benedetto & G. Montorsi, "Unveiling Turbo Codes : Some Results on Parallel Concatenated Coding Schemes", IEEE Transactions on Information Theory, vol. 42, No. 2, march 1995, pp. 409-428.
- [33] H. Nickl, J. Hagenauer and F. Burkert, "Approaching Shannon's Capacity Limit by 0.27 dB Using Simple Hamming Codes", IEEE Communications Letters, vol. 1., No.5, September 1997, pp. 130-132.
- [34] P. Elias, "Error-Free Coding," IRE Transactions on Information Theory, PGIT-4, pg 29 to 37, September 1954.
- [35] R. Tanner, "A Recursive Approach to Low Complexity Codes," IEEE Transactions on Information Theory , Volume IT-27, No. 5, September 1981.
- [36] S. Lin & D. J. Costello, "Error Control Coding : Fundamentals and Applications", Prentice-Hall, USA, 1983, pp. 274-277.
- [37] J. Lodge, R. Young, P. Hoeher & J. Hagenauer, "Separable MAP "Filters" for the Decoding of Product and Concatenated Codes", proceedings of IEEE International Communications Conference (ICC), May 1993, Geneva, Switzerland, pp. 1740-1745.
- [38] M. Moher, "Decoding via Cross-entropy Minimisation", proceedings of IEEE GlobeCom Conference 1993, pp. 809-813.
- [39] R.M. Pyndiah, "Near-Optimum Decoding of Product Codes : Block Turbo Codes", IEEE Transactions on Communications, vol. 46, No. 8, August 1998.
- [40] A. Picart & R. Pyndiah, "Adapted Iterative Decoding of Product Codes", proceedings of IEEE GlobeCom Conference, December 1999, Rio de Janeiro, Brazil, pp. 2357-2362.

- [41] “Technical Description of Turbo Product Codes”, Efficient Channel Coding Inc., USA, June 1999 – <http://www.eccincorp.com>.
- [42] J. Lodge, P. Hoeher and J. Hagenauer, “The Decoding of Multidimensional Codes Using Separable MAP Filtering”, in Proc. 16<sup>th</sup> Queen’s Biennial Symp. Commun. 1992, Kingston, Canada, pp. 343-346.
- [43] D. Rankin & T.A. Gulliver, “Asymptotic Performance of Product Codes”, proceedings of IEEE International Communications Conference (ICC), June 1999, Vancouver, Canada, pp 431-435.
- [44] D. Rankin & T.A. Gulliver, “Randomly Interleaved Product SPC Codes”, proceedings of International Symposium on Information Theory (ISIT), June 2000, Sorrento, Italy.
- [45] L. Ping, S. Chan and K.L. Yeung, “Iterative Decoding of Multi-dimensional Concatenated Single Parity Check Codes”, proceedings of IEEE International Communications Conference (ICC), June 1998, Atlanta, USA, pp. 131-135.
- [46] J. K. Wolf, “Efficient Maximum Likelihood Decoding of Linear Block Codes Using a Trellis”, IEEE Transactions on Information Theory, vol IT-24, No. 1, January 1978, pp. 76-80.
- [47] S. Lin, T. Kasami, T. Fujiwara & M. Fossorier, “Trellises and Trellis-Based Decoding Algorithms for Linear Block Codes”, Kluwer Academic Publishers, USA, 1998.
- [48] D. Chase, “A Class of Algorithms for Decoding Block Codes with Channel Measurement Information”, IEEE Transactions on Information Theory, vol. IT-28, No.1, January 1972, pp. 170-182.
- [49] M. P. C. Fossorier & S. Lin, “Chase-Type and GMD Coset Decodings”, IEEE Transactions on Communications, vol. 48, No. 3, March 2000, pp. 345-350.
- [50] E. Fishler, O. Amrani & Y. Be’ery, “Geometrical and Performance Analysis of GMD and Chase Decoding Algorithms”, IEEE Transactions on Information Theory, vol. 45, No. 5, July 1999, pp. 1406-1422.
- [51] M. P. C. Fossorier & S. Lin, “Computationally Efficient Soft-Decision Decoding of Linear Block Codes Based on Ordered Statistics”, IEEE

- Transactions on Information Theory, vol. 42, No. 3, May 1996, pp. 738-750.
- [52] B. Sklar, "Digital Communications : Fundamentals and Applications", Prentice Hall, USA, 1988.
- [53] X. Huang, N. Phamdo & L. Ping, "BER Bounds on Parallel Concatenated Single Parity Check Arrays and Zigzag Codes", proceedings of IEEE GlobeCom Conference, December 1999, Rio de Janeiro, Brazil.
- [54] J. S. K. Tee & D. P. Taylor, "Multiple Parallel Concatenated Single Parity Check Codes", submitted to IEEE International Communications Conference (ICC), June 2001, Helsinki, Finland.
- [55] J. S. K. Tee and D. P. Taylor, "Multiple Serially Concatenated Single Parity Check Codes", proceedings of IEEE International Communications Conference (ICC), June 2000, New Orleans, USA, paper number MNC 5\_5
- [56] E. K. Hall & S. G. Wilson, "Design and Analysis of Turbo Codes on Rayleigh Fading Channels", IEEE Journal on Selected Areas in Communications, vol. 16, No. 2, February 2000, pp. 160-174.
- [57] G. Ungerboeck, "Channel Coding with Multilevel/Phase Signals", IEEE Transactions on Information Theory, vol. IT-28, No. 1, January 1982, pp. 55-67.
- [58] G. J. Pottie & D. P. Taylor, "Multilevel Codes Based on Partitioning", IEEE Transactions on Information Theory, vol. 35, No. 1, January 1989, pp. 87-98.
- [59] A. R. Calderbank, "Multilevel Codes and Multistage Decoding", IEEE Transactions of Communications, vol. 37, No. 3, March 1989, pp. 222-229.
- [60] U. Wachsmann, J.B.Huber and P. Schramm, "Comparison of Coded Modulation Schemes for the AWGN and the Rayleigh Fading Channel", proceedings of ISIT'98, August 1998.
- [61] E. Zehavi, "8-PSK Trellis Codes for a Rayleigh Channel", IEEE Transactions on Communications, vol. 40, No. 5, May 1992, pp. 873-884.

- [62] Y. Kofman, E. Zehavi & S. Shlomo (Shitz), "A Multilevel Coded Modulation Scheme for Fading Channels", *AEU (International Journal of Electronics and Communications)*, No. 6, 1992, pp. 420-428.
- [63] G. Caire, G. Taricco & E. Biglieri, "Bit-Interleaved Coded Modulation", *IEEE Transactions on Information Theory*, vol.44, No.3, May 1998, pp. 927-946.
- [64] S. A. Al-Semari & T. E. Fuja, "I-Q TCM : Reliable Communication Over the Rayleigh Fading Channel Close to the Cutoff Rate", *IEEE Transactions on Information Theory*, vol. 43, No. 1, January 1997, pp. 250-262.
- [65] U. Hansson, "Efficient Digital Communication over the Time Continuous Rayleigh Fading Channel", Ph.D Thesis, Chalmers University of Technology, Goteborg, Sweden, 1997.
- [66] P. Schramm, "Multilevel Coding with Independent Decoding on Levels for Efficient Communication on Static and Interleaved Fading Channels", proceedings of the 8<sup>th</sup> IEEE International Symposium on Personal, Indoor and Mobile Radio Communication, 1997, pp. 1196-1200.
- [67] G. D. Forney, "Convolutional Codes I : Algebraic Structure", *IEEE Transactions on Information Theory*, vol. IT-16, November 1970, pp. 720-738.
- [68] G. D. Forney, "The Viterbi Algorithm", proceedings of IEEE, vol. 61, No. 3, March 1973, pp. 268-278.
- [69] G. Ungerboeck, "Trellis-Coded Modulation with Redundant Signal Sets Part I : Introduction", *IEEE Communications Magazine*, vol. 25, No. 2, February 1987, pp. 5-11.
- [70] G. Ungerboeck, "Trellis-Coded Modulation with Redundant Signal Sets Part II : State of the Art", *IEEE Communications Magazine*, vol. 25, No. 2, February 1987, pp. 12-21.
- [71] G. D. Forney, R. G. Gallager, G. R. Lang, F. M. Longstaff, S. U. Qureshi, "Efficient Modulation for Band-Limited Channels", *IEEE Journal on Selected Areas in Communications*, vol. SAC-2, No. 5, September 1984, pp. 632-647.

- [72] A. R. Calderbank & N. J. A. Sloane, "Four-dimensional Modulation with an Eight-state Trellis Code", *AT&T Technical Journal*, vol. 64, May-June 1985, pp. 1005-1018.
- [73] G. D. Forney & L.-F. Wei, "Multidimensional Constellations – Part I : Introduction, Figures of Merit, and Generalised Cross Constellations", *IEEE Journal on Selected Areas in Communications*, vol. 7, August 1989, pp. 877-892.
- [74] G. D. Forney, "Multidimensional Constellations – Part II : Voronoi Constellations", *IEEE Journal on Selected Areas in Communications*, vol. 7, August 1989, pp. 941-958.
- [75] S. S. Pietrobon, R. H. Deng, A. Lafanechere, G. Ungerboeck & D. J. Costello, "Trellis-coded Multidimensional Phase Modulation", *IEEE Transactions on Information Theory*, vol. 36, 1990, pp. 63-89.
- [76] S. S. Pietrobon & D. J. Costello, "Trellis Coding with Multidimensional QAM Signal Sets", *IEEE Transactions on Information Theory*, vol. 39, March 1993, pp. 325-336.
- [77] D. Divsalar & M. D. Simon, "The Design of Trellis Coded MPSK for Fading Channels : Performance Criteria", *IEEE Transactions on Communications*, vol. 36, No. 9, September 1998, pp. 1004-1012.
- [78] D. Divsalar & M. D. Simon, "The Design of Trellis Coded MPSK for Fading Channels : Set Partitioning of Optimum Code Design", *IEEE Transactions on Communications*, vol. 36, No. 9, September 1998, pp. 1013-1022.
- [79] C. Schlegel & D. J. Costello, "Bandwidth Efficient Coding for Fading Channels : Code Construction and Performance Analysis", *IEEE Journal on Selected Areas in Communications*, vol. 7, No. 9, December 1989, pp. 1356-1368.
- [80] B. Vucetic, "Bandwidth Efficient Concatenated Coding Schemes for Fading Channels", *IEEE Transactions on Communications*, vo. 41, No.1, January 1993, pp. 50-61.
- [81] H. Imai & S. Hirakawa, "A New Multilevel Coding Method Using Error-Correcting Codes", *IEEE Transactions on Information Theory*, vol. IT-23, No. 3, 1977, pp. 371-377.

- [82] G. J. Pottie, "Multilevel Codes Based on Partitioning", Ph.D Thesis, McMaster University, 1989.
- [83] H. Herzberg, Y. Be'ery & J. Snyders, "Concatenated Multilevel Block Coded Modulation", IEEE Transactions on Communications, vol. 41, No. 1, January 1993, pp. 41- 49.
- [84] N. Seshadri & C.-E. W. Sundberg, "Multilevel Trellis Coded Modulations for the Rayleigh Fading Channel", IEEE Transactions on Communications, vol. 41, No. 9, September 1993, pp. 1300-1310.
- [85] J. Wu & S. Lin, "Multilevel Trellis MPSK Modulation Codes for the Rayleigh Fading Channel", IEEE Transactions on Communications, vol. 41, No. 9, September 1993, pp. 1311-1318.
- [86] R. van Nobelen, "Coding for the Rayleigh Fading Channel", Ph.D Thesis, University of Canterbury, February 1996.
- [87] J. Huber & U. Wachsmann, "Capacities of Equivalent Channels in Multilevel Coding Schemes", Electronics Letters, vol. 30, No. 7, 31<sup>st</sup> March 1994, pp. 557-558.
- [88] J. Huber, "Multilevel Codes : Distance Profiles and Channel Capacity", in ITG-Fachbericht 130, Conference Records, October 1994, Munchen, Germany, pp. 305-319.
- [89] J. Huber & U. Wachsmann, "Design of Multilevel Codes", in Proceedings of IEEE Information Theory Workshop (ITW), Rydzyna, Poland, June 1995, paper 4.6
- [90] U. Wachsmann, R. Fischer & J. B. Huber, "Multilevel Codes : Theoretical Concepts and Practical Design Rules", IEEE Transactions on Information Theory, vol. 45, No. 5, July 1999, pp. 1361-1391.
- [91] Y. Kofman, E. Zehavi & S. Shamai (Shitz), "Analysis of a Multilevel Coded Modulation System", in 1990 Bilkent International Conference of New Trends in Communications, Control, and Signal Processing, Conference Records, Ankara, Turkey, July 1990, pp. 376-382.
- [92] Y. Kofman, E. Zehavi & S. Shamai (Shitz), "Performance Analysis of a Multilevel Coded Modulation System", IEEE Transactions on Communications, vol. 42, No. 2/3/4, February/March/April 1994, pp.299-312.

- [93] R. G. Gallager, "Information Theory and Reliable Communications", Wiley, New York, 1968.
- [94] T. M. Cover & J. A. Thomas, "Elements of Information Theory", Wiley, New York, 1991.
- [95] A. J. Viterbi, J. K. Wolf, E. Zehavi & R. Padovani, "A Pragmatic Approach to Trellis-Coded Modulation", IEEE Communications Magazine, July 1989, pp. 11-19.
- [96] C. Heegard, S. Lery & W. Paik, "Practical coding for QAM transmission of HDTV", IEEE Journal of Selected Areas in Communications, vol. 11, January 1993, pp. 111-118.
- [97] M. L. Moher, J. H. Lodge, "TCMP – A Modulation and Coding Strategy for Rician Fading Channels", IEEE Journal of Selected Areas in Communications, vol. 7, December 1989, pp. 1347-1355.
- [98] P. K. Ho, J. K. Cavers & J. K. Varaldi, "The Effects of Constellation Density on Trellis Coded Modulation on Fading Channels", IEEE Transactions on Vehicular Technology, vol. 42, August 1993, pp. 318-325.
- [99] U. Hansson & T. Aulin, "Channel Symbol Expansion Diversity", Electronics Letters, vol. 31, No. 18, 31<sup>st</sup> August 1995, pp. 1545-1546.
- [100] U. Hansson & T. Aulin, "Channel Symbol Expansion Diversity – Improved Coded Modulation for the Rayleigh Fading Channel", proceedings of IEEE International Communications Conference (ICC), June 1996, Dallas, USA, pp. 891-895.
- [101] M. Hook, C. Edholm, N. Edvardsson, S. Javerbring, F. Miller, P. Schramm and J. Skold, "Coded Modulation for Evolution of Mobile Radio Systems", proceedings of ICT'98
- [102] G. Caire, G. Taricco & E. Biglieri, "Capacity of bit-interleaved channels", Electronic Letters, vol. 32, No. 12, 6<sup>th</sup> June 1996, pp. 1060-1061
- [103] U. Wachsmann & J. Huber, "Power and Bandwidth Efficient Digital Communications Using Turbo Codes in Multilevel Codes", European Transactions on Telecommunications (ETT), vol. 6, 1995, pp. 557-567.
- [104] K. Fazel & L. Papke, "Combined Multilevel Turbo-code with 8-PSK

- Modulation”, 1995?
- [105] K. Fazel & L. Papke, “Combined Multilevel Turbo-code with MR-modulation”, proceedings of IEEE International Communications Conference (ICC), May 1995, Seattle, Washington, USA, vol. 2, pp. 668-672.
- [106] P. Robertson & T. Worz, “Coded Modulation Scheme Employing Turbo Codes”, *Electronic Letters*, vol. 31, No. 18, August 1995, pp. 1546-1547,
- [107] P. Robertson & T. Worz, “A Novel Bandwidth Efficient Coding Scheme Employing Turbo Codes”, proceedings of IEEE International Communications Conference (ICC), June 1996, Dallas, USA, pp. 962-967.
- [108] P. Robertson & T. Worz, “Extensions of Turbo Trellis Coded Modulation to High Bandwidth Efficiencies”, proceedings of IEEE International Communications Conference (ICC), 1997, pp. 1251-1255.
- [109] P. Robertson & T. Worz, “Bandwidth-Efficient Turbo Trellis-Coded Modulation Using Punctured Component Codes”, *IEEE Journal on Selected Areas in Communications*, vol. 16, No. 2, February 1998, pp. 206-218.
- [110] W. J. Blackert & S. G. Wilson, “Turbo Trellis Coded Modulation”, proceedings of CISS 1996.
- [111] S. Benedetto, D. Divsalar, G. Montorsi & F. Pollara, “Parallel Concatenated Trellis Coded Modulation”, proceedings of IEEE International Communications Conference (ICC), June 1996, Dallas, USA.
- [112] S. Benedetto, D. Divsalar, G. Montorsi & F. Pollara, “Serial Concatenated Trellis Coded Modulation with Iterative Decoding : Design and Performance”, proceedings of IEEE GlobeCom Conference 1997, pp.38-43.
- [113] X. Li & J. A. Ritcey, “Bit-Interleaved Coded Modulation with Iterative Decoding”, *IEEE Communications Letters*, vol. 1, No.6, November 1997, pp.169-171.
- [114] X. Li & J. A. Ritcey, “Trellis Coded Modulation with Bit Interleaving

- and Iterative Decoding”, *IEEE Journal on Selected Areas in Communications*, vol. 17, No. 4, April 1999, pp. 715-724.
- [115] X. Li & J. A. Ritcey, “Bit-Interleaved Coded Modulation with Iterative Decoding”, *IEEE International Communications Conference (ICC)* June 1999, Vancouver, Canada.
- [116] S. Le Goff, “Performance of bit-interleaved Turbo-Coded Modulations on Rayleigh Fading Channels”, *Electronic Letters*, vol. 36, No. 8, 13<sup>th</sup> April 2000, pp. 731-733.
- [117] R. F. H. Fischer, J.B. Huber and U. Wachsmann, “Multilevel Coding : Aspects from Information Theory”, *proceedings of IEEE Globecom Conference*, November 1996, London, UK, pp. 26-30.
- [118] T. M. Duman & M. Salehi, “Performance Bounds for Turbo-Coded Modulation Systems”, *IEEE Transactions on Communications*, vol. 47, No. 4, April 1999, pp. 511-521.
- [119] A. J. Goldsmith & S-G Chua, “Adaptive Coded Modulation for Fading Channels”, *IEEE Transactions on Communications*, vol. 46, No. 5, May 1998, pp. 595-602.
- [120] M. J. Mihaljevic & J. Dj. Golic, “A Method for Convergence Analysis of Iterative Probabilistic Decoding”, *IEEE Transactions on Information Theory*, vol. 46, No. 6, September 2000, pp. 2206-2211.
- [121] B. Sklar, “A Primer on Turbo Code Concepts”, *IEEE Communications Magazine*, December 1997, pp. 94-101.
- [122] G. Caire, G. Taricco & G. Battail, “Weight Distribution and Performance of the Iterated Product of Single Parity Check Codes”, *proceedings of GlobeCom 94, Communications Theory Mini Conference*, Nov-Dec 1994, San Francisco, USA, pp. 206- 211.
- [123] G. Battail, “On Random-like Codes”, *Lecture Notes in Computer Sciences*, No. 1133, Springer, pp. 76-94.
- [124] E. Soljanin & Rudiger Urbanke, “On the Performance of Recursive Decoding Schemes”, *proceedings of International Symposium on Information Theory 1997 (ISIT '97)*, June-July 1997, Ulm, Germany, pp. 9.
- [125] O. Y. Takeshita, M. P. Fossorier & D. J. Costello, “A New Technique

- for Computing the Weight Spectrum of Turbo-Codes”, IEEE Communications Letters, vol. 3, No. 8, August 1999, pp. 251-253.
- [126] O. Y. Takeshita, O. M. Collins, P. C. Massey & D. J. Costello, “On the Frame Error Rate of Concatenated Turbo Codes”, IEEE Transactions on Communications, vol. 49, No. 4, April 2001, pp. 602-608.
- [127] M. Fossorier & S. Lin, “Error Performance Analysis for Reliability-Based Decoding Algorithms”, proceedings on International Symposium on Information Theory 2000 (ISIT '00), June 2000, Sorrento, Italy, pp. 64.
- [128] “Special Issue on Codes and Graphs and Iterative Algorithms”, IEEE Transactions on Information Theory, vol. 47, No. 2, February, 2001.